Engineering a Tumor Microenvironment Based on Bioresponsive Alginate

Nataliya Debera

MASTHER THESIS

MESTRADO INTEGRADO EM BIOENGENHARIA – BIOTECNOLOGIA MOLECULAR

Faculdade Engenharia da Universidade do Porto

Instituto de Ciências Biomédicas Abel Salazar

October, 2020

Engineering a Tumor Microenvironment Based on Bioresponsive Alginate

Nataliya Debera

Dissertation for Master in Bioengineering

SUPERVISOR:

Sílvia Bidarra, PhD i3s

CO-SUPERVISOR:

Ruben Pereira, PhD i3s

Cristina Barrias, PhD i3s

i3S – Instituto de Investigação e Inovação em Saúde, Universidade do Porto

"Life is short and information endless:
nobody has time for everything"

Aldous Huxley, Brave New World Revisited

Acknowledgments

Este primeiro parágrafo dedico aos meus orientadores. Pelo apoio constante que me proporcionaram durante o trabalho experimental que não poderia ter atingido os níveis aqui apresentados sem o seu vasto conhecimento e experiencia. Agradeço em particular a Sílvia por ter acompanhado este trabalho tão de perto com um entusiasmo contagiante e dedicação sem fim. Ao Rúben pelas discussões pontuais que aclaravam as ideias. Aos dois pelo grande apoio e motivação na reta final. Não posso deixar de agradecer também a Cristina Barrias pela oportunidade que me foi dada.

Não posso deixar de agradecer aos meus pais pelas oportunidades que criaram para mim. Eles são o pilar para cada etapa que eu vou ultrapassando.

Considero que tive bastante sorte no meu percurso universitário. Tive a oportunidade de aprender com a peculiaridade de cada pessoa que fez parte deste percurso. Mas sem dúvida que a melhor parte é saber que foram criadas amizades duradouras que se traduzem em pequenos gestos que fazem uma grande diferença. Entre almoços no bar de minas, a tangerinas na porta do i3s e a gossip infinito que todos tanto gostamos criamos um tipo de relação simbiótica difícil de explicar.

As minhas babes biotecas por viverem comigo os momentos mais desafiantes e serem uma fonte de apoio constante. Aos amigos de Peniche pelas piadas, boatos e todo o tipo de discussões random, sei que levo a vossa amizade para além destes 5 anos. E fica muito mais por dizer mas ninguém tem tempo para tudo!

The research described in this thesis was financially supported by:

Project ANGIONICHE, refª POCI-01-0145-FEDER-028744 and PTDC/MED-ECT/28744/2017, financed by FEDER funds via COMPETE-POCI (PT2020) and Portuguese funds via Fundaçao para a Ciencia e Tecnologia (FCT)

Abstract

Breast Cancer (BC) is the second most frequently diagnosed cancer and one of the major causes of death in women. Triple Negative Breast Cancer (TNBC) is a particularly aggressive and heterogeneous subtype of BC. Thus, the identification of actionable targets for this disease is a complex task, and until today chemotherapy is still the standard care for this subtype of cancer with poor clinical outcome. Therefore, efforts should be made to optimize treatment efficacy, based on the tailoring of standard systemic treatment and further personalization strategy.

The study of cancer biology and drug response has been based on *in vivo* animal models. However, they fall short in represent accurately the human-specific conditions. In the early stages of cancer research, 2D *in vitro* models provided insightful knowledge, but now they are obsolete. Nowadays, it is well-accepted that cancer biology can no longer be limited to cancer cell characteristics, but should be considered alongside cells' microenvironment. 2D models fail short in recreating 3D cell-cell and cell-matrix interactions that occur in the tumor microenvironment (TME). As an alternative, 3D models have been gaining attention in this field of study, since they allow the incorporation of different TME components in a more relevant physiological setting.

The endeavor to engineer such a model should attain the cellular composition of the tissue, vasculature formation, signaling molecules, and ECM biochemical and biomechanical cues. However, the recreation of a relevant ECM equivalent is the bottleneck of 3D systems development. The fine balance between bioactivity and mechanical properties is not easy to achieve. In this context, the present work had the main objective of developing an ECM equivalent with tunable biochemical and biomechanical properties (e.g. stiffness, the density of cell-adhesion ligands and protease-sensitive moieties), based on ultra-pure alginate. The main advantages of using ultra-pure alginate are the low batch-to-batch variability, defined and xeno-free composition, and tailorable biochemical and mechanical properties.

First, we introduced a highly reactive maleimide molecule into the alginate backbone without compromising its viscoelastic properties nor ionic gelation ability. Second, we observed that this molecule was capable to participate in thiol "click" reactions with a bifunctional MMP sensitive crosslinker and a mono-cysteine RGD ligand. Third, the mechanical properties of these bifunctionalized hydrogels were enhanced by this dual crosslinking mechanism.

Then, we evaluated the biological response of this ECM equivalent and observed that fibroblast were able to establish a cell network within these matrices. Moreover, the stiffness of these bioresponsive hydrogels fell within the natural stiffness of breast tissue. Furthermore, after establishing the optimal formulation for MDA-MB-231 3D culture we evaluated their outgrowth capability, MMP production, and drug resistance.

Furthermore, the functionalization with maleimide, and the consequent orthogonal chemistry in which it can participate, allows an accurate tethering of the polymer with biochemical cues. Thus, in the future, this formulation can be used to test the effect of other biologically relevant peptides and allow to elucidate their influence in cancer cell behavior in a controlled and well established environment.

Table of Contents

Acknowledgments vi
Abstract viii
List of Figures xii
List of Tables xv
List of Abbreviations xvi
1. Introduction 1
1.1 Context 1
1.2 Goal 3
2. 3D models: more than adding a dimension 5
3. Organotypic 3D models of breast cancer 7
3.1 Tumor cells and fibroblasts 7
3.2 Tumor cells and endothelial cells 10
3.3 Tumor cells and other stromal cells 11
4. Alginate: Borrowing from nature 16
5. Materials & Methods 21
5.1 RGD-Alginate synthesis 21
5.2 Maleimide-modified Alginate synthesis 21
5.3 Quantification of Coupling Efficiency 23
5.4 Hydrogel Formation and Characterization 24
5.5 3D cell culture within Bioresponsive Alginate 25
5.6 Treatment with anti-cancer drug Paclitaxel 28
5.7 RGD-Scaffold filling with bioresponsive alginate 29
5.8 Statistical Analysis 29
6. Results and Discussion 30
6.1 Design Considerations 30
6.2 Alginate Modification and characterization 32
6.3 3D Cell Culture 38
6.4 TME development and analysis 46
6.5 Paclitaxel Drug resistance 52
6.6 Preliminary results to test the applicability of the bioresponsive alginate in the development of 3D tri-culture platform 54
7. Concluding remarks and future perspectives 58
References 61

Supplementary Information 68

List of Figures

Figure 1 - Schematic representation of TME design based on bioresponsive alginate. Strategy A results in a more heterogeneous distribution of MMP cleavable sites and RDG moieties due to mixture of alginate with different modifications. Strategy B results in a more homogeneous material due to in situ addition of both RGD and MMP sensitive peptide to alginate maleimide.A4 and B4 - the hypothetical response of human mammary fibroblasts (hMF) 4

Figure 2 - The tumor microenvironment (TME) complexity and its key players. Evolution of 3D models and their level of physiological relevance directly proportional to the number of elements incorporated from the TME. More relevant in vitro models will allow for therapeutic drug development and mechanistic studies of cancer biology. Adapted from *[22]*..... 6

Figure 3 - Alginate structure and chain conformation - A. The two different monomers: (1,4)-linked β-D-mannuronic acid and (1,4-)α-D-guluronic acid ; Monomers arrangement in the alginate chain: B)G – blocks; C) M – blocks; D) MG – blocks, alternating M and G 17

Figure 4- Scheme of Alginate Modification chemistries. A – RGD-Alginate synthesis by carbodiimide chemistry; B – Maleimide-Alginate synthesis using DMTMM as coupling reagent; B1 – Thiol-Michael Addition reaction of MMP sensitive peptide; B2 - RGD peptide coupling by thiol-Michael addition reaction..... 23

Figure 5 - Schematic representation of cell embedding within bioresponsive alginate hydrogel. Small drops of cell-laden alginate were applied on top of a Teflon plate between two spacers and then another Teflon plate was placed on top of those spacers. After gelation, 3D matrices were obtained. 26

Figure 6 - Schematic representation of bioresponsive alginate hydrogels design. a) AlgRGD synthesis by aqueous carbodiimide chemistry; b) AlgM synthesis using DMTMM as coupling reagent; c) and d) represents two different strategies adopted for RGD introduction in final hydrogel composition. 32

Figure 7 - H-NMR spectra of alginate modified with maleimide with different degree of carboxylic group activation and varying amount of substituent added. 33

Figure 8 - Visual representation of viscosity increase after MMP sensitive peptide crosslinking at different ratios. Strategy A (1:1 AlgRGD/M1) after 5 and 15 min and Strategy B (AlgM1) after 5 min..... 35

Figure 9 - Calibration curve plotted from absorbance values of GI-linker and table of absorbance values of the samples tested and percentage of free thiol..... 36

Figure 10 - Gelation kinetics. a) MMP crosslinking of Strategy A; b) Dual crosslinking of Strategy A; c) MMP crosslinking of Strategy B; d) Dual crosslinking of Strategy B 38

Figure 11 - Rheological characterization of cell laden hydrogels. a) Strategy A – gelation kinetics (R3); b) Strategy B – gelation kinetics (R1); c) Strategy A – stiffness of cell laden hydrogels with hMF with R4 (240 μM) and R2 (120 μM; d) Strategy B – stiffness of cell laden hydrogels with hMF with R2 (240 μM) and R1 (120 μM). Results are presented as mean ± standard deviation. $p>0.05$..... 40

Figure 12 - Cell viability and morphology accessed by Live/Dead assay. From left to right: representative CLSM images of hMF cultures after 14 days of culture within 1:1 AlgRGD/M1 hydrogels with GI-linker (R1 = 60µM), (1:1 AlgRGD/M1-R1), control without GI-linker (1:1 AlgRGD/M1-R0) and control without AlgM1 (AlgRGD). Live cells are stained by calcein AM (green) and dead cells by ethidium homodimer-1 (red). Top images, scale bar = 200 µm; bottom images, scale bar = 100 µm)..... 41

Figure 13 - Overview of hMF culture during 14 days within bioresponsive alginate hydrogels without (R0) and with GI-linker (R2). After 14 days of culture within a dually crosslinked hydrogel cells were able to adhere and spread, showing clear protrusions through F-actin staining (green). Cells were stained for F-actin (green), *fibronectin (grey) and DAPI (nuclei, blue).* Scale bar = 200 µm. 43

Figure 14 - Representative CLSM images of hMF morphology after 1 day of different alginate formulation: R0 (no GI-linker, control); R1, R1.5 and R2. . From left to right we have a closer look over the cell morphology. Black and with images represent fibronectin deposition. Cells were stained for F-actin (green), fibronectin (grey) and DAPI (nuclei, blue). Left column, scale bar = 200 µm; middle and right column, scale bar = 50 µm. 44

Figure 15 - Representative CLSM images of hMF cultures at day 14 *within* different alginate formulation: R0 (no GI-linker, control); R1, R1.5 and R2 *(scale bar = 200 µm). We have a closer look over the cell morphology in condition R1 and R1.5 (scale bar = 50 µm). Black and with images represent fibronectin deposition.* Cells were stained for F-actin (green), fibronectin (grey) and DAPI (nucleu, blue). 45

Figure 16 - Morphological evolution of MDA-MB-231 cells within different alginate formulation: R0 (no GI-linker, control); R1, R1.5 and R2. a) From top to bottom evolution with time of cell cultures (1, 7 and 14 days). From left to right increasing concentration of GI-linker (scale bar = 100 µm). B) Close up of condition R1, evidencing the spheroid formation (scale bar = 50 µm). 48

Figure 17 - Spheroid diameter of MDA_MB-231 after 7 days in culture within different alginate formulations: R0 (no GI-linker, control); R1, R1.5 and R2. . There was significant statistical difference between R0, R1 and R1.5 (****$p<0.0001$) and no significant difference between R0 and R2 ($p>0.05$) (n=200 spheroids for each condition) 49

Figure 18 – Cellular outgrowth in fibrin hydrogel. MDA-MB-231 laden alginate hydrogels (R0 and R1) cultured for 7 days were placed between two layers of fibrin. Live/dead staining was performed after 3 days in fibrin and images acquired with CLSM . Live cells are stained by calcein AM (green) and dead cells by ethidium homodimer-1 (red). I – alginate hydrogel; II – fibrin hydrogel; dotted line represents the interface of the two hydrogels. 50

Figure 19 – A –Gelatinase zymogram of MDA-MB-231 cultured in R0 and R1 alginate. B – Quantitative densiometric analysis of MMP production (n=1). 51

Figure 20 – Immunostaining of co-cultures of hMF and MDA-MB-231 embedded within R1 alginate after 7 days of culture. A. Overview of cell distribution (scale bar = 50 µm). B. Zooming 4x zone confined by a dashed white square where it is possible to observe spheroids formation (dashed circles) and elongated cells (arrows indicate possible fibroblasts) in close contact observed under CLSM. Cells were stained for F-actin (cyan), collagen type I (Col I, green), Vimentin (red) and DAPI (nucleu, blue). Scale bar = 25 µm..... 52

Figure 21- Metabolic activity of mono-cultures of MDA-MB-231 and co-cultures of MDA-MB-231 with hMF after treatment for 72h with increasing paclitaxel concentrations relative to 0.01% DMSO. a) Response of mono-cultures in 2D culture (blue bars) and 3D maintained for 1 day (3D-D1, red bars) or 7 days (3D-D7, green bars) in culture before treatment. b) Response of co-cultures of in 2D and 3D maintained for 1 days or 7 days before drug treatment. Data is presented as means ± stdev (n=3). 54

Figure 22 - Schematic representation of the 3D tri-culture platform that combined an epithelial cell-laden bioresponsive hydrogel with a pre-vascularized scaffold. Adapted from Filipa Teixeira MSc thesis 55

Figure 23 - Mosaic assembly of cross-sections of cell laden R1 hydrogel seeded on top of RGD alginate scaffolds after 1 and 7 days of culture, showing hydrogel penetration throughout the porous scaffold. From left to right we can see an overlapped image of the cell distribution and the scaffold structure at brightfield. Cells were labelled with CellTrackerGreen and DAPI (nuclei in blue) Scale bar = 500 µm. 56

Figure 24 - Morphology of MDA-MB-231 embedded within R1 alginate and added to the porous scaffolds after 1 and 7 days of culture. Cells were able to proliferate within the scaffold and formed spheroids, which was monitored by taking brightfield images and by imaging labelled cells with CellTrackerGreen and DAPI (*nuclei in* blue). Scale bar = 50 µm. 57

Supplementary Figure 1 - ^{1}H-NMR spectrum of AlgM1 and the integrals of the TSP (0.05M) standard (1.00) at 0.00 ppm and the maleimide signal (0.85) at 6.9 ppm. 68

Supplementary Figure 2 –Top view of hMF cultured within bioresponsive alginate hydrogels after 7 and 14 days of culture within different alginate formulation: R1 and R1.5. Cells were stained for F-actin (green), fibronectin (grey) and DAPI (nucleu, blue). Images were taken by CLSM. Scale bars = 200 µm. 70

Supplementary Figure 3 - Effect of DMSO in metabolic activity of mono-cultures of MDA-MB-231 and co-culture of MDA-MB-231 with hMF after 72 hours. a) Response of mono-cultures and b) of co-cultures in 2D culture (blue bars) and 3D maintained for 1 day (3D-D1, red bars)) or 7 days (3D-D7, green bars)) in culture before adding DMSO. Values were normalized considering culture in DMEM as 100% of viability . Data is presented as means ± st*andard deviation* dev (n=3). 70

Supplementary Figure 4 – Brightfield images of MDA-MB-231/hMF spheroids (top row) and MDA-MB-231spheroids (bottom row). At day 0, cells aggregated, forming spherical structures. Co-cultures present higher cell cohesion, originating spheroids with smaller diameter. After 1 day, co-culture*d* spheroids seem*ed* to lose their initial cohesion and circularity. On t*h*e other hand, mono-cultures spheroids seems to slightly decrease their diameter..... 71

List of Tables

Table 1 – Molecular classification of breast carcinomas. Adapted from *[27]* 7

Table 2 – Summary of heterotypic in vitro 3D breast cancer models..... 14

Table 3 – Different extents of alginate modification with 1-(2-Aminoethyl)maleimide, theoretical drees of substituition (tDS) and the percentage of COOH activation and reagent used. 22

Table 4 - Coupling efficiencies of different chemistries for RGD grafting onto alginate backbone and final concentrations in 1% w/v hydrogels of each strategy. 34

Table 5 - Table of ratios of peptide crosslinker to maleimide, final peptide concentration in 1% hydrogels composed of 100% of AlgM1 and the corresponding amount of thiol groups. This values are adjusted with the hydrogel polymer concentration and the amount of maleimide-alginate used 36

Supplementary Table 1 - Calculus of the percentage of functionalization and the efficiency of the reaction based on quantitative NMR analysis. 68

Supplementary Table 2 - Table of ratios of peptide crosslinker to maleimide, final peptide concentration in 1% hydrogels composed of 100% of AlgM1 and the corresponding amount of thiol groups. This values are adjusted with the hydrogel polymer concentration and the amount of maleimide-alginate used, e.g ratio R5 in a hydrogel with 50% of AlgM1 is equivalent to a peptide concentration of 300µM..... 69

List of Abbreviations

2D - two-dimensional

3D - three-dimensional

α-SMA - α-smooth muscle actin

3DμTP - 3D breast cancer microtissue model

ADSC - Adipose-Derived Stem Cells

AlgM – Alginate modified with maleimide

BC – breast cancer

BCA – Bradford Calorimetric Assay

BME - Basement Membrane Extracts

BMi - Bone-mimicking Microenvironment

BOKL - Katushka-expressing Bone Seeking Clone

CAAs - Cancer Associated Adipocytes

CAFs - Cancer Associated Fibroblasts

CG4RGDSP – cysteine-(glycine)4-arginine-glycine-aspartic acid-serine-proline

CLSM - Confocal Laser Scanning Microscope

CMFDA - 5-chloromethylfluorescein diacetate

DCs - Dendritic Cells

DMEM – Dulbeco's Modified Eagle Medium

DMEM – 50/50 – mixture of high and low glucose DMEM medium

DMSO - Dimethyl Sulfoxide

DMTMM - 4-(4,6-Dimethoxy-1,3,5-triazin-2-yl)-4-methylmorpholinium chloride

DOX - Doxorubicin

EC - Endothelial Cells

ECM - Extracellular Matrix

EDC - 1-ethyl- (dimethylaminopropanyl)carbodiimide

EMT - Epithelial-to-Mesenchymal Transition

ER - Estrogen Receptor

FAP - Fibroblast Activator Protein

FBS - Fetal Bovine Serum

FGF - Fibroblast Growth Factors

FSP-1 - Fibroblast Stimulating Protein

GDL - Glucono-δ-Lactone

G4RGDSP - (glycine)4-arginine-glycine-aspartic acid-serine-proline

HA - Hyaluronic Acid

HBSS - Hank's Balanced Salt Solution

HEPES (N-(2-Hydroxyethyl)piperazine-N'-(2-ethanesulfonic acid)

HER2 - Human Epidermal Growth Factor Receptor 2

hESC - human Embryonic Stem Cells

hMF - human Mammary Fibroblasts

hSAP - human Subcutaneous Preadipocytes

HUVEC - Human Vein Endothelial Cells

iPSC - induced Pluripotent Stem Cell

MDSCs - Myeloid-Derived Suppressor Cells

MES - -(N-morpholino)ethanesulfonic acid

MMP - Matrix Metalloproteases

MSC - Mesenchymal Stem Cells

NHS - N-hydroxy-sulfosuccinimide

NK - Natural Killer

NMR – Nuclear Magnetic Resonance

OA - oxidized alginate

OEC - outgrowth endothelial cells

PDGF - Platelet Derived Growth Factor

PDMS - poly-dimethyl-siloxane

PEG - polyethylene glycol

PFA – Paraformaldehyde

PGA – polyglycolide

PLA – polycaprolactone

PR - Progesterone Receptor

RGD – Arginine-Glycine-Aspartic acid

RT – Room Temperature

SDS - Sodium Dodecyl Sulfate

TAMs - Tumor-Associated Macrophages

TGF-β – Tumor Growth Factor Beta

TIL - Tumor Infiltrating Lymphocytes

TME - Tumor Microenvironment

TMS - Tissue Matrix Scaffold

TNBC - Triple Negative Breast Cancer

Tregs - regulatory T cells

TSP - trimethylsilylpropanoic acid

VEGF - Vascular Endothelial Growth Factor

1. Introduction

1.1 Context

The human body is a construction of perfectly coordinated tissues with their complex morphology and vital functions. Being the cells its building blocks, each one of them working through countless life cycles until its death. All the information for correct cell function is stored in the DNA and during their lifetime, cells undergo several changes, some of them may cause damages to the DNA. Adding to this, we are inserted in an environment that although is life-sustaining is quite hostile and can act as a cause for DNA damage. When a cell is severely damaged and cannot be fixed by internal mechanisms it is condemned to die and restore the equilibrium. The problem appears when the cell exits this programmed route and starts to behave abnormally dividing without control, forming a mass of abnormal cells, damaging the surrounding tissue and in some cases invading other tissues, in a process called metastasis. Cancer is a term used to describe this abnormal behavior and it can affect any tissue of the body thus each cancer has a set of characteristics that resemble the normal tissue but are in some way altered and malfunctioning.

According to the 2020s World Health Organization report on cancer, in 2018 there were 18 million cases of cancer in the world and 9.6 million people died from the disease. It is expected that the incidence and deaths will increase in the next years especially in Low and Lower Middle Income Countries. Breast Cancer (BC) is the second most frequently diagnosed cancer and one of the major causes of death in women [1]. To fight cancer and consequently damper the raise of these numbers, an accurate understanding of the disease is required in order to provide the molecular and cellular basis for the development of new therapies with improved clinical efficacy.

To understand cancer the question we must ask ourselves is 'What is and isn't normal?'. One shall seek to comprehend the differences between normal cells and cancer cells and the mechanisms of fundamental processes such as cell growth, the transformation from normal to a cancer cell, and the spread or metastasis of cancer cells. Another aspect to take into account is the symbiotic relationship of the cancer cell with the tumor microenvironment (TME), composed of the extracellular matrix (ECM) and cells from the stroma [2]. Insights into cancer related processes could lead to the development of new cancer treatment strategies. Currently, there are three approaches to model the TME: *in vivo*, *ex vivo*, and *in vitro* models [3]. Each model has their advantages and disadvantages but in the end the information gathered from them enables to answer some of the issues stated above and lead to the development of new cancer treatment strategies.

As with most human cancers, BC is used to refer to different tumors concerning histopathological appearance, molecular alterations, presentation, and clinical outcome [4]. Triple Negative Breast Cancer (TNBC) represents 15% of breast carcinomas and is defined by the

absence of three main BC biomarkers, lack of expression of estrogen receptors and progesterone receptors, and lack of amplification or overexpression of HER2 (also known as ERBB2) [5]. This is a very heterogeneous group of tumors that are associated with a more aggressive phenotype with significantly higher rates of metastasis and a poorer clinical outcome [6]. From a clinical point of view, TNBC is a very relevant group because patients cannot benefit from endocrine or anti-HER2 therapy, and consequently chemotherapy is the only established therapeutic option [7]. Once metastasized, TNBC has a high predisposition to involve vital organs such as lung, liver and brain, leading to a significantly shorter median overall survival than other cancers. Therefore, efforts should be made to optimize treatment efficacy, based on the tailoring of standard systemic treatment and further personalization strategy. Despite an overwhelming amount of pre-clinical research on breast cancer and chemotherapeutic strategies, the probability of approval of an oncology drug after completing Phase 1 trials is only 8.3% [8]. The major cause of this inefficient translation of pre-clinical findings is that the development of cancer drugs have been based on the drug's cytotoxicity in two-dimensional (2D) models which fail to recapitulate relevant physiological conditions and the actual response to drug treatment [3]. One promising approach expected to improve the success rates in drug development, is the design of new preclinical models that better recapitulate *in vivo* biology and microenvironmental factors. It is now well-accepted that three-dimensional (3D) systems better emulate the *in vivo* environment than traditional 2D monolayer cultures. Because they are more biologically relevant, 3D cell cultures are becoming more prominent in drug discovery due to higher predictive value for therapeutic outcome. In addition, 3D cell culture models using human cells can circumvent drawbacks of mouse models that, aside from the high cost and ethical considerations, may not be representative of human-specific conditions.

The challenge lays in the development of a suitable *in vitro* model for the study of breast cancer that can recapitulate the biologic setting for tumor cells, mimicking the natural TME with the correct architecture and multicellular components of the stroma. Hopefully, these demands can be satisfied by organotypic 3D models that have been gaining an important role in the study of cancer biology. The promise of an accurate 3D model lies in the possibility to reflect the distinct higher-order cell processes that are inherently 3D.

To this day multicellular spheroids are the golden standard of 3D cell culture, however recent advances allowed for the development of new 3D experimental systems. Biomaterial-based platforms traditionally associated with tissue engineering approaches have been translated into cancer research, creating improved models to study tumor biology [9][10]. The advantage of engineered biomaterials is the ability to accurately tune multiple properties, such as matrix stiffness, degradation, and inclusion of ECM proteins, that are important for tumor progression, invasion and metastasis [11]. Another consideration to take into account is the type of material used for the construction of this model. Some of the key characteristics are biocompatibility, biodegradability, tunable mechanical properties, and cost. *In vitro* models comprising tumor

ECM-mimetic hydrogels exhibit great potential as matrices for 3D cell culture and organization [12].

1.2 Goal

The goal of this thesis is to design a breast tumoroid of TNBC that recreates a tumor-like compartment. To achieve this goal we sought to engineer bioresponsive ultra-pure alginate with tunable biochemical and biomechanical properties (e.g. stiffness, the density of cell-adhesion ligands, and protease-sensitive moieties). The great advantages of ultra-pure alginate are the low batch-to-batch variability, defined and xeno-free composition, and their precisely customizable biochemical and biophysical properties. For alginate modification two alternative chemical routes for carboxylic group activation will be investigated: the traditional aqueous carbodiimide chemistry (EDC/NHS) and DMTMM activated amidation. These alginate derivatives should be capable not only to promote integrin-mediated cell adhesion but also to generate a hydrogel degradable by proteases, enhancing cell-cell contact. Different formulations will be explored, selected and further used for the embedding of MDA-MB-231, a human breast cancer cell line. In a near future, this model can be further adapted to incorporate patient-derived cells for *ex vivo* assessment of therapeutic efficacy using precision medicine approaches for translational research.

Specific targets of the present thesis are:

a. Synthesis and characterization of molecularly-design ECM-like alginate 3D matrices (two alternative chemical routes will be explored).
b. Assess the biological effect of different alginate formulations, more specifically the impact of hydrogel degradation via cleavage of MMP-sensitive peptides on cell morphology. To better visualize cell-cell contact and spreading within the 3D matrix fibroblast cells will be used (Figure 1).
c. Embedding of MDA-MB-231 within modified alginate matrices previously optimized. Alginate with different concentrations of MMP-sensitive peptides will be considered. The behavior of MDA-MB-231 cells within a 3D environment will be studied regarding: spheroids formation, outgrowth migration, MMP production and drug response.

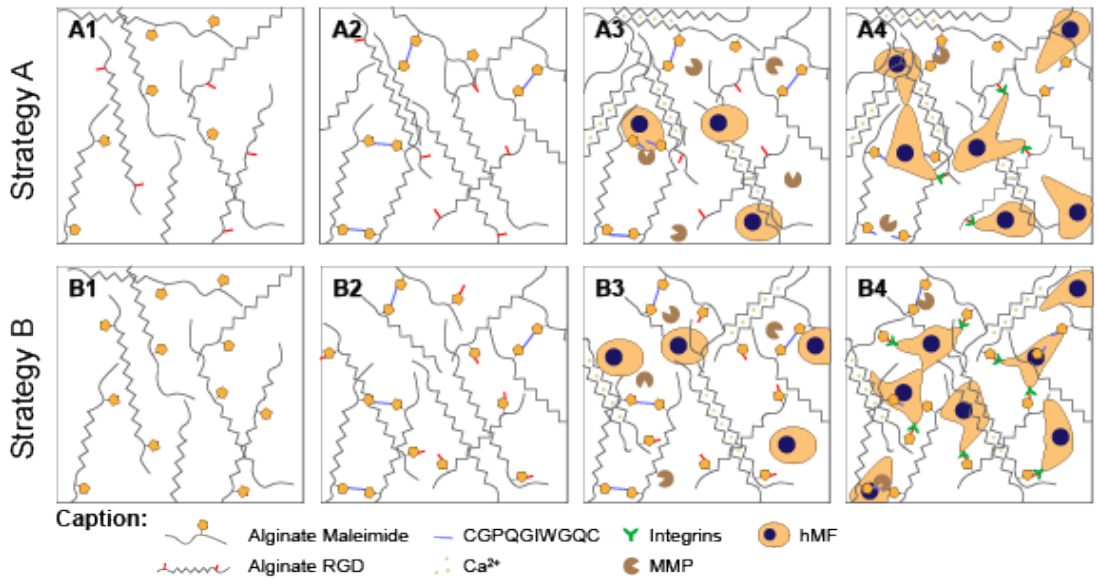


Figure 1 - Schematic representation of TME design based on bioresponsive alginate. Strategy A results in a more heterogeneous distribution of MMP cleavable sites and RDG moieties due to mixture of alginate with different modifications. Strategy B results in a more homogeneous material due to in situ addition of both RGD and MMP sensitive peptide to alginate maleimide.A4 and B4 - the hypothetical response of human mammary fibroblasts (hMF)

2. 3D models: more than adding a dimension

Most of the knowledge of cancer related events and drug screening comes from 2D monolayer cell cultures and animal models but in the past few years, their limitations have been thoroughly analyzed. *In vitro* 2D monolayers fail short in reproducing a relevant physiological environment because it is now widely accepted that tumors are not merely a mass of transformed proliferating cancer cells but there also exist an evolving 3D network of stromal, immune and endothelial cells within a dynamic ECM that supports and mediates tumor therapeutic sensitivity and resistance. Without the complexity of this TME there is no accurate representation of the cell-cell and cell-ECM interactions which can lead to false results in drug development. Although, animal models have been used to resemble the*in vivo* tumor progression and incorporate components of the physiologically relevant microenvironment their use should be limited due to ethical concerns. Furthermore, animal models and humans have inter-specific variability with genetic, molecular, and physiological limitations [13] and the complexity of an *in vivo* environment makes it difficult to study specific interactions between different tumor components. Therefore, results in animal models and clinical trials have an average rate of concordance of approximately 8% [14]. The development of 3D *in vitro* models is motivated by the need for cellular models that better capture the complexity of TME and an ideal model would eliminate the differences related to species. More sophisticated 3D *in vitro* models could be able to recapitulate the complexity of the tumor microenvironment its cellular heterogeneity, cell-cell interactions, and spatial architecture [15] (Figure 2).

The most commonly explored 3D *in vitro* tumor models are the 3D multicellular tumor spheroids, due to several advantages such as ease of assembly, high-throughput of drug screening, and relatively low cost. These multicellular structures mimic *in vivo* tumor growth via formation of cell aggregates that exhibit a central necrotic core, an intermediate layer of quiescent cells, and an outer layer of proliferating cells as well as a solute/ion gradient from the periphery to the center, and a 3D spatial organization [16]. Spheroids can be composed of a single cell type or a co-culture of different cell types which gives them some level of heterogeneity. Although cells can secrete ECM proteins, spheroids are considered ECM-free models. The lack of a pre-existing ECM makes these models inadequate to represent the ECM guidance and influence of cancer cells and stromal cells from the onset, failing to provide the initial cues for characteristic cancer phenotypes to arise [15].

Although useful in the past to unravel cancer cell behavior in a 3D setting it is time for spheroids as 3D cancer models to become obsolete. As depicted in Figure 2, spheroids represent very poorly the complex composition of the TME. Engineered 3D models based on hydrogels as ECM equivalents have been climbing the ladder of physiological relevance. For this purpose, hydrogels of natural or synthetic origin have been explored [10][17][18]. Cell culture within hydrogels can combine more elements from the TME. Besides cancer cells, they allow for the

inclusion of other cell types and most importantly a physical equivalent of the ECM (Figure 2). The most commonly explored hydrogels for tissue engineering purposes are naturally derived alginate, collagen, hyaluronic acid (HA) and fibrin and synthetic polymers such as polyethylene glycol (PEG), polycaprolactone (PLA), and polyglycolide (PGA) [19]. Among these, ultra-pure alginate hydrogels present advantages such as low batch-to-batch variability, well defined and xeno-free composition, and precisely customizable biochemical/physical properties [20][21]. The manipulation of hydrogel properties and the combination of several culture techniques may allow the development of heterotypic models that better emulate the TME. Heterotypic models aim to combine not only different types of cells but also the structural features of the tumor stroma (e.g vascularization) and therefore might be the closest candidates to animal model substitution in therapeutic drug development and mechanistic studies of cancer biology. In the next chapter are described the efforts to bioengineer the TME of breast cancer having in mind the stromal cell used and the hydrogel composition to mimic the ECM.

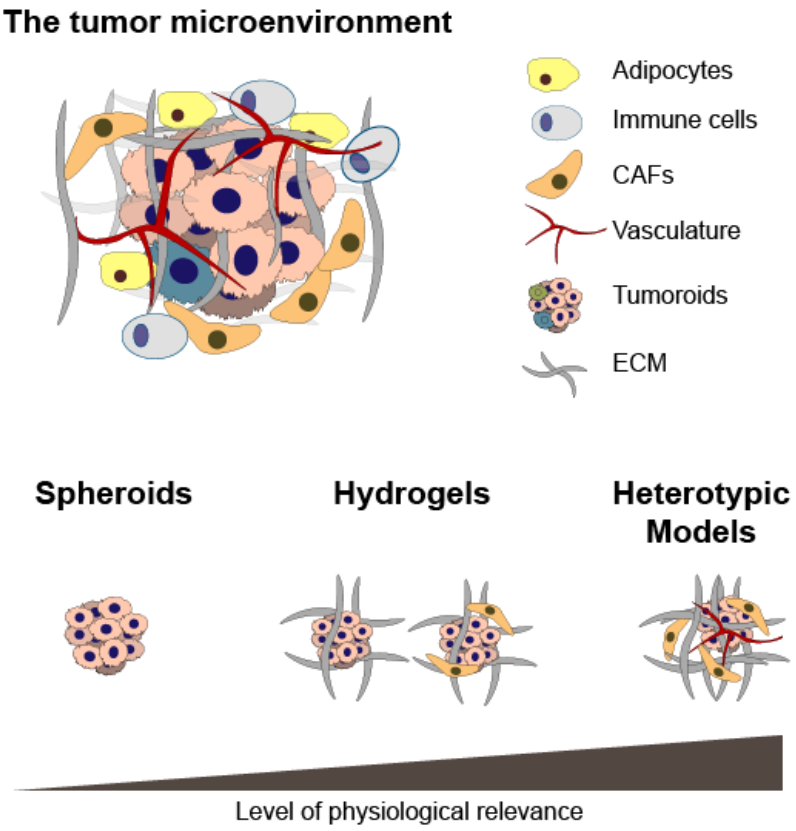


Figure 2 - The tumor microenvironment (TME) complexity and its key players. Evolution of 3D models and their level of physiological relevance directly proportional to the number of elements incorporated from the TME. More relevant in vitro models will allow for therapeutic drug development and mechanistic studies of cancer biology. Adapted from *[22]*.

3. Organotypic 3D models of breast cancer

The tumor microenvironment role in tumor progression has been increasingly analyzed and implicated in cancer related events. The stromal cell types present in the TME of breast cancer include fibroblasts, macrophages, adipocytes, endothelial cells, and other infiltrating leucocytes supported by the structural extracellular matrix with a tissue specific signature of signal molecules entrapped in it [23]. These are critical components of TME that take part in the induction of malignancy in breast cancer through various mechanisms. Tumor cells and the microenvironment induce reciprocal changes in their phenotype and function that cause events such as migration, proliferation, and drug resistance [24][14]. The intercommunications of different cell types cannot be ignored in the process of construction of an *in vitro* model as well as the tissue architecture. Therefore, a successful 3D *in vitro* tumor system should encompass an ECM-like matrix that support cancer cells and other cells from TME, allowing nutrient, gas, and signal exchanges among cells [25].

In this chapter, are reviewed organotypic 3D models for breast cancer that include breast cancer cell lines co-cultured with stromal cells, and analyzed their significance in recapitulating the *in vivo* environment and downstream applications. Since a variety of BC cell lines are available and used in the studies described below, the immune profile of the representative established cancer cell lines are represented in Table 1 [26][27]. Noteworthy, breast cancer is a very heterogeneous disease and molecular profiling allowed to classify it into different subtypes attending the following immunohistochemical biomarkers: estrogen receptor (ER), progesterone receptor (PR), and human epidermal growth factor receptor 2 (HER2). According to their expression profile, they can be classified as luminal A, luminal B, basal, claudin-low, and HER2.

Table 1 – Molecular classification of breast carcinomas. Adapted from *[27]*

Classification	Immunoprofile	Example of cell lines
Luminal A	ER(+); PR(+); HER2(-)	MCF-7, T47D, SUM185
Luminal B	ER(+);PR(+);HER2(+)	BT474; ZR-75
Basal	ER(-);PR(-);HER2(-)	MDA-MB-468; SUM190; HCC1143
Claudin-low	ER(-);PR(-);HER2(-)	BT549; MDA-MB-231
HER2	ER(-);PR(-);HER2(+)	SKBR3, MDA-MB-453

3.1 Tumor cells and fibroblasts

Fibroblasts are responsible for producing and reorganizing various ECM proteins, which are essential elements in normal tissue homeostasis and function. They synthesize components of ECM such as collagens, proteoglycans, and fibronectin as wells as many enzymes, such as matrix metalloproteases (MMPs) that can degrade ECM and release growth factors and cytokines harbored or embedded within the ECM. Therefore they influence epithelial cell features and

cancer phenotype by altering ECM composition [28]. Normal fibroblasts display a quiescent phenotype but can become activated under multiple stimuli from cancer cells or the microenvironment becoming cancer associated fibroblasts (CAFs). CAFs are heterogeneous cells that have been described to have implications in tumor progression and also immune modulation. Activated fibroblast in tumors have been associated to myofibroblast phenotype similar to the one present in wound healing processes [29][30]. They can have different origins, such as activated local fibroblasts, vascular smooth muscle cells, and mesenchymal stem cells (MSCs). Consequently, CAFs exhibit different markers, for example, fibroblast activator protein (FAP), α-smooth muscle actin (α-SMA), platelet derived growth factor α and β receptor (PDGF-α and β), fibroblast stimulating protein (FSP-1) and vimentin [31]. CAFs influence events, such as epithelial-to-mesenchymal transition (EMT), angiogenesis, and metastasis, furthermore by altering ECM composition they decrease chemotherapeutic uptake in tumors and alter tumor sensitivity to a variety of chemotherapies [32]. It only seems logical to study the interaction between CAFs and breast cancer cells in a relevant physiological environment. Thus, several studies have been carried out in that direction trying to develop a relevant 3D *in vitro* model.

Using an improved 3D spheroid culture method Anastasov *et al.,* were capable of generating heterotypic 3D microtissues with primary human dermal fibroblasts (NHDF) and three different mammary cancer cell lines (T47D, MDA-MB-361, and MDA-MB-231) [33]. They observed that the co-culturing of MDA-MB-231 with fibroblast allowed these cells to form a 3D-microtissue as opposed to the diffuse growth when in monoculture, stressing out the importance of the TME. They also confirmed that the sensitivity to drug treatment was lower in the presence of a tumor stroma cell type.

Brancato *et al.* compared two heterotypic 3D culture models, the golden standard spheroid model and a 3D breast cancer microtissue model (3D - µTP) [34]. The cellular component in both models included cancer associated fibroblasts (CAFs) and luminal phenotype breast cancer cells, MCF-7. In the µTP model, cells were seeded into porous biodegradable microcarriers made of gelatin. Spheroids were generated using rounded bottom non-tissue culture treated 96-well plates. In general, both heterotypic models with CAFs exhibit higher drug resistance than homotypic cultures. Nevertheless, spheroids showed higher levels of resistance related to the diffusion coefficient of the tested drug, doxorubicin (DOX). The study demonstrates that the diffusion coefficient increases with the complexity of the system, from homotypic to heterotypic culture and from no ECM (spheroid) to the presence of ECM structure (µTP). Furthermore, the compact nature of the spheroid structure limited the diffusion of the drug to the inner layers. Also, cells proliferated slower on µTP than in spheroids which can also explain the increase in resistance. They also evaluated the expression of adhesion molecules and compared both models to an *in vivo* tumor model. They conclude that µTP models expression profiles were similar to the *in vivo* grown tumor. The µTP model has an upper hand on spheroids in terms of recreating a relevant physiological microenvironment, which makes it a useful tool for *in vitro* drug screening.

In another study, Gudjonsson et al. aiming to recreate the correct microenvironment for human breast cancer used the luminal breast cancer cell line MCF-7 in co-culture with hTERT immortalized fibroblast cell line that displayed a myofibroblast phenotype [35]. A hydrated collagen I gel was used as the matrix substitute. They mainly focused on the identification of genes regulated on tumor cell-fibroblast interaction and were able to identify a hitherto undescribed gene, EPST11. Upregulation of EPST11 can be involved in the transition of fibroblasts to myofibroblasts, a population of cells that is absent in normal breast tissue but is an abundant stromal cell type in human breast cancer. With this 3D heterotypic breast cancer model it was possible to understand the activation pathways from normal stromal cells to cancer associated ones.

Rijal and colleagues have developed a model using a tissue matrix scaffold (TMS) derived from decellularized mice breast tissue, they were able to use the TMS in both forms as a porous scaffold and as a hydrogel [36]. To increase architectural stability, cross-linking was promoted by using UV light and adding tyrosinase as a crosslinker. The approach involved seeding of MDA-MB-231 cell line on the porous scaffold, followed by a layer of TMS hydrogel without cells and on top a layer of GM637 (human fibroblasts)-laden hydrogel, allowing the polymerization of the hydrogels in between. Using this layered approach they could observe the migration of both cancer cells and fibroblasts into the blank gel layer, which allows to study cells invasive behavior. To validate the performance of this model in testing anticancer drugs and predicting treatment efficacies they cultured T47D and BT474 cancer cell lines in 2D and 3D culture, using for the latter one also a scaffold of collagen. They observed that the effect of drugs was less pronounced in 3D cultures and with higher post-treatment recovery of cell proliferation. Also when compared to collagen scaffolds cells proliferated better in TMS scaffolds and showed higher resistance to drug treatment. The authors were able to create a compartmental TMS system that is convenient not only to observe multiple cell phenotypes of different cell populations in a single system, but also to perform drug screening. Nevertheless, the use of decellularized mice breast tissue raises awareness to the amount that is necessary to produce this models in large scale since one of the goals of developing *in vitro* models is to reduce animal use.

Overall, these models prove that cells cultured in 3D show different phenotypes, have slower proliferation rates, and exhibit higher resistance to anticancer treatment. Adding a stromal cell type, such as fibroblasts, in co-culture with cancer cell types might be insufficient to fully represent the effect of the TME in tumor response to drug treatment. As described by the above studies, the introduction of the ECM compartment slows cells proliferation rate, affecting their spatial distribution and making them less compact. This synergic effect alters the drug sensitivity, implying the importance of ECM in recreating a faithful tumor design for drug screening.

3.2 Tumor cells and endothelial cells

Tumor vasculature plays an essential role in tumor development and progression [37]. Endothelial cells (EC) are responsible for the formation of new vessels in tumors, in a process called angiogenesis that is triggered by hypoxia and by a variety of growth factors and chemokines [38]. ECs migration toward and into the tumor involves ECM degradation by proteolytic enzymes releasing, therefore, matrix bound growth factors such as vascular endothelial growth factor (VEGF) and fibroblast growth factors (FGF) that further enhance the angiogenic process [39]. The formation of vasculature in the tumor allows for oxygen and nutrient supply promoting cell survival and also providing a way for metastasis to occur. Therefore understanding the underlying mechanisms of tumor angiogenesis provides a way to identify new targets for cancer therapy. Thus, establishing 3D co-culture systems that allow studying the interaction of endothelial cells with cancer cells will allow for the identification of new therapeutic targets and validate the development of anti-angiogenic therapies. Some attempts have been made in that order reporting co-culture of EC with cancer cells either in spheroids or with scaffold. A common type of EC used in different works are human vein endothelial cells (HUVEC), a mature primary EC. However the results are not always promising on this demand for EC organization. For example, co-cultured spheroids of HUVEC with MCF-7 or MDA-MB-231 did not result in EC organization into tubular networks [40]. They observed that in co-culture EC had proliferated and formed a cluster within the spheroid. This suggests that co-culture with certain cancer cell lines is not sufficient to induce HUVEC organization. There is a need to use a different stimuli to achieve the correct cells phenotype such as addition of pro-angiogenic factors or an ECM that can support this cell behavior.

In a recent study, Swaminathan *et al*., bioprinted pre-formed spheroids of breast epithelial cell lines into a co-culture six-layer collagen-alginate grid structure to study the interactions of MCF-7, MDA-MB-231 and MCF10A with HUVEC [41]. They observed that the bioprinted spheroids maintained cell viability, 3D architecture, polarization, and function. They also saw that chemoresistance to paclitaxel, a cell mitotic arrest inducer drug, increased in 3D bioprinted spheroids when compared with individually bioprinted cells. However, this increased resistance was not observed in co-culture with EC. In co-cultures they observed that most of the HUVEC cells were dead after treatment with paclitaxel and the breast tumor spheroids lost their structure and were dispersed within the bioprinted structure.

Langer *et al.*, took advantage of the 3D bioprinting technique to establish a scaffold-free bioprinted tumor tissue that consisted of a cancer cell core surrounded by several stromal cell types [42]. For the tumor core they used different subtypes of breast cancer cell lines: MCF-7, SKBR3, HCC1143, and MDA-MB-231. The stromal compartment included primary human mammary fibroblasts (hMF) and HUVEC. Cells were bioprinted in hydrogel-based bioinks that were removed during subsequent culture. In the cancer compartment, they observed that the MDA-MB-231 cells rapidly migrated into and dispersed among the stromal cells, as for the other subtypes they maintained the original printed structure with a cancer cell core. In the stromal

compartment in all subtypes, HUVEC self-organized into a capillary-like network and there was an increase in collagen deposition with time except for the bioprinted tissue with MDA-MB-231. Furthermore, they also bioprinted to the stromal compartment, alongside hMF and HUVEC, primary human subcutaneous preadipocytes (SAP) and primary human bone-marrow-derived mesenchymal stem cells (MSC). The addition of adipocytes influenced tumor phenotype by secreting leptin, a pro-inflammatory mediator. MSC increased collagen deposition within the stromal compartment, indicative of a more reactive and desmoplastic TME. As for drug screening, they tested two chemotherapeutic drugs, doxorubicin, and paclitaxel and observed an increase in drug resistance in the 3D models. They also evaluated the response of the model to anti-angiogenic treatment with Sunitinib, which inhibits VEGFR in tumor cells, and observed a decrease in endothelial cell network. There is evidence that anti-VEGF therapy can promote tumor aggressiveness by increasing collagen deposition. Bioprinted tissues with MDA-MB-231 cells showed an increase in collagen deposition after treatment with Sunitinib. The same results were obtained in *in vivo* orthotopic xenografts of MDA-MB-231 suggesting the recapitulation of *in vivo* phenotypes by these bioprinted tissues.

Taubenberger *et al.* developed a matrix metalloproteinase degradable biohybrid PEG-heparin hydrogel to engineer an artificial ECM and study the influence of specific ECM binding factors [43]. They used a four-arm PEG, modified with MMP sensitive peptide and three different adhesion peptides RGD, IKVAV, and GFOGER derived from fibronectin, laminin-111, and collagen type I respectively and crosslinked with maleimide modified heparin. To establish the tumor-angiogenesis constructs tumor cells were cultured in hydrogels to form spheroids that were harvested and combined in a new hydrogel co-culture with HUVEC and MSC. This required the addition of extra amount of RGD and growth factors such as VEGF, SDF-1 and FGF-2 to the PEG-heparin mixture. Since MDA-MB-231 did not form spheroids further analyses were conducted in MCF-7 constructs. What they could observe was that IKVAV and GFOGER did not have any significant effect on MCF-7 spheroid morphology or proliferation when compared to RGD. Also no major differences were observed in HUVEC network formation for the different peptides regarding vessel length and network density. Although they claim that their model is suitable for evaluating specific cell-ECM interactions in a systemic way, the approach seems rather complicated involving modification of two different polymers and requiring further addition of growth factors. Furthermore, the use of heparin raises some questions since the authors do not specified the origin of the molecule nor its chemical properties. Also it might not be appropriate to form angiogenic constructs since the role of heparin in angiogenesis is inconclusive, with conflicting data reported in literature [44] .

3.3 Tumor cells and other stromal cells

Other cells such as immune cells and adipocytes also are present in the mammary gland. Fat-filled adipocytes comprise a large proportion of the stromal fat pad, in fact, they are the most abundant component surrounding breast cancer cells, nevertheless, their role in tumor initiation, growth, and metastasis is a relatively new area of investigation [45][28]. Normal

adipocytes are transformed into cancer associated adipocytes (CAAs) by signals from tumor cells. CAAs are characterized by a fibroblast-like phenotype, overexpression of collagen IV and they secrete significant amounts of pro-inflammatory mediators (CCL2, CCL5, IL-1β, IL-6, TNF-α, VEGF, leptin, etc.) this leads to accumulations of macrophages and can promote invasion and metastasis in BC [46].

The infiltration of immune cells, which can be either from the innate or adaptive immune system, into the tumor and its microenvironment is an early event, also the influence of the infiltrates have been demonstrated in tumor progression, tumor suppression and the efficacy of anticancer therapies. Cytotoxic (CD8+) T cells, T helper (CD4+) cells, Natural Killer (NK) cells, and dendritic cells (DCs) are all involved in the effective immune response, while M2 tumor-associated macrophages (TAMs), FOXP3+ regulatory T cells (Tregs), and myeloid-derived suppressor cells (MDSCs) are associated with suppression of the immune response. TILs populations, tumor infiltrating lymphocytes that make part of the adaptive immune systems, are usually used as biomarkers to predict if the response will be effective or suppressed. The evaluation of the effect on cancer cells, of the immune cells present in TILs and the molecular mechanism behind it, are still poorly understood. Therefore, establishing an *in vitro* 3D model to study this interaction in a more controlled and specific way could be an important step to shed some light on these events [47].

Only a few 3D culture systems were established to evaluate the influence of lymphocytes in breast cancer. Augustine *et al.*, established a heterotypic 3D culture system using BC cells, MCF-7 and MDA-MB-231, Tregs and NK cells [48]. The authors point out that a critical factor of investigation with Treg lymphocytes is the phenotypic characterization. Without a definitive phenotype, isolated population may contain contaminating effectors cells that contribute to conflicting results about the role of this cells in breast cancer. The cells were cultured in the commercially available Matrigel in four different groups for each of the cell line: Treg-NK-BC cells (EXP), NK-BC, Treg-BC and BC. Co-culture with immune cells lead to decrease in cell mass and disruption in cell network more prominent in EXP and NK-BC groups. The tissue remodeling was associated with MMP production and confirmed by decrease in matrix viscosity and expression levels of CCL4 that was higher in EXP and NK-BC groups. Overall, the matrigel-based culture system seems suitable for downstream applications, such as gene expression, immunolocalization of tumor biomarkers, and cytokine analysis. Noteworthy, matrigel present some limitations such as, uncertainty in the biological activity of its components and batch-to-batch variation. Therefore, it would be of great advantage to recreate this experiment with another type of ECM equivalent.

In a more complex study Benton *et al.*, developed a 3D microtumor model of breast cancer including either MCF-7 or MDA-MB-231 breast cancer cell lines co-cultured into spheroids with adipose derived human mesenchymal stem cells (hMSC).These spheroids were then added to a tubular structure formed by HUVEC also co-cultured with hMSC [49]. The structures were

cultured in basement membrane extracts (BME) obtained from Trevigen Inc. and supplemented with collagen-1 that provided an ECM like structure. These microtumors were compared to 2D and 3D monocultures of MCF-7 and MDA-MB-231. They observed that stromal cells enhance BC cell proliferation in a cell-line depend manner, the addition of hMSC was sufficient to increase proliferation of MDA-MB-231 cell line but the MCF-7 cells required the addition of both hMSC and HUVEC. Furthermore, the addition of hMSC increased the invasiveness of both cell lines, directing also the development of tumor architecture, MCF-7 displayed a multi-lobular phenotype and MDA-MB-231 showed a wavy, invasive phenotype. They also evaluated the effect of two chemotherapeutic drugs fluorouracil and paclitaxel. A more selective resistance was observed in microtumor models over that in 2D and 3D monocultures, while MCF-7 revealed to be more resistant, MDA-MB-231 showed more sensitivity to the drug treatment. Overall the results in microtumors were similar to the ones reported for xenograft models. They observed that the treatment with paclitaxel also inhibited the recruitment of tubular networks to the breast cancer microtumor. Therefore, this model besides evaluating tumor cells directly also provides a mechanism to evaluate other cell populations in the growing tumor tissue.

In a recent study, S.Chanji *et al.* optimized a commercial extrusion-based bioprinter to print a 3D model of breast cancer cells (MCF-7) and adipose-derived stem cells (ADSC) pre-differentiated to mature adipocytes [50]. For the bioink, they used a 3:2 alginate to gelatin hydrogel, a formulation that they chose based on printability and adequate structural support for cells with sufficient degradation to allow cell proliferation. They observed that the cells maintained post-printing viability either in mono- or co-culture. By confocal microscope analysis, they observed that cells in co-culture tended to cluster together in the innermost part of the 3D hydrogel, also the lipids in co-culture appeared more clustered together than in mono-cultures of ADSC, suggesting an effect of cancer cells in adipocyte behavior. The cell viability assay also demonstrated some necrotic centers, but overall there was an increase in DNA content and metabolic activity suggesting cell proliferative capacity during the culture time. This 3D model shows some recapitulation of the TME with intact adipocytes and cancer cells after printing, the main advantage of obtaining a viable 3D model through bioprinting is that it can be used as a platform for high-throughput screening and identification of breast cancer treatment options using patient's cancer cells and adipocytes. It would be interesting to test this model with minor alterations on the bioink formulation. It seems that the use of both alginate and porcine gelatin has the purpose to combine the good printability of alginate and the cell interactive properties of gelatin. Nevertheless, gelatin is a derivative of collagen and it is from animal origin therefore it has batch-to-batch variation which could affect the reproducibility of the model.

Table 2 – Summary of heterotypic in vitro 3D breast cancer models

Model	BC cell line	Stromal cell type	ECM
Spheroid microtissue [33]	T47D, MDA-MB-361, and MDA-MB-231	primary human dermal fibroblasts (NHDF)	ECM free
3D – µTP [34]	MCF-7	Cancer associated fibroblasts (CAFs)	Porous gelatin scaffolds
Collagen I 3D model [35]	MCF-7	hTERT immortalized fibroblast cell line	Collagen I hydrogel
TMS [36]	MDA-MB-231, T47D, and BT474	Human normal fibroblasts (GM637) cell line	decellularized mice breast tissue
Spheroids [40]	MCF-7 and MDA-MB-231	Human Umbilical Vein Endothelial Cells (HUVECs)	ECM free
Bioprinted spheroids [41]	MDA-MB-231	HUVECs	Collagen-alginate bioink
Bioprinted tumor tissue [42]	MCF-7, SKBR3, HCC1143, and MDA-MB-231	HUVECs, Human Mammary fibroblasts (HMFs), primary human subcutaneous pre-adipocytes (SAPs) and Mesenchymal Stem Cells (hMSCs)	ECM free
Biohybrid PEG-heparin hydrogel [43]	MCF-7, MDA-MB-231	HUVECs and bone marrow-derived MSCs	PEG-peptide and heparin-maleimide
Matrigel 3D culture system[48]	MCF-7, MDA-MB-231	Blood derived regulatory T lymphocytes (T_{REG}) and natural killer (NK)	Matrigel
3D microtumor model [49]	MCF-7 and MDA-MB-231	adipose derived human mesenchymal stem cells (hMSCs) and HUVECs	Basement Membrane proteins supplemented with collagen-1
Bioprinted 3D model[50]	MCF-7	Adipose derived stromal cells (ADSCs)	3:2 5% alginate to gelatin bioink

Spheroids, although widely used, are not as representative as an ECM based model for purposes of drug screening. Their lack of ECM component from the start leads to high rates of cell proliferation and consequently the formation of very dense structures which alter drug diffusion giving misleading results for some chemotherapeutic agents. Therefore, the development of ECM based models can be a more appropriate way to study cancer biology. As we can see from Table 2, the models described either use purified ECM proteins (e.g collagens), basement

membrane extracts (isolated from Engelbreth-Holm-Swarm mouse sarcoma), or decellularized matrices from *in vivo* tissues. These are commonly used mainly because of their inherent biocompatibility, cell interactivity through naturally present adhesion peptides, and motifs sensitive to protease action giving the ability to cells to modulate the architecture of the environment. However, they have large variations between batches, poor mechanical properties and poorly defined composition with limited ability to modulate chemical and physical properties which can complicate a systematic comparison between models [11].

Another promising approach used to engineer the TME is microfluidics. Microfluidic devices simulate the TME in small chips with microchannels allowing perfusion at tailorable flow rates. Therefore they are used for studying angiogenesis, intravasation, extravasation, mechanotransduction pathways, cancer cell behavior, and drug response under shear stress [3]. These devices are useful to study metastasis to other tissues or organs. Since breast cancer cells mostly metastasize to bone several microfluidic devices recapitulate breast-to-bone metastasis. For example, Jeon *et al.* developed a microfluidic device fabricated with poly-dimethyl-siloxane (PDMS) using soft lithography techniques to evaluate BC cell extravasation into bone [51]. In their study they used a katushka-expressing bone seeking clone (BOKL) of MDA-MB-231. Their system contains a 1.3 mm wide central hydrogel region flanked by two lateral media channels. The hydrogel region corresponds to the microvascular network enclosed by a bone-mimicking microenvironment (BMi) matrix that is generated by embedding hBM-MSC, osteo-differentiated primary hBM-MSC, and HUVEC in fibrin gel. The channels flanking the hydrogel allow the addition of cancer cells, biochemical factors, and flow across the vasculature formed in the gel channel. They compared cancer cell extravasation into the BMi matrix with a muscle microenvironment and a matrix without stromal cells. The highest rate of extravasation was to BMi followed by only matrix and with the lowest rate to muscle environment. This complex design makes microfluidic devices a useful tool to develop more complex 3D models, allowing the study of cancer metastases under biologically and biophysically controlled 3D microenvironments. Moreover they are compatible with high-throughput drug screening techniques allowing a more efficient testing platform. Nevertheless, the fabrication techniques of microfluidic devices are still expensive and time consuming. 3D-printing is emerging as a new fabrication technique of microfluidic devices but it is still struggling with the resolution of the printed structures and the optimal material for printing that has good biocompatibility and surface properties [52].

Overall, the major factor affecting the success of a reliable 3D model seems to be the adequate choice of material to recapitulate the ECM. The key characteristics are biocompatibility, mechanical properties, degradation, and mass transport properties. Hydrogels are widely explored for this purpose either from the natural or synthetic origin, an ideal hydrogel should allow precise control over mechanical properties and biochemical cues.

4. Alginate: Borrowing from nature

The choice of biomaterial to engineer a 3D model is of great importance, it must resemble the native TME which means it has to provide physical, mechanical and biochemical cues. Therefore, when designing engineered models the dynamics between the cells, ECM and signaling molecules in the TME should be taken into consideration [12]. Additionally it has to be compatible with 3D cell culture techniques and allow downstream applications. Advances in tissue engineering have enabled the fabrication of mimetic TME that can be used to study the communication of the tumor and its surrounding environment and allow drug screening of potential anti-cancer compounds.

Hydrogels are water-swollen crosslinked polymeric networks produced by the simple reaction of one or more monomers. They exist in a wide range of chemistries, can be tuned to different material properties, have the potential to bind a large amount of water upon crosslinking and are soft by nature just like the ECM which makes them suitable for engineering the TME. Cell culture in hydrogels involves either embedding of viable cells within the material or seeding on top of a matrix. Therefore, the factors that play an important role in selecting a hydrogel for 3D tissue culture are cell adhesion, stability in culture, biophysical properties, mild gel formation process and hydrogel digestion for cell recovery for downstream applications. Hydrogels can be either naturally-derived polymers (alginate, collagen, hyaluronic acid (HA), fibrin, etc.) or synthetic polymers (polyethylene glycol (PEG), polycaprolactone (PLA) and polyglycolide (PGA)) [53]. Natural polymers derived from purification of ECM proteins or basement membrane extracts have similar characteristics to the tissue microenvironment, however disadvantages such as low mechanical properties and batch-to-batch variations reduce their consistency and reproducibility [22]. Synthetic materials can be produced with controlled properties but they have less biological properties than natural polymers and can degrade to form by-products that may alter the local microenvironment [54]. An approach that could overcome some of this issues would be to use a natural polymer that could offer control over mechanical and biochemical properties maintaining at the same time its natural biocompatibility.

Alginate's bio-inert property, for a long time, was perceived as a disadvantage, but truly it is an opportunity to incorporate highly specific and quantitative models for cell-ECM interactions. Alginate is a naturally occurring polysaccharide composed of (1,4)-linked β-D-mannuronic acid and its epimer α-D-guluronic acid, arranged in M-blocks, G-blocks and alternating MG-blocks (Figure 3). It is commercially available in various grades of molecular weight, composition, and distribution patterns depending on the extraction source [55]. Alginate can be found in the cell walls of brown algae, including *Macrocystis pyrifera, Laminarea hyperborean* and *Ascophyllum nodosum*. It is also an exopolysaccharide of bacteria including *Pseudomonas aeruginosa* and can be obtained by biosynthesis [56]. Nevertheless, current commercially available alginate comes strictly from algae sources. The extraction process is straightforward but multistage and requires

further purification steps to remove mitogens and cytotoxic impurities, obtaining in the end a water soluble alginate salt, usually sodium alginate which is the most investigated in the pharmaceutical and biomedical field [57].

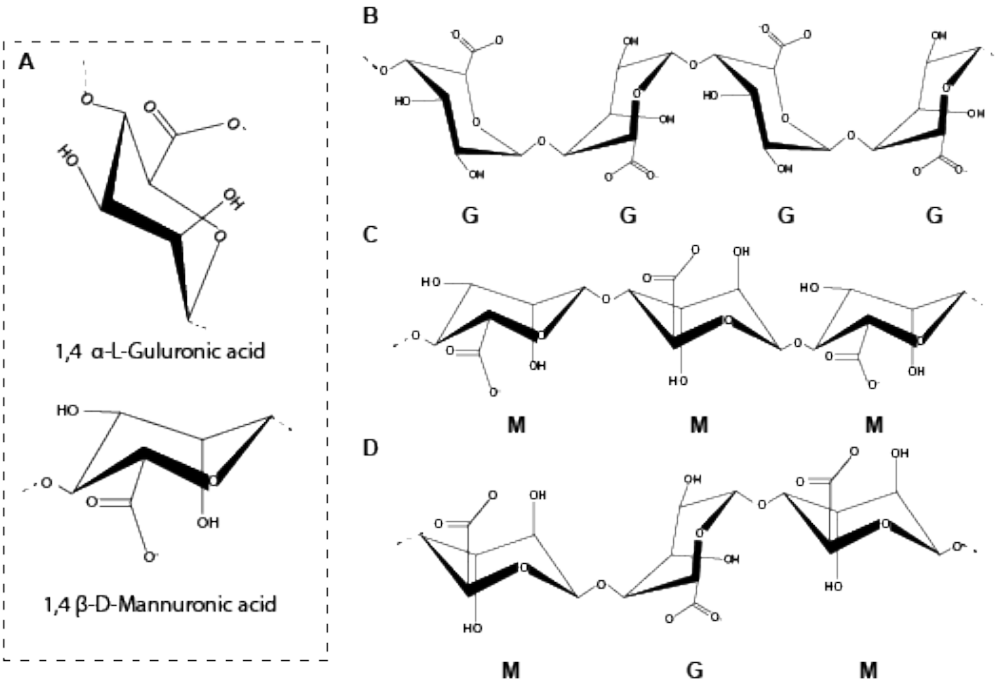


Figure 3 - Alginate structure and chain conformation - A. The two different monomers: (1,4)-linked β-D-mannuronic acid and (1,4-)α-D-guluronic acid ; Monomers arrangement in the alginate chain: B)G – blocks; C) M – blocks; D) MG – blocks, alternating M and G

Alginate can be cross-linked to form hydrogels under mild conditions. The most common way is the ionic cross-linking in the presence of divalent cations such as Ca^{2+}, Sr^{2+} and Ba^{2+}. Divalent ions bind to G-blocks from different polymer chains that allow a higher degree of coordination, forming a hydrogel through what is termed the “egg box” model of cross-linking. The rate of ionic gelation process can be controlled by mixing alginate solution with calcium carbonate ($CaCO_3$), which is insoluble in water at neutral pH. Then Glucono-δ-Lactone (GDL) is added to the mixture to lower the pH and trigger the release of Ca^{2+}. The release of Ca^{2+} initiates the gelation in a more gradual manner which results in more uniform gels with better mechanical properties [58].

The advantages of using alginate hydrogels for cell culture are their gelation at physiological conditions, gentle dissolution for cell retrieval, transparency for microscopic evaluation, gel pore network that allow nutrient and waste material diffusion and the non-animal origin. Furthermore, alginate can be easily modified via chemical and physical reactions to obtain derivatives with various structures, properties, functions and applications from drug delivery systems to *in vitro* 3D cell culture systems. Tuning properties such as biodegradability, mechanical strength, gelation properties and cell response can be achieved through

combination with other biomaterials, immobilization of different ligands and physical or chemical cross-linking [59].

Alginate derivatives containing peptides chemically introduced as side-chains have been mostly exploited to promote cell adhesion. The cell adhesion peptides can be introduced to the alginate backbone using carbodiimide chemistry to couple them via the carboxylic groups of the sugar residues. Peptides including the sequence arginine-glycine-aspartic acid (RGD) have been extensively used as model adhesion ligands, due to the wide-spread presence of integrin receptors for this ligand on various cell types [60]. A minimum concentration of RGD peptides in alginate gels is needed for the adhesion and growth of cells, this minimum is dependent of cell type [61]. Different peptides have also been investigated for alginate modification, including DGEA and YIGSR and found to improve the adhesion of various cells. Nevertheless, RGD is the most frequently used because it is soluble in aqueous media, easy to manufacture at a high purity in automated peptide synthesis and it is well characterized [62].

Cell-adhesive alginates alone or combined with other hydrogels have been widely used as cell culture substrates in 3D-culture, and as scaffolds in tissue engineering applications, such as tissue regeneration, cell differentiation, *in vitro* models and bioprinting . For example, human embryonic stem cells (hESC) and induced pluripotent stem cell (hiPSC) derived embryonic bodies have been encapsulated in RGD-alginate hydrogels (0.5% and 1%w/v) and hyaluronic acid (HA) hydrogels to generate retinal tissue [63]. They observed that the 0.5% w/v RGD-alginate matrix enhanced the generation of 3D derived retinal tissue and accelerated the maturation of the neural retina. On the other hand, HA hydrogels did not show any improvement when compared with embryonic bodies cultured in suspension without any hydrogel. By characterizing the hydrogels properties they conclude that the polymer concentration, cell-matrix binding motifs and, 3D surface morphology (pore wall smoothness and pore sizes) are key factors that affect cell differentiation. The polymer concentration will affect rheological properties and therefore vary the stiffness of the matrix that can be matched to the stiffness of natural tissue in this case the retina.

Another study used RGD-alginate to engineer a 3D *in vitro* model of gastric mucosa for stomach permeability studies [64]. To mimic the extracellular matrix and cellular compartment of the *lamina propria* they embedded normal stomach fibroblast in RGD-alginate hydrogel, on top of which they seeded a moderately differentiated adenocarcinoma stomach cell line (MKN74) to represent the gastric barrier. Culture of fibroblast in RGD-alginate, at an optimal cell density, showed increased cell proliferation, protein production and metabolic activity over time and after 7 days of culture fibroblasts were spread and had an elongated morphology. This demonstrated that the initial cell density and the nature of the artificial matrix are important for a successful model. Here they used a low polymer density (1% w/v) with calcium-mediated external crosslinking that generated a soft and highly permeable alginate hydrogel, although with some polymer concentration gradient due to the gelation mechanism.

Bidarra *et al.,* developed a 3D model based on RGD-alginate to study the interconversion between epithelial and mesenchymal states and its reverse [10]. They cultured EpH4 murine breast epithelial cell line within soft RGD alginate matrix. The hydrogel was described to have a relevant concentration of RGD peptide and resemble the biomechanical properties of natural breast tissue, namely an elastic modulus of approximately 200 Pa, thus supporting breast epithelial morphogenesis. Since the alginate matrix do not promote EMT by itself to study this event hydrogel cultures were treated for 7 days with TGF-β1, an EMT inducer. They were able to identify key-EMT phenotypic alterations such as loss of cell-cell contact (loss of functional E-cadherins) and expression of fibronectin and vimentin. When TGF-β1 was removed, they identified cells expressing both epithelial and mesenchymal markers. Their 3D model proved to be reliable to investigate the role of the microenvironment on cancer-related events such as EMT.

Certain cell processes are dependent of ECM degradation so it is of great interest to introduce this characteristic in alginate hydrogels. As it is well known alginate is not degradable by mammals as they lack the proper enzyme. However, this hydrogels are soft and due to the nature of the crosslinking mechanism they can slowly dissolve through exchange reactions of divalent cations with monovalent ions such as sodium present in the surrounding medium. Furthermore degradation can be manipulated by controlling the molecular weight and composition of polymers[65]. Another strategy is to incorporate alginates with different lengths of G-blocks which introduces mismatches between the crosslinking blocks[65]. Another chemical method to induce faster degradation of the alginate is partial oxidation with sodium periodate [66]. This reaction alters the conformation of the uronate residues to an open-chain adduct which makes it susceptible to hydrolysis. Degradation rate is dependent on the degree of oxidation, pH and temperature. Jia *et al.* used alginate with various degrees of oxidation as a bioink to print human adipose-derived stem cells (hADSCs) into lattice-structured, cell-laden hydrogels[67]. Moreover, they modified the oxidized alginate (OA) with RGD peptide. They observed that after printing OA can effectively promote cell proliferation and spreading when compared to the non-oxidized alginate bioink. Also, OA with different degrees of oxidation had distinct cell spreading which can be exploited to adapt the bioink to the desired tissue engineering application. In another example, oxidized alginate modified with RGD peptide is used to guide the assembly of outgrowth endothelial cells (OEC) and mesenchymal stem cells (MSC) into vascularized microtissues. During *in vitro* cultures OECs were capable of forming capillary-like networks and after transplantation of in mice the microgels not only preserved the capillary-like network but also lead to *de novo* formation of human vascular networks. This demonstrates the eclectic applications of alginate derivatives in tissue engineering with promising results [18].

Nonetheless, this degradation methods are based on the physicochemical properties of the alginate and depend on several other factors that are external to cells. They are mostly employed in tissue engineering for regenerative medicine to aid in the clearance of alginate from

human body. Introduction of protease sensitive peptides into the polymer is one way to give back the control over the ECM degradation to the cells. This way it would be expected that the degradation of the artificial ECM would match the growth and proliferation cycles of cells.

For example, Fonseca *et al.* developed a system for hMSC delivery based on MMP sensitive alginate hydrogel [68]. The approach was based on their previous work were they developed a double end grafted alginate with PVGLIG protease degradable peptide [69]. They compared cell behavior whithin PVGLIG-alginate and not modified alginate. They observed that PVGLIG-alginate promoted a higher outward cell migration *in vitro* and *in vivo.* These results show that the degradation of the hydrogel is cell mediated and can be tailored to the desired function or cellular need.

In another study a different approach was used to develop a cell-adhesive and cell-degradable alginate hydrogel, based on methacrylated alginate [70]. Firstly, the RGD peptide was grafted to the alginate by a Michael-type reaction between a thiol group and methacrylate. Secondly, the system was dually crosslinked via a MMP sensitive peptide flanked by two thiol groups by a Michael-addition reaction and the exposed to UV light to trigger radical polymerization of methacrylate and form the final hydrogel structure. They cultured an osteosarcoma cell line within this hydrogel and observed rapid cell proliferation and spreading when compared only to alginate without the MMP sensitive crosslinker. Furthermore, they investigated the use of this material in microfabrication techniques in particular photolithography to obtain micro patterned hydrogels.

5. Materials & Methods

5.1 RGD-Alginate synthesis

PRONOVA UP LVG (Batch: BP-0907-02), ultrapure low viscosity (≈199 mPa) sodium alginate with an approximate content of guluronic acid of 70% was modified with G_4RGDSP peptide using aqueous carbodiimide chemistry (Figure 4 – A). Briefly, 1-ethyl-(dimethylaminopropanyl)carbodiimide (EDC) is used to form amide linkages between amide containing molecules and the carboxylate moieties on the alginate polymer backbone. A co-reactant, N-hydroxy-sulfosuccinimide (sulfo-NHS), is used to stabilize the reactive EDC-intermediate and prevent the competing hydrolysis reaction. Alginate (1% w/v) was dissolved in MES buffer (0.1M MES, 0.3M NaCl, pH 6.5) and left with magnetic stirring overnight at RT. The reagents EDC and sulfo-NHS were added in a proportion of 2:1 per gram of Alginate respectively. Subsequently, G_4RGDSP dissolved in MES buffer and added in a proportion of 100mg per gram of alginate. The mixture was left to react for 20h (while stirring) and the reaction was quenched by adding 18mg of hydroxylamine per gram of Alginate. The dialysis was performed using dialysis tubing (MWCO 3500). First, the membranes were left to soak in ultra-pure (UP) water for 30 minutes to remove the azide, then the solution of Alginate was poured into the membranes and clamped. These were placed in 5L buckets and dialyzed in decreasing solutions of NaCl in deionized water for 3 days. After the dialysis the alginate was purified using activated charcoal that was removed by filtration. The alginate was freeze-dried and stored at -20ºC until use. The amount of grafted RGD was quantified using BCA Protein Assay (Thermo Scientific) detailed later on.

5.2 Maleimide-modified Alginate synthesis

Maleimide was introduced into the backbone of alginate by amidation of the carboxyl groups of alginate with the amine groups of 1-(2-Aminoethyl)maleimide, using the 4-(4,6-Dimethoxy-1,3,5-triazin-2-yl)-4-methylmorpholinium chloride, DMTMM (Mw: 276.72) as the coupling reagent (Figure 4 - B). Briefly, Alginate (1% w/v) was dissolved in UP water, then DMTMM was added to activate the polysaccharide carboxyl groups (e.g. 100% COOH activation: 1.34g of DMTMM/ 1g of alginate) and left to react for 30min. Then, maleimide was added according to Table 3 and the mixture was stirred at RT for 24h. The reaction products with different degrees of substitution were dialyzed against decreasing solutions of NaCl in UP water for 3 days. Finally, the samples were filtered and lyophilized to remove the water from M-Alginate and stored at -20ºC for further use. Maleimide coupling was assessed by ^{1}H-NMR. Spectra were acquired on a 400MHz Bruker spectrometer and analysed using the MestReNova software. NMR samples were prepared between 8 and 9 mg in 0.6 mL of D_2O and TSP (trimethylsilylpropanoic acid) at 0.05M was added as an internal standard.

Table 3 – Different extents of alginate modification with 1-(2-Aminoethyl)maleimide, theoretical drees of substituition (tDS) and the percentage of COOH activation and reagent used.

	mg of maleimide/ g of alginate	(tDS) (%)	COOH activation (%)	DMTMM:ALG molar ratio
AlgM4	84,8	9.5	100%	1:1
AlgM2	42,4	4.8	100%	1:1
AlgM1	21,2	2.4	100%, 50%, 25%	1:1; 1:2; 1:4
AlgM0.5	10,6	1.2	100%	1:1

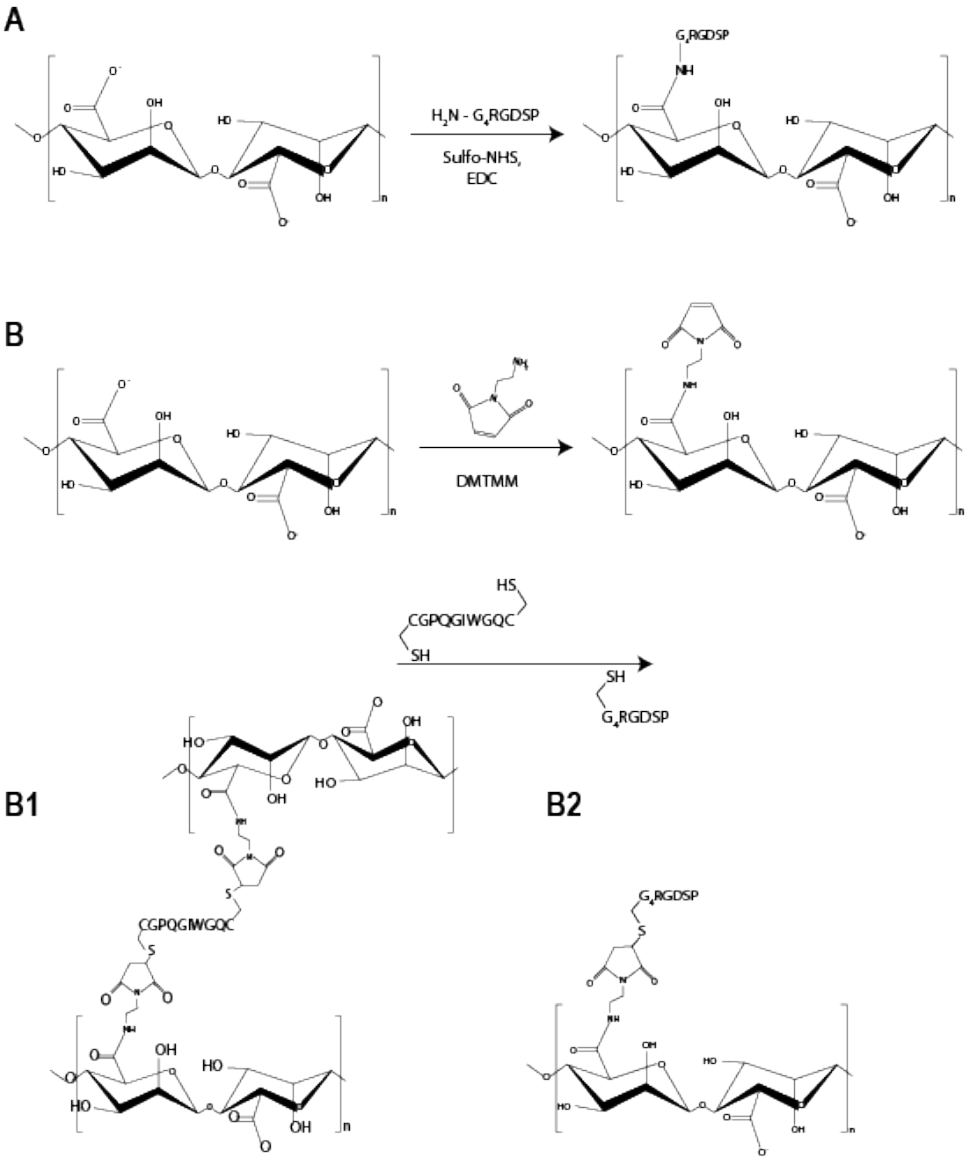


Figure 4- Scheme of Alginate Modification chemistries. A – RGD-Alginate synthesis by carbodiimide chemistry; B – Maleimide-Alginate synthesis using DMTMM as coupling reagent; B1 – Thiol-Michael Addition reaction of MMP sensitive peptide; B2 - RGD peptide coupling by thiol-Michael addition reaction.

5.3 Quantification of Coupling Efficiency

RGD-Alginate Coupling Efficiency by Carbodiimide Chemistry. The RGD bound to the alginate was determined using the Pierce BCA protein assay kit from Thermo-Scientific. Three different solutions were prepared: 2% (w/v) blank-alginate solution that is the alginate that went through all the steps of modification but without the addition of the RGD peptide; 1% (w/v) RGD-alginate solution; 2mg/mL RGD peptide solution. The peptide solution was mixed with the blank-alginate to obtain the pattern concentrations of peptide: 1, 0.5, 0.25, 0.13, 0.06, 0.03, 0.015 and 0 mg/mL. 20µL of each pattern solution and sample (RGD-alginate) were transferred to a 96 well plate and 200µL of BCA substrate was added to each well. The samples were incubated for 1h

at 37ºC protected from light. The absorbance was measured in a 96 well plate at λ=562nm in a micro plate reader. The peptide immobilized on alginate was calculated from the equation of the trend line fitted on the standard curve plotted from the pattern concentrations. The synthesis's yield was calculated by:

$$Yield\ (\%) = \left(\frac{[peptide] \times 100}{mg\ of\ peptide\ used} \right) per\ g\ of\ alginate \qquad \text{(Eq.1)}$$

RGD-Alginate Coupling Efficiency by Thiol-Michael Addition. This reaction occurs by adding a CG_4RGDSP peptide to the maleimide-alginate, where the thiol group of the cysteine can react with the double bound of the maleimide ring by Thiol-Michael Addition reaction (Figure 4 – B2). Alginate (1% w/v) was dissolved in Hank's Balanced Salt Solution (HBSS, pH≈7.4) and the RGD added directly to the alginate solution to a final concentration of 200 µM and left to react for 5 min. The solution was dialyzed to remove the peptide that was not successfully coupled to the alginate. After the dialysis the alginate was purified using activated charcoal that was removed by filtration. The alginate was freeze-dried and used in the quantification assay that was performed as described above. A blank alginate was also prepared.

5.4 Hydrogel Formation and Characterization

Two strategies were used to form bioresponsive alginate hydrogels.

In the first strategy a solution at 2% (w/v) of 1:1 RGD-alginate to maleimide-alginate was prepared in HBSS. The alginate was then sequentially crosslinked by the addition of MMP sensitive peptide, CGPQG↓IWGQC (0-600 µM, the arrow indicates the site of cleavage) (Figure 4– B1) and by the presence of divalent Ca^{2+} ions ($nCa^{2+}/nCOO^{-}$ = 0.288). The ions were released from $CaCO_3$ by acidification of the solution due to addition of Gluco-δ-lactone (GDL) ($nCaCO_3/nGDL$ = 0.125). Resulting in a dual crosslinking mechanism. The polymer concentration was reduced to 1.5% (w/v).

In the second strategy only a solution of Maleimide-Alginate was prepared (2% (w/v)). To allow cells to adhere to maleimide-modified alginate, the CG_4RGDSP peptide was grafted to alginate backbone by the thiol-Michael addition reaction (Figure 4 – B2) to a final concentration of 200µM, then the solution was crosslinked in the same way as described previously, reaching a final alginate concentration of 1% (w/v).

Rheological characterization. All analyses were performed using a Kinexus Pro rheometer (Malvern). The gelation kinetics with the MMP crosslinker was evaluated by the single frequency oscillation assay. Maleimide-alginate was dissolved in HBSS and immediately after adding the crosslinker the hydrogel precursor was placed between the rheometer plates at a final concentration of 1.5% (w/v) for strategy A and 1% (w/v) for strategy B. To evaluate the dual crosslinking effect hydrogels were prepared the same way as described above with addition of $CaCO_3$, peptide and GDL and immediately transferred to the plates of the rheometer. Also, the effect of cells in the geling process was assessed by transferring the hydrogel precursor solution

to a cell suspension of hMFs at a final cell density of 8×10^6 cells/mL. The parameters used for this assay were: frequency(Hz)=0.05; shear strain(%)=1; Gap(mm)=0.5; Temperature(°C)=37. The storage modulus (G') and the loss modulus (G'') were monitored.

To characterize the storage modulus (G') of cell-laden hydrogels, these were left to incubate for 24 h at 37 °C. After 24 h samples were incubated with medium containing HEPES (N-(2-Hydroxyethyl)piperazine-N'-(2-ethanesulfonic acid)) to buffer the media in air. All samples were assayed using a plate-and-plate geometry (4 mm diameter, sand blasted surfaces) and 4 mm cylinders were punched from the original hydrogels prior analysis in a humidified environment at physiological temperature (37°C). A frequency sweep ([0.01-1] Hz at 1% shear strain) was run on swollen samples with 20% of compression, the height of the hydrogels were determined using a digital caliper. The values of the G'(Pa) that are presented correspond to a frequency of 0.1 Hz which is within the linear viscoelastic regime based on previous work in the group.

Determination of free thiol group content. The crosslinking of the maleimide-alginate with the MMP sensitive peptide (CGPQG↓IWGQC) or from now onwards also referred to as GI-linker implies that the thiol terminal group of both ends has to react with the maleimide by the thiol-Michael addition reaction. To determine whether this double connection occurs, the content of free thiol groups was determined by Ellman's reagent reaction as described previously [71], with modifications. A phosphate buffer solution was prepared by dissolving 76.8 mM Na_2HPO_4 and 22.5 mM $NaH_2PO_4.H_2O$ in MilliQ water. Ellman's reagent (4mg) was dissolved in 1mL of phosphate buffer. Standards of MMP sensitive peptide were prepared (1mM; 0.75mM; 0.5mM; 0.25mM; 0.125mM; 0.065mM and 0mM) in phosphate buffer. Modified alginate was dissolved in HBSS to 1% w/v and crosslinked with variable degrees of peptide to maleimide ratios (Table 5) followed by crosslinking in the presence of divalent Ca^{2+} ions. Hydrogels were washed with HBSS for 30 min to remove excess of peptide. Then, to each 20 µL of standard and to the samples 4 µL of Ellman's reagent and 200 µL of phosphate buffer were added. Afterwards, samples were incubated for 1 h and 30 min (at RT) until the color of the solution matched the color of the hydrogels. Finally, 100 µL of standard and sample were transferred to a 96-well-plate and absorbance was measured at 412 nm (UltroSpec 100 Pro). The concentration of thiol groups were determined from the MMP sensitive peptide calibration curve.

5.5 3D cell culture within Bioresponsive Alginate

Primary human mammary fibroblast (hMF) and TNBC cell line MDA-MB-231 were embedded within bioresponsive alginate. hMF were cultured in DMEM (4.5 g/L D-Glucose, Gibco) supplemented with 10% fetal bovine serum (FBS, Biowest) and 1% of penicillin and streptomycin (PenStrep) in 5% CO_2 at 37 °C in tissue culture polystyrene flasks. MDA-MB-231 cells were maintained in DMEM (1 g/L D-Glucose, Gibco) supplemented with 10% FBS and 1% PenStrep in 5% CO_2 at 37 °C in tissue culture polystyrene flasks.

For the cell embedding within bioresponsive alginate hydrogels (Figure 5), first cells were trypsinized and centrifuged at 1100 rpm for 5 min. The cell pellet was ressuspended in HBSS and the gel precursor solution with different concentrations of GI-linker (R2; R1.5; R1 and R0) was added to the cell suspension to a final cell density of 8×10^6 cells/mL for hMF and 5×10^6 cells/mL

for MDA-MB-231. Then droplets of 20µL were placed between Teflon plates and the alginate left to polymerize for 10 min. at 37 °C. The hydrogels were transferred to 24-well plates with cell culture medium, the medium was changed after 30 min due to acidification by GDL. The cell-laden hydrogels were maintained in cell culture medium that was exchanged every 48h for a maximum of 14 days. For co-culture of MDA-MB-231 with hMF the bioresponsive alginate was used with a degree of GI-linker of R1, the cell density was of 5×10^6 cells/mL with equal parts of MDA-MB-231 and hMF. The co-culture was maintained in a mixture of 50% of high glucose DMEM and 50% of low glucose DMEM supplemented with 10% FBS and 1% Pen/Strep, from now on DMEM-50/50.

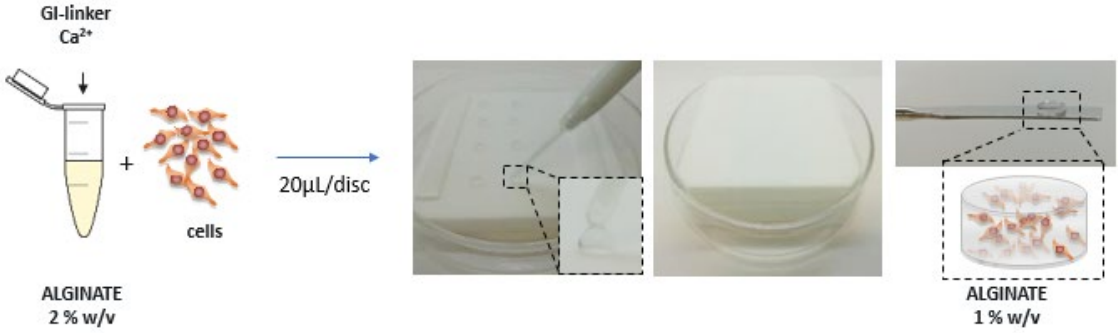


Figure 5 - Schematic representation of cell embedding within bioresponsive alginate hydrogel. Small drops of cell-laden alginate were applied on top of a Teflon plate between two spacers and then another Teflon plate was placed on top of those spacers. After gelation, 3D matrices were obtained.

Live/dead viability assay. hMF cultured in hydrogels from strategy A were washed with DMEM without phenol red and incubated with ethidium homodimer and calcein for 45 min. in 5% CO_2 at 37 °C. The ethidium homodimer stock solution (2mM in DMSO:ddH_20, 1:4) and the calcein stock solution (1mg/mL) were diluted in DMEM 1:400 and 1:500, respectively. Then 250 µL of each solution were added to the samples. After 45 min samples were washed and observed under a confocal laser scanning microscope (CLSM, Leica TCS-SP5 AOBS, Leica Microsystems).

Morphology analysis. The cell laden hydrogels were washed with HBSS to remove cell culture medium and fixed with 4% v/v paraformaldehyde in HBSS, then discs were washed to remove the remaining paraformaldehyde. The samples were incubated with a blocking buffer (1.5% w/v BSA in HBSS) for 1 h to minimize non-specific adsorption of the antibodies. Then, samples containing hMF were incubated overnight at 4 °C with fibronectin (1:200 in 1.5% BSA) and phalloidin 488 for F-actin staining (1:100, Flash Phalloidin Green 488). On the next day, samples were washed and incubated with the secondary antibody Alexa Fluor 594 goat anti-rabbit (1:1000, A11072) and DAPI for nuclei staining (1:500) for 1 h.

MDA-MB-231-laden hydrogels were permeabilized with 0.2% v/v Triton X-100 for 10 min, washed twice and then incubated with blocking buffer for 1h. Then, samples were incubated overnight at 4 °C with flash phalloidin 647 (1:100, Flash Phalloidin Red 647) and with primary antibody mouse anti-vimentin (1:50, Santa Cruz, SC-6260) for actin and vimentin staining

respectively. On the next day, samples were washed and incubated with secondary antibody Alexa Fluor 594 goat anti-mouse (1:1000) and DAPI for 1h at RT.

The samples were washed with HBSS and incubated with vectashield at 4°C until imaging. The samples were extensively rinsed and imaged on a CLSM.

MMP Production. To evaluate the influence of the MMP sensitive peptide in MMP production (MMP2 and MMP9) cell culture supernatants were analysed by gelatin-zymography. After 12 days of 3D culture in MMP sensitive hydrogel and a control without the GI-linker, discs were transferred to a new well and incubated with DMEM supplemented with 1% of FBS. After 48 h of culture the media were collected and loaded into gelatin-SDS polyacrylamide gels. The gel was run in 1× Tris-Glycine SDS running buffer at 80V (Mini Protean Tetra Cell system, BioRad). After electrophoresis, gels were washed twice and incubated with MMP substrate buffer for 16h at 37°C. Afterwards, gels were washed and stained with Coomassie Brilliant Blue R-250 (Sigma). MMPs proteolytic activity was evident by the presence of clear bands against a blue background of Coomassie Blue-stained gelatin substrate.

ECM Production by hMFs in co-culture. Samples were fixed with 4% v/v paraformaldehyde in HBSS at days 1, 3 and 7 of culture. First hydrogels were permeabilized with 0.2% v/v Triton X-100 for 10 min, washed twice and then incubated with blocking buffer for 1 h. Afterwards, samples were incubated overnight at 4 °C with flash phalloidin 647 (1:100, Flash Phalloidin Red 647), primary antibodies rabbit anti-collagen I (1:100, Rockland 600-401-103-0.1) and mouse anti-vimentin (1:50, Santa Cruz, SC-6260) for actin, collagen I and vimentin staining respectively. On the next day, samples were washed and incubated with secondary antibodies Alexa Fluor 594 goat anti-rabbit (1:1000, A11072) and Alexa Fluor 594 goat anti-mouse (1:1000, A11029) and DAPI for 1h at RT. Samples were washed with HBSS and storage in vectashield at 4°C until imaging. The samples were on a CLSM.

MDA-MB-231 Outgrowth Assay in Fibrin. After 7 days of culture cell laden hydrogels of MDA-MB-231, crosslinked with MMP sensitive peptide (R=0.1) were embedded between two layers of fibrin hydrogel in ibidi 4 well chamber slides. To from fibrin hydrogels two precursor solution A and B were prepared. Solution A was composed of fibrinogen, aprotinin and culture medium. Solution B contains thrombin diluted in PBS that triggers fibrinogen transformation into fibrin hydrogel. The solutions were mixed in a proportion of 5A:4B. A bottom layer was made by pipetting the mixture into a well that was left to polymerize for 25 min at 37 °C. The cell laden alginate hydrogel was transferred to the middle of the fibrin layer then gently another layer of fibrin was made by pipetting again the mixture of A and B on top of the structure and leaving it to polymerize. The final structure was maintained in cell culture medium and after 3 days of culture a live/dead assay was performed.

5.6 Treatment with anti-cancer drug Paclitaxel

2D cell culture. Mono-culture of MDA-MB-231 and co-culture of MDA-MB-231 and hMF were seeded at a cell density of 100 000 cells per well in a 24-well plate. Mono-culture was maintained in DMEM low glucose and co-culture in DMEM-50/50 for 24 h to allow cell attachment and afterwards incubated with Paclitaxel.

Spheroid formation. Spheroids were produced using commercially available MICROTISSUES® technology (size L, 9×9 array, fits 12 well-plate, (MicroTissue Inc.). Briefly, 12-series agarose micro-molds were prepared using 2% agarose in 0.9% of NaCl. To assure sterile conditions agarose was autoclaved prior dissolution and also filtered afterwards with 0.22 µm sterile filters. Micro-molds were placed in 12-well plates and equilibrated with DMEM and DEMEM-50/50, 24 h before cell seeding. MDA-MB-231 were resuspended in 200 µL of DMEM and seeded at a cell density of 3.24×10^5 cells/micro-mold, corresponding approximately to 4000 cells per spheroid. For co-cultures, hMF were mixed with MDA-MB-231 in 1:1 ratio, the cell mixture was seeded with a cell density of 3.24×10^5 cells/micro-mold. After 2 hours, to allow cell deposition into the micro-molds, additional medium was finally added to the wells. Mono-cultures were grown in DMEM and co-cultures in DMEM-50/50 for 3 days prior incubation with Paclitaxel. Images were acquired at day 0 and day 1 with an inverted light microscope.

3D cell culture within bioreponsive alginate. Cell-laden hydrogels were prepared as described above using a degree of crosslinker of R1. Both MDA-MB-231 monocultures and cocultures were immobilized with a cell density of 5×10^6 cells/mL, which corresponds approximately to 100 000 cells per hydrogel. Then, hydrogels were cultured for 24 h and 7 days prior incubation with paclitaxel to evaluate the effect of the drug on single cell and on spheroids formed within the 3D matrix.

Incubation with Paclitaxel. Paclitaxel ($C_{47}H_{51}NO_{14}$, Mw: 853.9) was dissolved in DMSO and diluted in cell culture media to following concentrations: 20, 2, 0.2 and 0.02 µM. The solutions were prepared in such way that the percentage of DMSO in cell culture media was of 0.01% v/v. As controls, cell culture media alone and cell culture media with 0.01% v/v of DMSO were used. Mono-cultures and co-cultures in 2D, spheroids and cell-laden hydrogels were incubated with Paclitaxel for 72 h and metabolic activity was measured by resazurin-based assay as previously described.

Metabolic Activity. The metabolic activity was measured by a resazurin-based assay. Briefly, the resazurin working solution at 20% v/v was added to each well and the samples were incubated at 37 °C for 2 h, protected from light. Then, the supernatant was transferred to a black 96 well plate and the resofurin fluorescence was read using a microplate spectrofluorometer (Synergy MX, Biotek), the samples were excited at 530nm and the emission was measured at 590nm.

5.7 RGD-Scaffold filling with bioresponsive alginate

RGD-Scaffold Preparation. A solution of RGD-alginate at 2.5% (w/v) was prepared, the alginate was left to dissolve overnight. NaCl was grained and particles between 150-250 µm were sieved. These NaCl particles were incorporated in the solution of alginate (3% and 6% per gram of alginate). A suspension of calcium carbonate ($CaCO_3$) in ultra-pure water at Ca^{2+} /COO^- molar ratio of 0.288 was added and the ionic crosslinking triggered by adding GDL solution at a $CaCO_3$/GDL ratio of 0.125. Next 250 µL of this solution was transferred to each well of a 96-well plate and left to form a gel for 45 minutes at RT. After the samples were frozen at -20ºC and freeze-dried at a pressure of 0,008 mbar and a temperature of -80ºC. The scaffolds were cut horizontally using a scalp, then the height was measured using a digital caliper. The structures were washed with ultra-pure water for 3 days, changing the water every 24h to allow the NaCl particles to leach out, giving rise to a high pores structure after freeze-dry.

Pre-staining with Cell-Tracker™ Green. MDA-MB-231 were pre-stained with Cell-Tracker™ Green CMFDA (5-chloromethylfluorescein diacetate, Mw: 464.9) with excitation at 492 nm and emission at 517 nm. The stock solution was prepared by dissolving the lyophilized product in DMSO to a concentration of 10 mM, then it was diluted in serum free medium to 15 µM and warmed to 37 °C. MDA-MB-231 cells were trypsinized and centrifuged to remove the cell culture medium. Afterwards, they were resuspended in pre-warmed Cell-Tracker working solution and incubated for 30 min in 5% CO_2 at 37 °C. Cells were again centrifuged to remove the staining solution, resuspended in fresh cell culture medium and incubated for 15 minutes. Finally, after removing the medium, cells were resuspended in HBSS to be further embedded in bioresponsive alginate (R1) at a cell density of 5×10^6 cells/mL.

Scaffold filling. To assure aseptic conditions prior culturing cells on the RGD-Scaffolds these were sterilized in 70% ethanol for 20 min. and washed several times with HBSS and cell culture medium. Meanwhile a cell laden hydrogel with pre-stained MDA-MB-231 was prepared (as described in section 5.5) and a 40 µL drop of the precursor solution was placed on top of the hydrated scaffold. The structures were centrifuged using a plate centrifuge at 1200 rpm for 2min and incubated at 37 °C for 20 min to allow polymerization of the filling alginate. The structures were maintained in culture with DMEM for 24 h and 7 days and then fixed with 4% v/v of PFA and stained with DAPI. Cell distribution throughout the scaffolds was assessed by CLSM.

5.8 Statistical Analysis

Statistical analysis was performed using GraphPad Prism 8.0 software version. One-way ANOVA test was used for the analysis of hydrogel stiffness and metabolic activity. A Kruskal-Wallis test was used for the analysis of spheroid size. Results for all analysis with ‘p’ value less than 0.05 were considered to indicate statistically significant difference.

6. Results and Discussion

During tumor progression from normal to neoplastic state eight hallmark capabilities are acquired by cancer cells, including: sustaining proliferative signaling, evading growth suppressors, resisting cell death, enabling replicative immortality, inducing angiogenesis, activating invasion and metastasis, reprogramming of energy metabolism and evading immune destruction [72]. To understand these mechanisms we can no longer limit our knowledge to cancer cell traits, instead we must also take into consideration the role of the TME in tumorigenesis. *In vitro* 3D models provide a platform that can be composed of cancer cells, stromal cells and ECM which allows to study cell-cell and cell-matrix interactions in a more specific and controlled manner. One of the major challenges when designing the TME is to recreate the extracellular matrix. Hydrogels are the material of choice to replicate the ECM due to their high water content and polymeric network structure that closely resembles the native ECM properties. Natural and synthetic hydrogels have been employed for this purpose though the control over biochemical and mechanical cues still remains a challenge [19].

6.1 Design Considerations

Alginate is a natural polymer capable of forming hydrogels under mild conditions. It is intrinsically bio-inert which is usually described as a disadvantage but we see it as an opportunity to explore the introduction of biochemical cues in a more controlled manner. The most common way to promote cell adhesion to alginate is to introduce cell binding peptides as side chains. Peptides including the sequence arginine-glycine-aspartic acid (RGD) have been extensively used as model adhesion ligands, due to the wide-spread presence of integrin receptors for this ligand on various cell types [62]. Furthermore, alginate is not degradable by mammalian cells because they lack the enzyme alginate lyase. One approach to make it cell degradable is by crosslinking alginate chains with MMP degradable peptides. MMPs functions are associated with enzymatic breakdown of ECM and basement membrane. In tumors, MMPs are implicated in 5 of the 8 hallmarks of cancer that are proliferation, evasion from apoptosis, angiogenesis, EMT and invasion [73]. The MMPs are produced by both cancer cells and cancer associated stromal cells, therefore the presence of a MMP sensitive crosslinker will allow cells to locally generate space within the hydrogel bulk. However, the cell mediated degradation of the hydrogel should not compromise its mechanical integrity in order to provide a stable support for cells over time. To have a better control over the mechanical properties a dual crosslinking mechanism is proposed: (1) alginate chains are crosslinked to a certain extent with MMP sensitive crosslinker, followed (2) by internal ionic crosslinking with Ca^{2+} ions. This kind of approach has already been explored by Fonseca and Bidarra in their work with double-end grafted alginate [69]. Their approach consisted on coupling both ends of a MMP sensitive peptide (PVGLIG) to low molecular weight alginate chains by carbodiimide chemistry. Obtaining at the end a soluble double-end grafted alginate polymer sensible to MMP proteolysis which they mixed with a RGD modified alginate and promoted ionic gelation *in situ*. Another work by Sun J *et al.* also exploited a dual crosslinking

mechanism by combining the crosslinking with a MMP sensitive peptide and UV mediated polymerization [70]. Their work is based on alginate functionalization with methacrylate. This group is available to participate in a Thiol-Michael addition reaction first with the thiol group of the cysteine present in the CRGD peptide and second with the thiols flanking the MMP sensitive crosslinker to obtain a protease degradable structure. Finally, the free-radical photopolymerization of methacrylates is triggered by exposure to UV light. The implementation of Michael-addition reaction in materials science has generated a great interest. This reaction has a highly modular "click" nature and is simple, robust and highly effective resulting in the formation C-C, C-N, C-O or C-S bonds under relatively facile reaction conditions. The Thiol-Michael addition reaction is the conjugate addition of thiols or thiolate anions to electron deficient C=C bonds. The typical Michael acceptors are electron-deficient -enes such as maleimides, vinyl sulfones, acrylates and methacrylates. Listed in order of C=C bond reactivity from highest to lowest [74].

Taking in scrutiny the previous work done with alginate our approach to develop a TME based on bioresponsive alginate hydrogels was designed in order to fulfil the following criterions:

1. The concentration of cell adhesion moieties should fall within the range of RGD densities found in commonly used biological matrices;
2. The hydrogel must be cell degraded by the action of cell-secreted MMPs in a controlled way;
3. The mechanical properties should match the natural properties of breast tissue and allow handling without compromising cell-cell and cell-matrix interactions;

To develop a biomaterial platform that addresses the mentioned design considerations, we selected alginate as the base polymer and a dual-crosslinking mechanism to allow the incorporation of thiolated-peptide sequences into the polymer backbone and provide precise control over the hydrogel mechanical properties. Maleimide-modified alginate was synthetized and explored to allow the formation of a lightly crosslinked and MMP-degradable hydrogel via thiol-Michael addition reaction between maleimides and cysteine residues in the peptide sequence. The protease sensitive sequence CGPQG↓IWGQC used or GI-linker is derived from the sequence GPQG↓IAGQ found in type I collagen and was chosen due to its susceptibility to cleavage by a wide range of MMPs (e.g 1,2,3 and 9) [75] secreted by several types of cells including hMF and MDA-MB-231 [76][77]. In previous work by Pereira RF *et al.* they demonstrated that this sequence was sensitive to collagenase II and the extent of degradation was dependent on the crosslinking density [78]. For the incorporation of cell adhesive peptides (RGD) we explored two different strategies:

- Strategy A, involved the combination of equal parts of RDG-modified alginate through carbodiimide chemistry with maleimide-alginate as illustrated in Figure 6 – a) and c). .

- Strategy B, only used maleimide modified alginate, mono-cysteine peptide CG_4RGDSP was incorporated via thiol "click" reaction during gel formation as depicted in Figure 6 - d).

In both cases MMP sensitive peptide (CGPQG↓IWGQC) and ionic crosslinking are sequentially performed resulting in final hydrogel at 1% w/v.

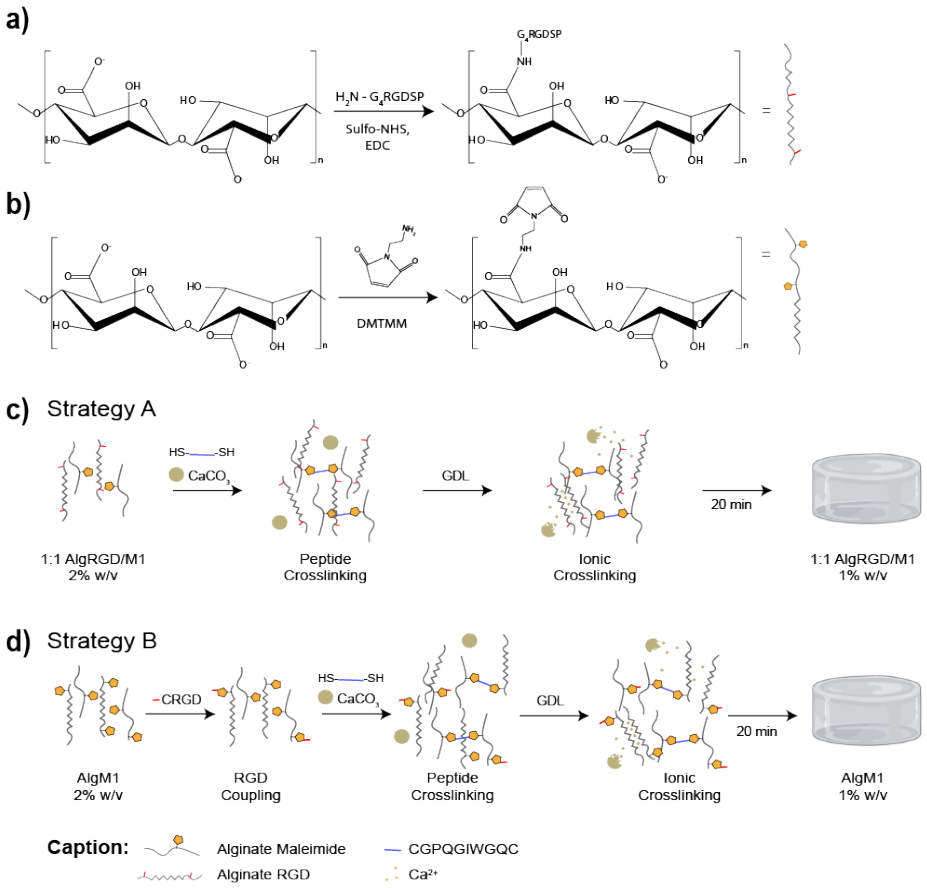


Figure 6 - Schematic representation of bioresponsive alginate hydrogels design. a) AlgRGD synthesis by aqueous carbodiimide chemistry; b) AlgM synthesis using DMTMM as coupling reagent; c) and d) represents two different strategies adopted for RGD introduction in final hydrogel composition.

6.2 Alginate Modification and characterization

Alginate-Maleimide. Alginate was functionalized with different amounts of 1-(2-Aminoethyl)maleimide (AlgM4, AlgM2, AlgM1 and AlgM0.5) using DMTMM as a coupling agent. DMTMM is an alternative activation agent of carboxylic groups. The main advantages over EDC/NHS chemistry are the stability in water solutions and the effective results in absence of pH control [79]. Also it has been described to held high yields of polymer amidation [80][81]. We observed that high degrees of maleimide lead to poor solubility of alginate derivatives, rendering the sample AlgM4 insoluble in water. In addition, it was also observed that the degree of maleimide substitution plays a major role on the ionic crosslinking ability of alginate by

determining the percentage of available (unmodified) carboxylic groups. In this regard, loss of ionic crosslinking ability under the tested conditions was observed for the sample AlgM2, despite its improved solubility. Therefore, AlgM1 and AlgM0.5 were used for further analysis.

Since we are working with low theoretical degree of substitution (Table 3) we proceed to study the effect of the amount of carboxylic group activation. The functionalization of alginate with maleimide was qualitatively confirmed in AlgM1 and AlgM0.5 samples by ^{1}H-NMR (Figure 7). The presence of maleimide was identified by the appearance of a new peak ~6.9 ppm corresponding to the protons in the double bond of the maleimide group. We can see that the intensity of the peak varies with the amount of maleimide added (Figure 7– A and D). Furthermore, when we added the same amount of maleimide but lowered the percentage of activeted carboxylic groups to 25%, it was possible to verify slight decrease in peak intensity as illustrated in Figure 7-C. . The calculation of the efficiency of the reaction is based on a quantitative NMR approach previously described [82] and the theoretical values in Table 3 (Supplementary Table 1). We found the efficiency of the reaction to be approximately 10% for sample AlgM1 which means that 1 g of alginate is likely to contain 1.2×10^{-5} mol of maleimide.

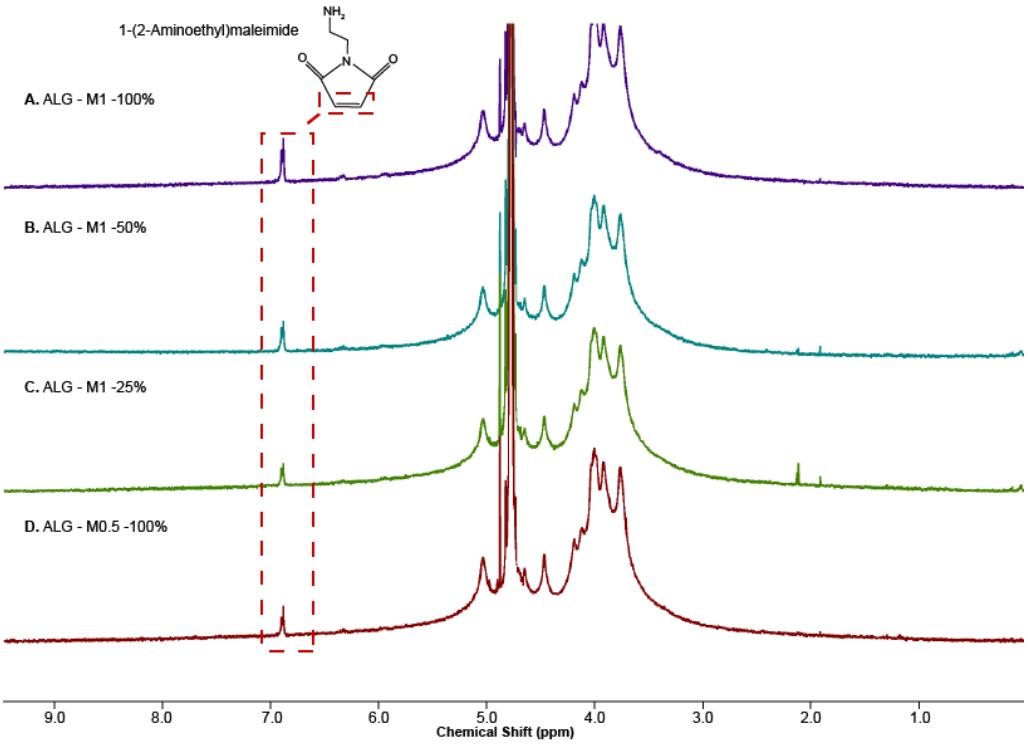


Figure 7 - H-NMR spectra of alginate modified with maleimide with different degree of carboxylic group activation and varying amount of substituent added.

AlgM0.5 was not considered for subsequent studies because it had less amount of maleimides available per gram of alginate. In strategy A, only a small amount of peptide crosslinking would be possible because the maleimides are halved due to the hydrogel formulation. The substrate for cell degradation could not be enough for a relevant biologic response. In strategy B, the

maleimides are needed in two reaction, RGD coupling and peptide crosslinking so we opted for an alginate with higher maleimide substitution (AlgM1).

Alginate-RGD. The activation of carboxyl groups with EDC/NHS chemistry to covalently bind peptides is the standard method for alginate functionalization and has been optimized to bind cell adhesive peptide containing the RGD sequence [60][69]. It is known that the concentration of RGD peptide is a factor that influences cell behavior and there is a minimum concentration to promote cell adhesion which is likely cell specific [83]. Two different chemistries were considered for the RGD coupling: a) carbodiimide chemistry and b) Thiol-Michael addition (Table 4).

Table 4 - Coupling efficiencies of different chemistries for RGD grafting onto alginate backbone and final concentrations in 1% w/v hydrogels of each strategy.

	Efficiency (%)	Concentration (↗M)
Carbodiimide (Strategy A)	27	177
Thiol-Michael Addition (Strategy B)	78	156

The coupling efficiency in both cases was calculated by the BCA Protein Assay. The coupling efficiency of carbodiimide chemistry was of 27% which is equivalent to 7 mM of RGD per mol of alginate. In a hydrogel at 1% w/v composed of 50% of alginate modified with RGD, as in strategy A, the concentration of this peptide is approximately 177 µM. On the other hand, the efficiency of RGD coupling by Thiol-Michael addition was higher - 78%. This efficiency represents a final RGD concentration of approximately 156 µM. Although further studies to optimize this coupling should be done, with this last strategy the amount of cell adhesion points is not limit to the amount of polymer pre-modified used. Moreover, the percentage of maleimides occupied with CG_4RGDSP peptide was only 7%, which did not compromise the crosslinking of GI-linker. Noteworthy, in both strategies the RGD concentration was within the range of RGD densities found in commonly used biological matrices, such as tumor-derived ECM [84]. It is important to mention that in strategy A to change the concentration of RGD we would need to alter either the final polymer concentration or the proportion of RGD modified alginate to a non-modified alginate. With this approach the optimization of RGD coupling to a specific final concentration is much harder. On the other hand, the strategy B affords a facile control over the final peptide concentration tethered to the polymer backbone by simply changing the initial amount of peptide added to reaction. Moreover, by sequentially adding desired amounts of different thiolated peptides, it would be possible to obtain a multi-peptide functionalized gel network via a straightforward functionalization strategy that avoids time consuming reaction and purification steps.

Alginate-GI linker. It is expected that the addition of GI-linker will increase the hydrogel viscosity due to the formation of a chemically crosslinked gel network. Since this alginate will be further used for 3D cell encapsulation, it is necessary to ensure that it viscosity does not preclude the

mixing with the cell suspension nor cause damage to the cell membrane during pipetting. Therefore, as proof of concept, we tested both strategies (A and B) with several GI-linker concentrations (R7, R5, R4, R3, R2, R1 and control R0 –Table 5) and evaluated their consistency and pipetting ability. The first readout was the qualitative measure of crosslinking that was perceived through an increase of solution viscosity (Figure 8).

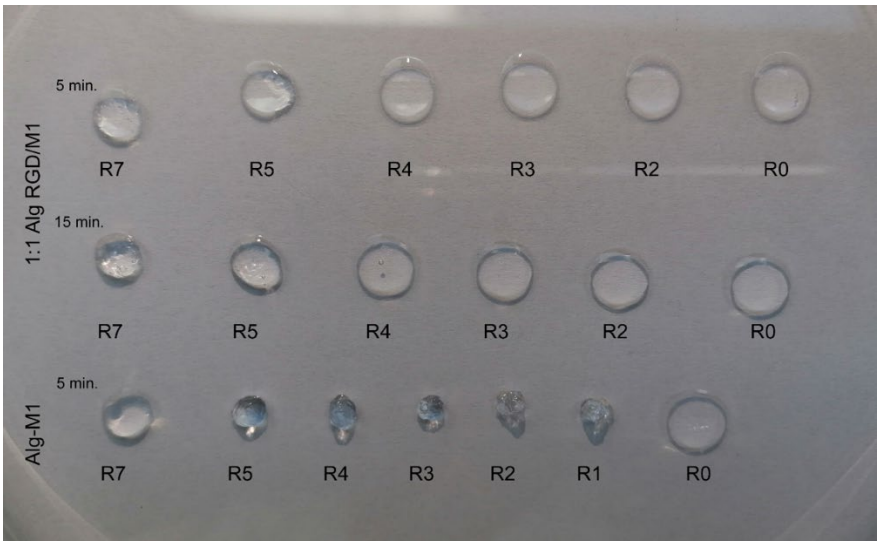
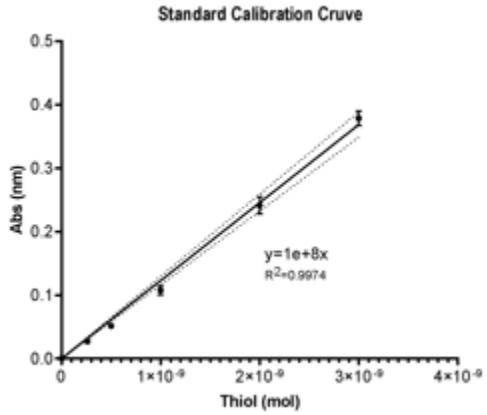


Figure 8 - Visual representation of viscosity increase after MMP sensitive peptide crosslinking at different ratios. Strategy A (1:1 AlgRGD/M1) after 5 and 15 min and Strategy B (AlgM1) after 5 min.

The extent of effective crosslinking was indirectly estimated by quantifying the amount of free thiols in dually crosslinked hydrogels by Ellman's test. The values established to test with the Ellman's reagent were based on the efficiency of maleimide modification and the principle that in order to occupy all the maleimides a proportion of thiol groups of 1:1 is needed (Supplementary Information table 2). The ratio R7 corresponds to the hydrogel containing an excessive amount of GI-linker that was calculated to be 40% of free thiol groups, while R5 is the ideal scenario of 1:1 (maleimide to thiol). The ratio R0 corresponds to the control hydrogel crosslinked only by Ca^{2+} (without GI-linker). We observed that in the R7 the amount of free thiol groups was of 23%. This can be explained by the fact that an excessive amount of GI-linker will preferentially connect by one end occupying the maleimides but not crosslinking two alginate chains. In the ideal amount of GI-linker (R5) were there exists a proportion of 1:1 thiol per maleimide we detected an amount of free thiol groups of 13%. One possible explanation could be related to the maleimides distribution within the polymer chains and the fact that the crosslinking will reduce the mobility of the chains decreasing the chances of the second thiol in the GI-linker to find its partner chain. Furthermore, with an increase of GI-linker concentration above the ideal scenario (R5) we observed a decrease in hydrogel viscosity. On the other hand, with lower GI-linker concentration (R4, R3) a higher viscosity was noticed. These alteration in viscosity were also observed by the rheological measurements (Figure 10). Overall, the effective crosslinking degree depends on the GI-linker concentration and is considered to be 100% effective bellow R5 concentration (~600µM) (Figure 9).

Table 5 - Table of ratios of peptide crosslinker to maleimide, final peptide concentration in 1% hydrogels composed of 100% of AlgM1 and the corresponding amount of thiol groups. This values are adjusted with the hydrogel polymer concentration and the amount of maleimide-alginate used

Strategy A		
Ratio GI/MAL	**GI-Linker (μM)**	**Thiol Groups (mol)**
R7	420	8.4×10^{-6}
R5	300	6.0×10^{-6}
R4	240	4.8×10^{-6}
R3	180	3.6×10^{-6}
R2	120	2.4×10^{-6}
R1	60	1.2×10^{-6}
Strategy B		
Ratio GI/MAL	**GI-linker (μM)**	**Thiol Groups (mol)**
R7	840	1.68×10^{-5}
R6	720	1.44×10^{-5}
R5	600	1.2×10^{-5}
R4	480	9.6×10^{-6}
R3	360	7.2×10^{-6}
R2	240	4.8×10^{-6}
R1	120	2.4×10^{-6}



Sample		Free Thiol	
	Abs(nm)	**mol**	**%**
R7	0.077	7.7E-10	23
R5	0.031	3.1E-10	13
R4	0.010	1.0E-10	5
R3	0	0	0
R2	0	0	0
R1	0	0	0
R0	0	0	0

Figure 9 - Calibration curve plotted from absorbance values of GI-linker and table of absorbance values of the samples tested and percentage of free thiol.

Gelation kinetics. In order to evaluate our third design consideration we had to characterize hydrogel mechanical properties. Rheology is the most common method for this purpose since it is quick, sensitive, requires small samples sizes and can reveal the differences in degree of crosslinking. The evaluation of the elastic (G') and viscous (G'') moduli can be done over time with constant frequency and strain which is used to evaluate the gelation of hydrogels since an increase in G' reveals a behavior toward a solid-like material [85].

Therefore, we selected a set of GI-linker concentrations to perform gelation studies, based on the results from the test depicted in Figure 8. We monitored the evolution of the elastic modulus (G') over time in Strategies A (R4, R3, R2) and B (R6, R3, R1) (Figure 10) using a rheometer. First we evaluated the gelation kinetics of the GI-crosslinking (MMP sensitive peptide crosslinking) as

shown in Figure 10 - a) and c). Since the Thiol-Michael addition reaction is very fast it was not possible to observe the exact crosslinking point. Figure 10 – a) shows the gelation kinetics of strategy A, where we could observe an increase in G' using higher concentration of GI-linker (R4). As expected from previous results, the lowest concentrations (R2) no longer exhibit an evident effect of the crosslinking. Interestingly, in strategy B we observed a slight increase in G' over time, but not a clear difference between GI-linker concentrations bellow the ideal scenario as the values of G' for R3 and R1 almost overlap. Also, as expected an excess of GI-linker (R6) resulted in a lower viscosity from onset and no evolution was observed over time (Figure 10 – c).

Secondly we evaluated the mutual effect of GI-crosslinking and ionic crosslinking on each other (Figure 10 – b) and d)). In Figure 10 – b), strategy A, there was a clear effect on the GI-crosslinking when combined with ionic gelation. This effect could be a delay or even an impairment on this mechanism. On the other hand, the evolution of G' over time shows no relevant difference when compared to ionically crosslinked alginate with no modifications (AlgBLK). This suggests that the hydrogel formation could be mostly due to the ionic crosslinking effect. On the contrary in Figure 10 - d), strategy B, the evolution profile of G' lies between the profile of GI-crosslinking and the ionic crosslinking of AlgBLK which suggests that both of the mechanism are contributing for the gelation process. Furthermore, we saw a stabilization of the hydrogel slightly sooner indicating a decrease in gelation time which allows hydrogel handling without breaking after 10 min of polymerization.

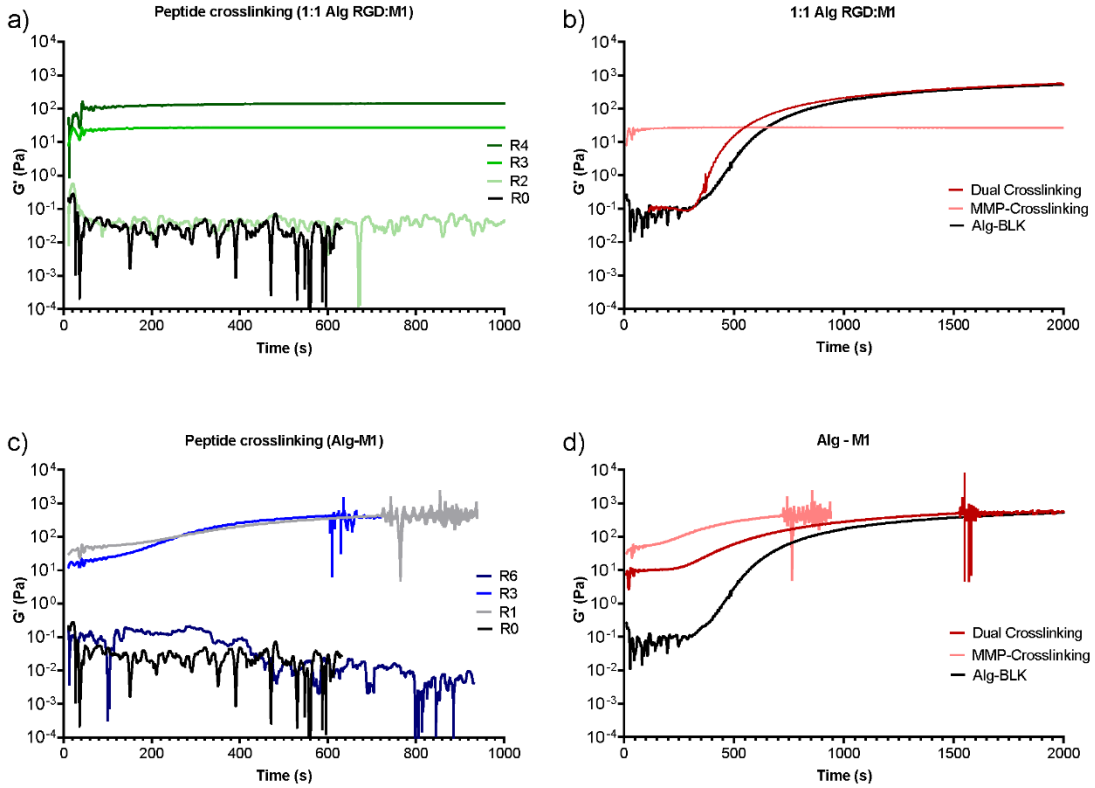


Figure 10 - Gelation kinetics. a) MMP crosslinking of Strategy A; b) Dual crosslinking of Strategy A; c) MMP crosslinking of Strategy B; d) Dual crosslinking of Strategy B

6.3 3D Cell Culture

Mechanical Characterization. The mechanical properties of a specific tissue depend on its function and are linked to its pathophysiological state. The breast is a soft tissue that undergoes several changes during a women life time. An important property of soft tissues is their elasticity which is altered in pathophysiological processes such as tumor development [86]. The breast tumor tissue is much stiffer (elastic modulus of 1000-4000 Pa) than the normal mammary gland (elastic modulus of ~200 Pa) [87][88]. To recreate an environment in which the tumor progression occurs the objective is to have an initial matrix stiffness closer to the normal mammary gland.

In order to obtain the cell laden hydrogels we had to study the gelation kinetics of the dual crosslinked hydrogels in the presence of cells (hMF) (Figure 11– a) and b)). Cells can constitute a physical impairment for the gelation process so it would be expected a slight delay in gelation time. When we analyze the profile of G' in Figure 11– a), strategy A, one can see that there is a difference between hydrogels with and without cells. Usually 20 min of polymerization are enough to allow handling of alginate hydrogels [10] but in the presence of cells we needed 30 min of polymerization to enable handling of the hydrogel. In strategy B, Figure 11 - b), there was no significant difference in the gelation kinetics, so the polymerization period in this strategy is shorter, around 10-15 min depending on the initial GI-linker concentration. Higher

concentrations of GI-linker allow higher degrees of crosslinking and since this reaction is so fast it the hydrogel stabilization happens sooner in time when compared to lower concentrations or no GI-linker.

To evaluate the stiffness of cell laden hydrogels with two concentrations of GI-linker we maintained them in culture for 24h to allow swelling stabilization and subsequently performed an oscillatory frequency sweep test using a shear strain of 1% (Figure 11 – c) and d)). In strategy A (Figure 10 – c)), hMFs are embedded in hydrogels with two different GI-linker concentrations (R4 = 240 µM; R2 = 120 µM) and compared to a hydrogel with no GI-linker (R0). As expected, higher concentration of GI-linker resulted in stiffer hydrogel but when we compared the stiffness of this hydrogels to R0 we see that the stiffness is nearly the double and higher than the native breast tissue. However, we cannot assign this increase in stiffness solely to the presence of the GI-linker but we also must consider that the polymerization time of these hydrogels is longer than the hydrogels with no GI-linker.

In strategy B (Figure 11 – d)), MDA-MB-231 cells are embedded in cell adhesive AlgM1 hydrogels using the same GI-linker concentrations that in this case correspond to R2 and R1. As expected the amount of GI-linker added is directly proportional to hydrogel stiffness, higher GI-linker concentration render higher hydrogel stiffness. We can see that although we have a dual crosslinking mechanism the hydrogel stiffness does not differ much from the R0. This can be also explained by the polymerization time of the hydrogels, R2 and R1 were left to polymerize for 10 min while the R0 needed 20 min to polymerize. With these results we can conclude that strategy B offers a greater control over the hydrogel stiffness that can be manipulated by the addition of different concentrations of GI-linker, polymerization time and changes in $nCa^{2+}/nCOO^{-}$ ratio.

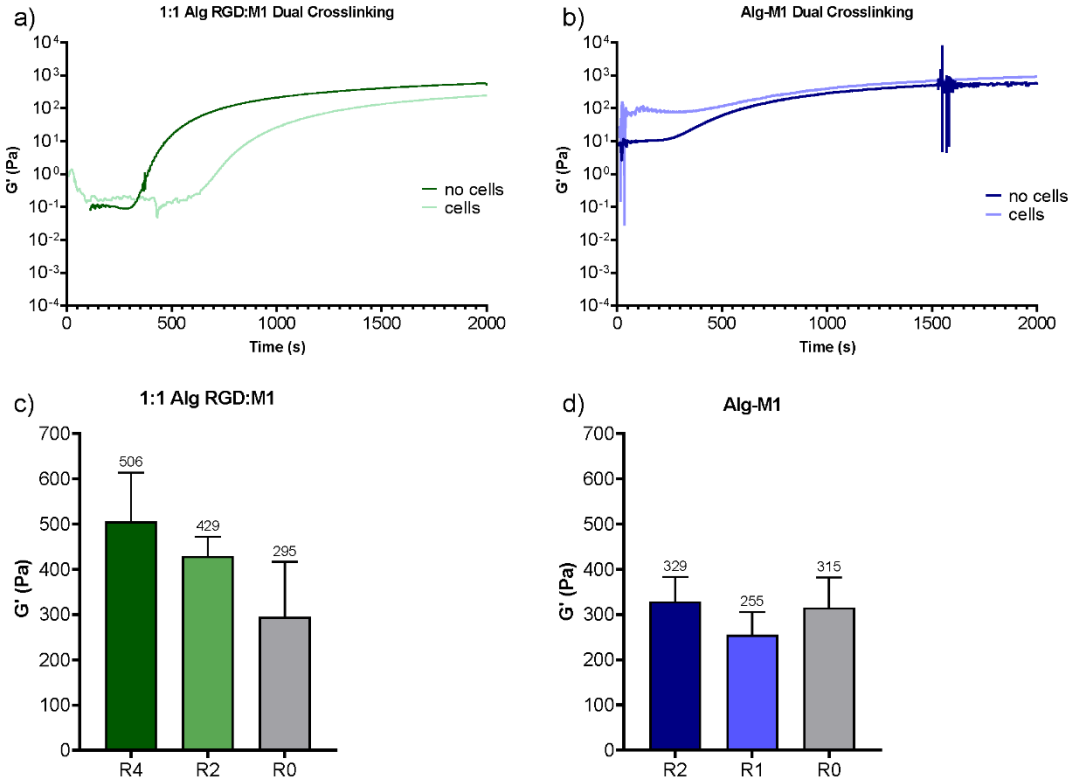


Figure 11 - Rheological characterization of cell laden hydrogels. a) Strategy A – gelation kinetics (R3); b) Strategy B – gelation kinetics (R1); c) Strategy A – stiffness of cell laden hydrogels with hMF with R4 (240 µM) and R2 (120 µM; d) Strategy B – stiffness of cell laden hydrogels with hMF with R2 (240 µM) and R1 (120 µM). Results are presented as mean ± standard deviation. p>0.05

Biological response. As the main aim of this study was to develop a cell-degradable alginate matrix, hMF were selected to evaluate cell spreading within the dual crosslinked hydrogels due to their characteristic spindle-shape morphology and MMP production for ECM remodeling [76].

To assess cell viability using the strategy A and evaluate the influence of GI-linker in cell morphology, hMFs were embedded within hydrogels 1:1 AlgRGD/M1 with and without GI-linker and AlgRGD (control). Cell-laden hydrogels were maintained in culture for two weeks and monitored with inverted light microscope for morphological changes. During the cell culture period cells maintained their round shape. After 14 days of culture live/dead staining was performed, revealing that the majority of cells were viable in all conditions (Figure 12). In fact, there was no difference in cell morphology in the presence of GI-linker. Most important, the presence of maleimides did not affect cell viability.

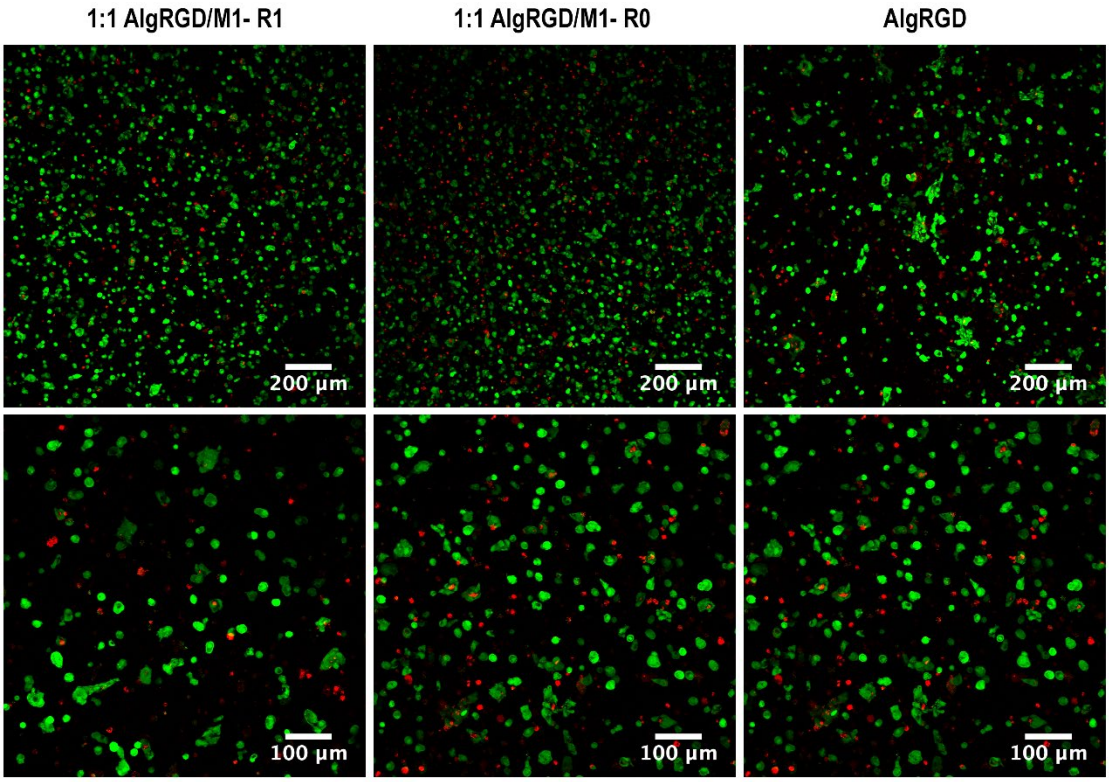


Figure 12 - Cell viability and morphology accessed by Live/Dead assay. From left to right: representative CLSM images of hMF cultures after 14 days of culture within 1:1 AlgRGD/M1 hydrogels with GI-linker (R1 = 60µM), (1:1 AlgRGD/M1-R1), control without GI-linker (1:1 AlgRGD/M1-R0) and control without AlgM1 (AlgRGD). Live cells are stained by calcein AM (green) and dead cells by ethidium homodimer-1 (red). Top images, scale bar = 200 µm; bottom images, scale bar = 100 µm).

In strategy A we are mixing the same polymer with different modifications meaning that half of the hydrogel will be crosslinked by GI-linker and the other half will present the cell-adhesion moieties. Both derivatives allow alginate to crosslink ionically therefore it will hold the structure together but at the same time compartmentalize cell-interactions with the polymer. In the chains where MMP-cleavable peptide is bound, there is no cell adhesion points. The distribution of cell-adhesion ligands affects specific cells behavior such as cell morphology and motility. Integrin mediated cell adhesion is important to create the traction force necessary for cell motility because of the crosstalk between the extracellular ligands and the cellular cytoskeleton [89]. At the interface between AlgRGD and AlgM1 cells could extend their protrusions to reach cell adhesive ligands, but if his not happen, cell will not able be able to attach to the matrix towards generating the necessary puling force for cell migration. This could be one of the reasons why cells remain round during the culture period together with increased stiffness of these hydrogels.

In order to achieve a more homogeneous distribution of cell interactive molecules we developed and optimized the strategy B, where both cell-adhesion ligands and MMP-degradable sites are expected to be uniformly distributed throughout the hydrogel network. To evaluate the

influence of GI-linker in cell morphology, hMFs were embedded in dual crosslinked AlgM1 hydrogels with varying concentrations of GI-linker (R2, R1.5, R1) and without GI-linker as control (R0). Cells were maintained in culture for 14 days and CLSM images were acquired at different time point. To evaluate cell spreading, cells were stained for F-actin, which is a marker of stress fibers necessary to generate contractile forces for cell migration, and fibronectin a ECM protein secreted by fibroblasts. First of all as depicted in Figure 13 we can see that hMF within GI/RGD alginate matrix are capable of spreading and establish several cell-cell contact and deposit fibronectin network. On the other hand, hMF within alginate without GI-linker remained mostly round and fibronectin is limited to cells vicinity. Second the cell spreading and distribution within the matrix over time is dependent on the GI-linker concentration (Figure 14). At day 1, R1 and R1.5 were very similar between them with a lot of spread cells and cell-cell contact. In R2 condition we observed both spread and round cells. Cells within R0 alginate presented a round morphology with only short cytoplasmic extensions around the cell. A closer look showed that in the three conditions with GI-linker cells displayed protrusions characteristic of cell spreading and similar patterns of fibronectin deposition. At day 14 we can see differences related to cell density within the different matrices (Figure 15). In condition R2, cells remained within the matrix at a considerable cell density, whereas conditions R1 and R1.5 presented fewer cells, suggesting higher cell escape ability. In fact, we were able to observe a dense cell network on the periphery of the alginate matrices. A top view at day 7 and day 14 of R1 and R1.5 conditions showed a large amount of spread cells and a dense fibronectin network (Supplementary Figure 3). From rheological characterization studies we know that lower concentrations of GI-linker lead to softer hydrogels. Although R1 and R1.5 have less MMP cleavable sites, their mechanical properties may allow a higher degree of cell mobility that leads to high cell escape. R2 provides a slightly stiffer matrix that is able to entrap cells for longer periods therefore at day 14 we see more cells within this matrix.

Here we demonstrated that cell spreading and proliferation within the dually crosslinked alginate is not only possible but also depends also on GI-linker concentrations which likely needs to be adjusted to different cell types.

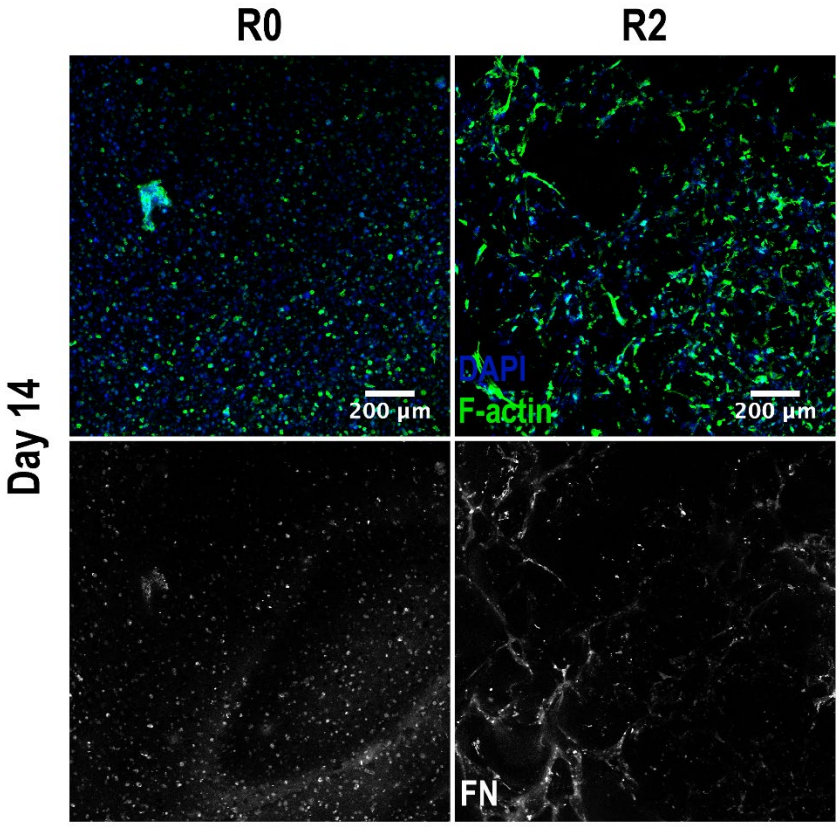


Figure 13 - Overview of hMF culture during 14 days within bioresponsive alginate hydrogels without (R0) and with GI-linker (R2). After 14 days of culture within a dually crosslinked hydrogel cells were able to adhere and spread, showing clear protrusions through F-actin staining (green). Cells were stained for F-actin (green), *fibronectin (grey) and DAPI (nuclei, blue).* Scale bar = 200 µm.

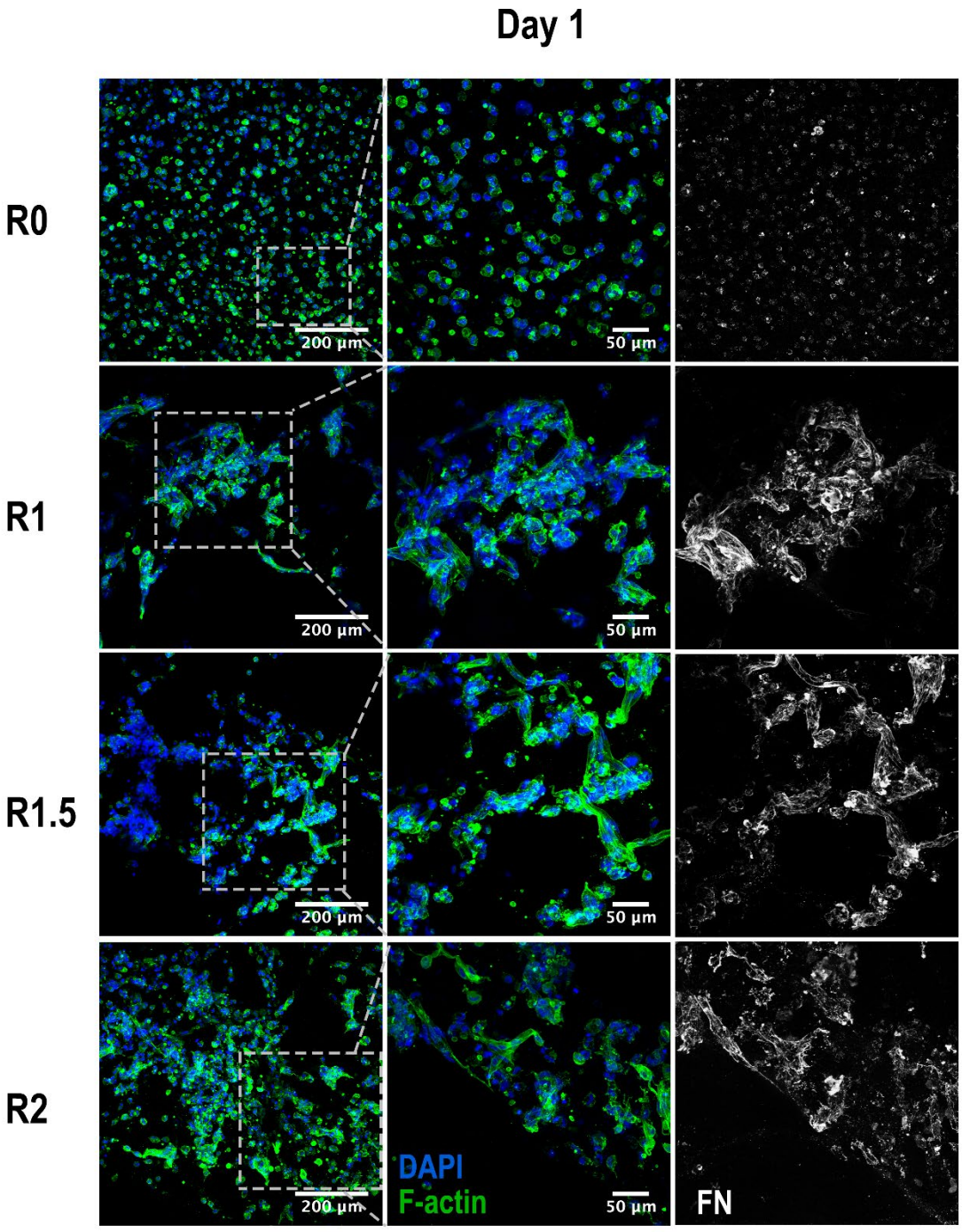


Figure 14 - Representative CLSM images of hMF morphology after 1 day of different alginate formulation: R0 (no GI-linker, control); R1, R1.5 and R2. . From left to right we have a closer look over the cell morphology. Black and with images represent fibronectin deposition. Cells were stained for F-actin (green), fibronectin (grey) and DAPI (nuclei, blue). Left column, scale bar = 200 µm; middle and right column, scale bar = 50 µm.

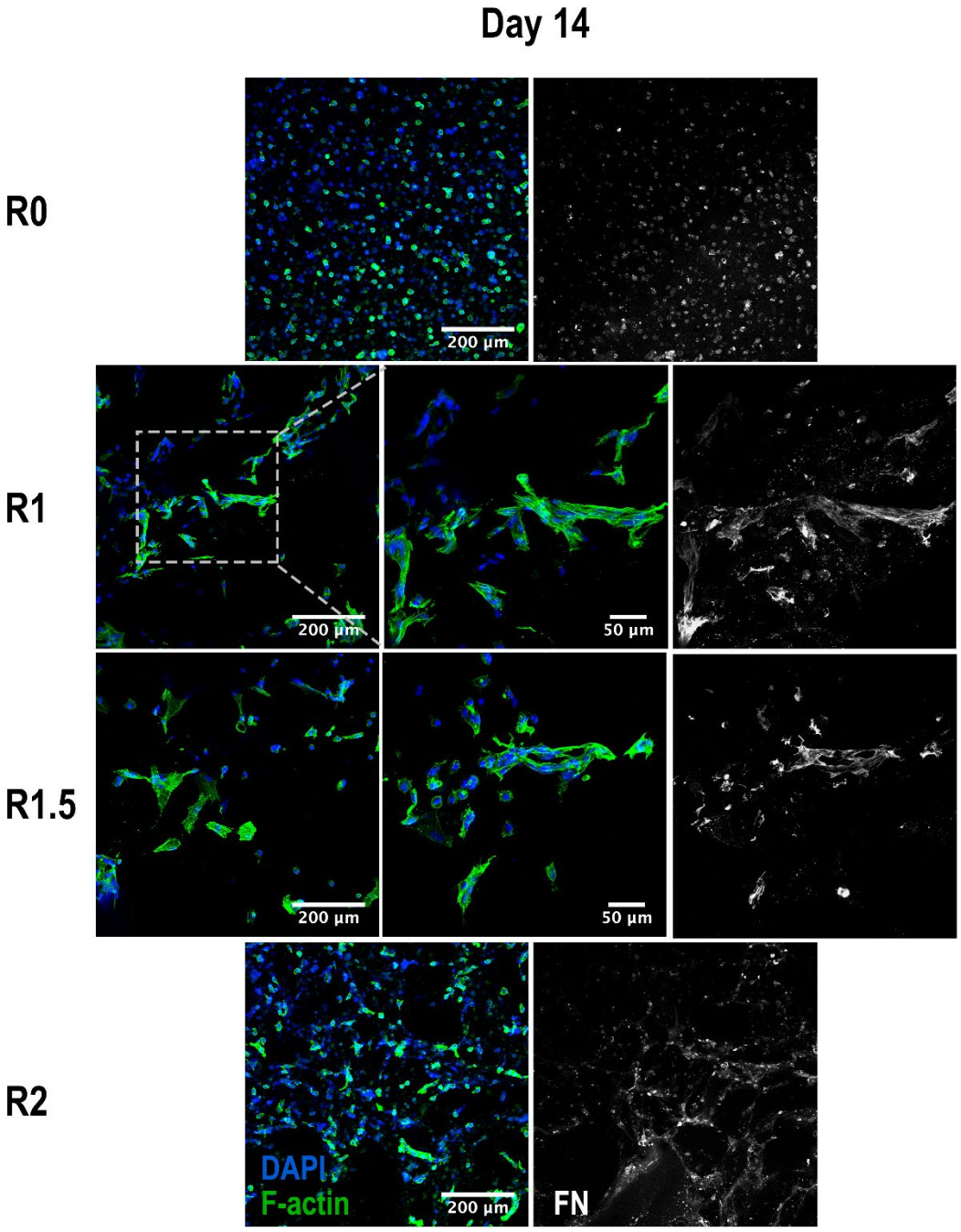


Figure 15 - Representative CLSM images of hMF cultures at day 14 *within* different alginate formulation: R0 (no GI-linker, control); R1, R1.5 and R2 *(scale bar = 200 µm). We have a closer look over the cell morphology in condition R1 and R1.5 (scale bar = 50 µm). Black and with images represent fibronectin deposition.* Cells were stained for F-actin (green), fibronectin (grey) and DAPI (nucleu, blue).

6.4 TME development and analysis

MDA-MB-231 is a widely used cell type to study breast cancer. However their poorly differentiated phenotype, lack of specific biomarkers (Table 1) and the ability to self-aggregate may difficult structural and biological characterization within 3D cultures [90]. Considering the examples described in Table 2 that use MDA-MB-231, three main observations can be taken. First, ECM-free approaches are not able to obtain spheroid structures. Second, ECM-based approaches report different outcomes regarding spheroid formation [36][43]. Third, fabrication techniques such as bioprinting allow for spatial control over 3D cell cultures, but this mechanism is directly related with the properties of the bio-ink formulation [41]. Anastasov *et al.* used the hanging drop method to form spheroids in mono-culture or co-culture with fibroblasts [33]. Although they were not able to form MDA-MB-231 spheroids in mono-culture, the co-culture allowed the 3D cell aggregation, stressing out the importance of the presence of stromal cells. Benton *et al.* reported a successful spheroid formation for MDA-MB-231 cell line but their approach is not entirely ECM free [49]. They resourced to a commercially available spheroid formation ECM in fluid form (Cultrex® Spheroid Formation ECM, Trevigen) to enhance cell-cell adhesion in low-adhesion 96-well plate. Although they successfully originate MDA-MB-231 spheroids, this approach does not offer any control over ECM biochemical and biophysical cues, which are important features during tumorigenesis. 3D cultures of MDA-MB-231 cells within ECM equivalents from onset should be able to provide not only the biochemical and biophysical signals that allow 3D cell organization, but also offer control over these cues. Therefore different ECM equivalent formulation can lead to different outcomes. For example, Taubenberger *et al.* embedded MDA-MB-231 in fully MMP-degradable PEG-heparin hydrogels and reported that cell remained single within the hydrogel [43]. Whereas within non-degradable PEG-heparin gels these cells were able to form spheroids. One possible explanation can be attributed to the high expression levels of MMPs and invasive feature of these cells, which allow them to disperse within the degradable matrix.

MDA-MB-231 culture within bioresponsive alginate. After confirming that we were able to fulfill all the criterions of our bioresponsive alginate design, we assessed the possibility of using this biomaterial in developing a TME. Acknowledging the impact that MMP sensitive linkers can have on MDA-MB-231 behavior, we started to study different GI-linker concentrations (R1, R1.5 and R0) on spheroid formation. For that purpose, cells were imaged under CLSM at different time points (Figure 16 – a)). Cells were stained for F-actin (red) , vimentin (green), which is a mesenchymal marker upregulated in MDA-MB-231 cell line [91], and nuclei (DAPI, blue). At day 1 cells remained mostly isolated in all conditions, although there were some differences in cell distribution in R1 comparing to the control (R0). This could be due to the initial hydrogel viscosity that is increased in hydrogels with dual crosslinking (Figure 11-d). After 7 days of culture there was a remarkable difference in the condition R1 with evident spheroid formation. In fact, R1 showed significantly higher spheroid diameter comparing to all the other conditions, with a

mean of 31.6 µm (Figure 17). In R1 condition, spheroids diameter present the highest heterogeneity, reaching a maximum of 56.91µm. On the other hand, R0 present the lowest mean (25.6 µm) and variation, which could be related to lack of cleavable sites within the matrix, which imposes higher mechanical confinement to cells restricting their spreading and migration (Figure 16). Noteworthy, R2 condition (spheroid mean of 25.8µm) showed no significant difference to the control. This could be related to stiffness values that we observed (Figure 11-c,d), in which higher amounts of GI-linker lead to increased stiffness. Consequently, this might be one of the reasons why higher amounts of cleavable sites did not lead to increased cell aggregation, pointing out to the importance of balancing the ratio between gel degradation and matrix mechanics in dual crosslinking. Spheroids from condition R1.5 presented an intermediate behavior between R1 and R2, with a spheroid mean of 28 µm.

In all conditions, spheroids continued to grow during the 2 weeks of culture as depicted in Figure 16a. In a close look to condition R1 (Figure 16b) it was possible to identify the formation of big spheroids with approximately 90 µm, but without a necrotic core. In fact, at day 14 some spheroids present some protrusions that could be related to invasive capacity of these cells and to fact that the matrix is cleavable. Noteworthy, it was possible to observe throughout the culture time a high number of cells that were able to escape from the alginate matrix, being this phenomenon more evident in R1 condition. To assess this behavior we have performed a cell outgrowth assay in fibrin for R1 and R0 (described below).

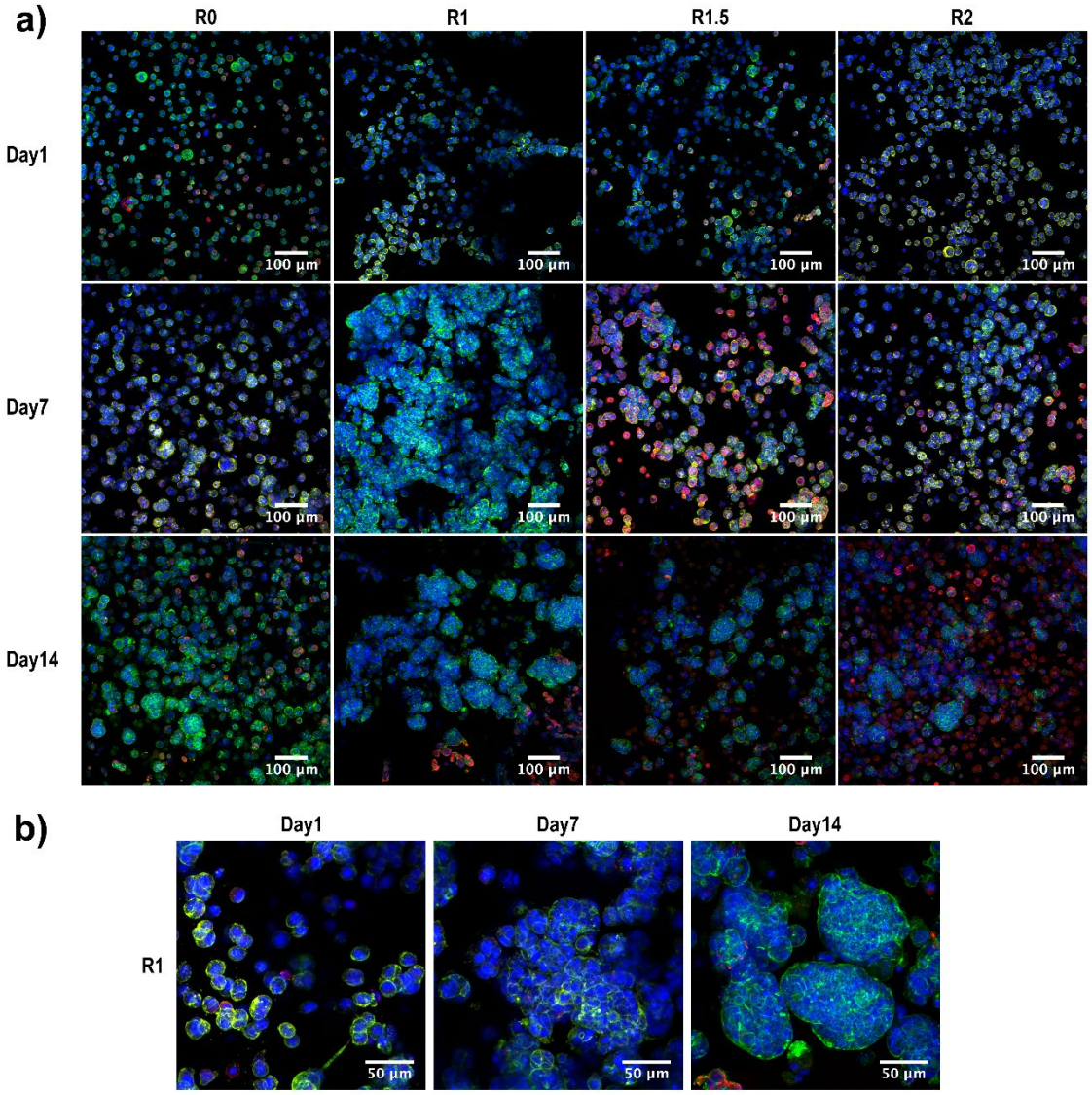


Figure 16 - Morphological evolution of MDA-MB-231 cells within different alginate formulation: R0 (no GI-linker, control); R1, R1.5 and R2. a) From top to bottom evolution with time of cell cultures (1, 7 and 14 days). From left to right increasing concentration of GI-linker (scale bar = 100 µm). B) Close up of condition R1, evidencing the spheroid formation (scale bar = 50 µm).

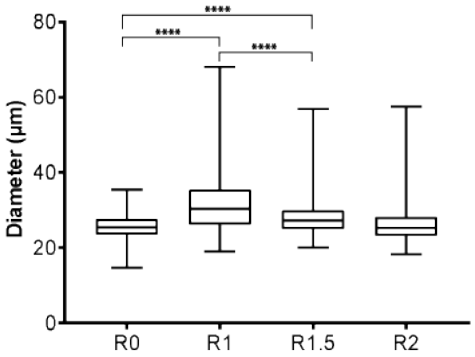


Figure 17 - Spheroid diameter of MDA_MB-231 after 7 days in culture within different alginate formulations: R0 (no GI-linker, control); R1, R1.5 and R2. . There was significant statistical difference between R0, R1 and R1.5 (****p<0.0001) and no significant difference between R0 and R2 (p>0.05) (n=200 spheroids for each condition)

Fibrin Outgrowth Assay. To confirm that R1 condition allow higher cell escape than the control (R0) we performed a cell outgrowth assay by embedding both cell laden hydrogels after 7 days of culture within fibrin hydrogel. Fibrin is the primary component of the coagulation cascade and serves as a scaffold for tissue repair after injury. It has a rich bioactivity providing signals and cues to direct cell behavior [92]. Therefore we used it as a chemotactic environment for our cells. It is expected that cells will migrate outward the alginate hydrogel into the fibrin as depicted in Figure 18. We were able to observe a differential patter in cell outgrowth when comparing the control to the bioresponsive alginate R1. As illustrated in Figure 18, there were less cells scattered within the fibrin (II) in the R0 (left picture) than in the R1 (right picture) ,which might correlate to an enhanced capability of cells to escape from the bioresponsive alginate with GI-linker (Figure 18 – R1 (II)). To escape from the alginate matrix R1, cells need to be able to produce MMPs that cleave the GI-linker, opening the alginate structure allowing spheroid growth and affording cell escape. To confirm MMP production we have performed a gelatin zymography.

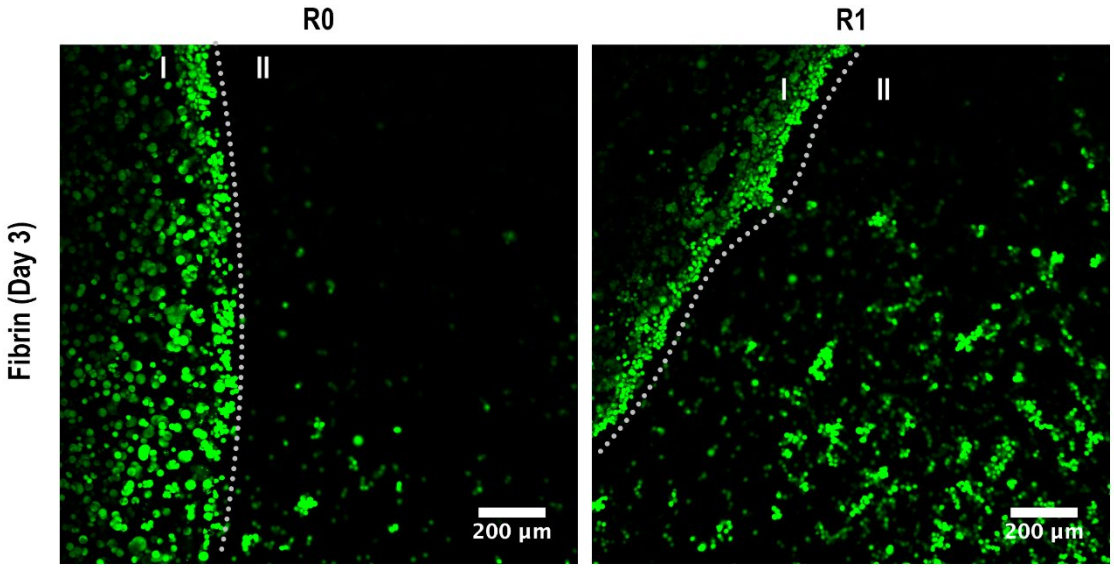


Figure 18 – Cellular outgrowth in fibrin hydrogel. MDA-MB-231 laden alginate hydrogels (R0 and R1) cultured for 7 days were placed between two layers of fibrin. Live/dead staining was performed after 3 days in fibrin and images acquired with CLSM . Live cells are stained by calcein AM (green) and dead cells by ethidium homodimer-1 (red). I – alginate hydrogel; II – fibrin hydrogel; dotted line represents the interface of the two hydrogels.

MMP Production. MDA-MB-231 is a particularly aggressive breast cancer cell line and has been described to produce high levels of MMPs namely, MMP-2 and MMP-9, during tumor progression [77]. In order to qualitatively access the influence of the GI-linker in MMP production, supernatants were collected from cells cultured with R1 hydrogel and R0 control. The MMP activity was evaluated by gelatin-zymography with the presence of clear bands at 72, 83 e 92 kDa as described in the literature for pro-MMP2, active MMP9 and pro-MMP9, respectively [93] (Figure 19-A). We observed that in the two conditions both MMPs were being secreted, but not major differences were observed (Fig 19-B). This assay needs to be repeated for other experiments and normalized to the total cell number. This normalization was not possible in this experiment, since we found some difficulties to dissolve the alginate with GI-linker, but tests with collagenase II and IV are ongoing.

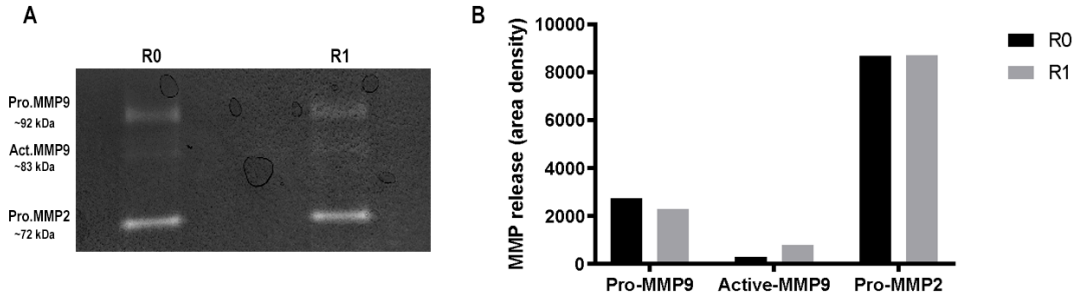


Figure 19 – A –Gelatinase zymogram of MDA-MB-231 cultured in R0 and R1 alginate. B – Quantitative densiometric analysis of MMP production (n=1).

ECM production by co-cultures. Fibroblasts are one of the key players in remodeling breast tissue during events related to a women life cycle and have been associated with tumor progression events. They are responsible for secreting ECM components such as collagens (I, III and V), proteoglycans, fibronectin and also basement membrane components such as laminin and collagen IV. In tumors they become activated and alter their ECM production patterns to higher levels of collagen deposition leading to increased tumor stiffness, cancer cell invasion and drug resistance [29]. In order to evaluate the ECM production of hMF in presence of MDA-MB-231, co-cultures were established and maintained for 7 days. CLSM images were acquired at different time points, but the most significant results, regarding collagen deposition and cell morphology, were observed at day 7 (Figure 20). Hydrogel discs were stained for F-actin, collagen I and vimentin. As depicted in Figure 20 we were able to observe spheroid formation, high collagen I deposition and vimentin expression. As said before, vimentin expression is upregulated in MDA-MB-231 but it is also a marker of cancer activated fibroblasts [76]. Since we do not use specific cell markers we can only speculate the cell type through their morphology. For instance, as pointed by the arrows in Figure 20-B, elongated cells are thought to be fibroblasts as observed in Figure 14 and not found in MDA-MB-231 3D cultures (Figure 16-a). On the other hand, cell clusters could result from both cells. Even though we saw phenotypic characteristics of both cell types such as spheroid formation and cell elongation, in future experiments co-culture conditions should be optimized regarding cell density and cancer to stromal cell proportion. Then, after establishing the optimal parameters the paracrine effects of cancer and stromal cell interaction could be evaluated in our bioresponsive hydrogel. To further validate this model, cultures could be screened for markers related to cancer activated fibroblasts such as α-SMA, fibroblast activation protein (FAP), fibroblast specific protein (FSP) among others [32]. Regarding ECM production, we could evaluate its impact in matrix stiffness over time.

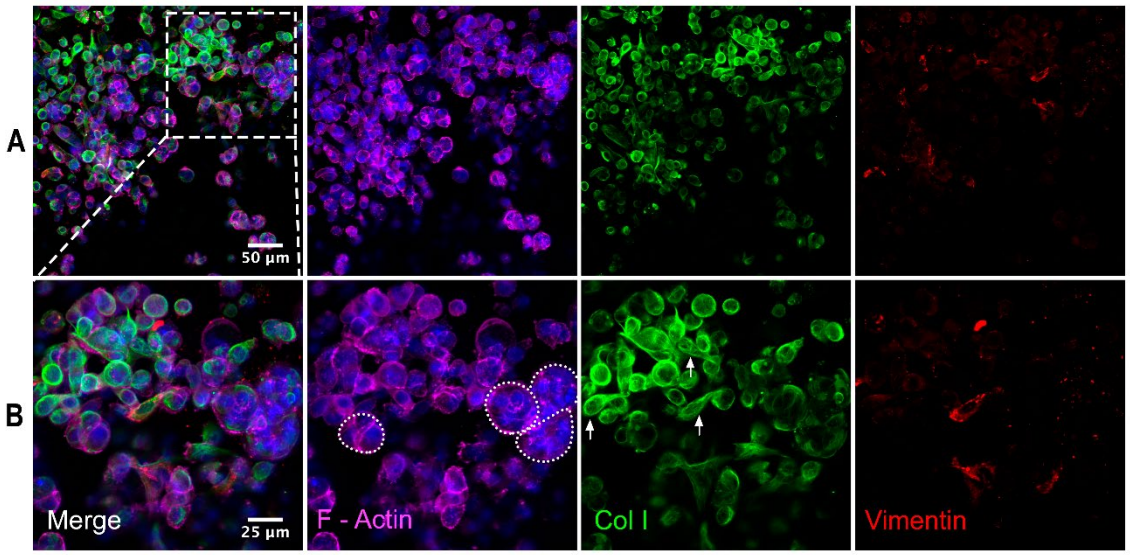


Figure 20 – Immunostaining of co-cultures of hMF and MDA-MB-231 embedded within R1 alginate after 7 days of culture. A. Overview of cell distribution (scale bar = 50 µm). B. Zooming 4x zone confined by a dashed white square where it is possible to observe spheroids formation (dashed circles) and elongated cells (arrows indicate possible fibroblasts) in close contact observed under CLSM. Cells were stained for F-actin (cyan), collagen type I (Col I, green), Vimentin (red) and DAPI (nucleu, blue). Scale bar = 25 µm.

6.5 Paclitaxel Drug resistance

Triple negative breast cancer is conveniently named due to the lack of three main breast cancer biomarkers (ER, PR and HER2).Therefore patients do not benefit from endocrine or anti-HER2 therapy, and chemotherapy is the mainstay of treatment for TNBC [5]. Despite their overall poor prognosis, patients with TNBC have a higher response to chemotherapy than patients with other breast cancer cell types, which is referred to as the TNBC paradox [7]. Paclitaxel, a member of taxanes, is an antineoplastic drug frequently used in treatment of different cancers including breast cancer [94]. Paclitaxel has an antimitotic effect by promoting polymerization and stabilization of microtubules. However lower concentrations of paclitaxel have been described to arrest cell division at the G2/M phase, a cell-cycle checkpoint which allows damaged cells to enter mitosis and undergo cell death [95].

As one of the most frequently used chemotherapeutic agents for breast cancer treatment we selected paclitaxel to evaluate MDA-MB-231 drug response within bioresponsive alginate in both mono- and co-culture. We compared results from 2D cultures and 3D cultures. 3D cultures were maintained for 1 (3D-D1) and 7 (3D-D7) days prior treatment with increasing concentrations of paclitaxel. All the conditions were incubated with the drug for 72h and the metabolic activity was measured by resazurin based assay (Figure 21). Two controls were used in each condition: i) cells cultured in normal conditions in DMEM (without vehicle and drug) and ii) cells cultured with the vehicle 0.01% DMSO. We compared the metabolic activity of both controls and although there was some decrease in metabolic activity it was not considered significant (Supplementary Figure 2). DMSO was used to dissolve the paclitaxel therefore to

subtract the effect that this component might have in the cell viability results were normalized relative to the condition 0.01% DMSO as illustrated Figure 19. In all tested conditions, paclitaxel reduced cell metabolic activity in comparison to the control. However, either in mono- or co-culture we do not see any significant differences among the lowest concentrations (0.02, 0.20, 2.00), whereas the highest concentration (20 µM) presented higher metabolic activity.

In mono-cultures, it seems that the 3D-D7 (Figure 21-a) exhibited a lower sensitivity for paclitaxel comparing to 3D-D1 and 2D, which could be due to the formation of cell clusters that impair drug diffusion. The lower metabolic activity observed in 3D-D1 could be related to the fact that this cells are more vulnerable as single cells dispersed in a 3D matrix.

Regarding co-cultures profile, there are no major differences between 3D-D1 and 3D-D7 for all tested concentrations. Interestingly, 3D co-cultures always present higher metabolic activity comparing to 2D culture. The decrease observed in 2D might be due to fibroblast death, which could be more susceptible to paclitaxel than MDA-MB-231 in the absence of any ECM-like matrix. A fibroblast mono-culture should be considered in future experiments.

In previous work, Zasadil *et al.* tested a range of paclitaxel concentrations from 0 to 50 µM and reported a concentration-depended effect in MDA-MB-231 cell cultures [96]. Their results are presented as percentage of mitotic index (number of cells in mitosis per total number of cells). They demonstrated that in response to increasing concentrations of paclitaxel, mitotic index peaks and then declines. The peak is found to occur for concentrations between 1-10 µM. Since the mitotic process is metabolically demanding it could be the reason why we saw an increase in metabolic activity for the 20 µM when compared to other concentrations. Therefore the resazurin based assay might not be the best way to evaluate the response of MDA-MB-231 to paclitaxel treatment.

Overall, the preliminary results herein presented correspond to one experiment, which unfortunately could not be repeated whithin the available time frame. As highlighted, further analyses are still needed.

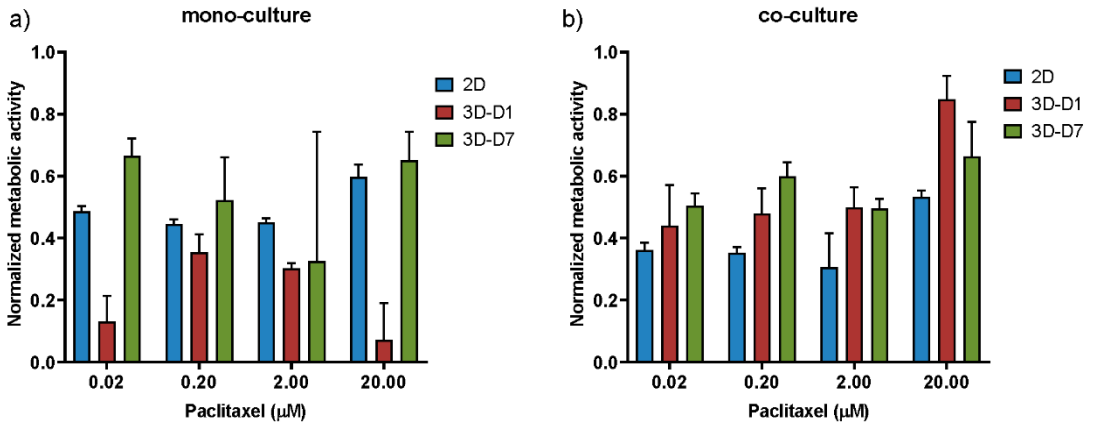


Figure 21- Metabolic activity of mono-cultures of MDA-MB-231 and co-cultures of MDA-MB-231 with hMF after treatment for 72h with increasing paclitaxel concentrations relative to 0.01% DMSO. a) Response of mono-cultures in 2D culture (blue bars) and 3D maintained for 1 day (3D-D1, red bars) or 7 days (3D-D7, green bars) in culture before treatment. b) Response of co-cultures of in 2D and 3D maintained for 1 days or 7 days before drug treatment. Data is presented as means ± stdev (n=3).

6.6 Preliminary results to test the applicability of the bioresponsive alginate in the development of 3D tri-culture platform

In previous chapters we described techniques for cancer cell embedding within hydrogels, though scaffold seeding is also a popular approach to study the cancer cell biology in a 3D environment. Solid scaffolds are generally used to model migration, invasion and metastasis of breast cancer. For example, 3D fibroin scaffolds were used to establish a co-culture with human osteoblast like cells (MG63) and MDA-MB-231 cells to mimic the 3D microenvironment of bone breast cancer [97]. Cancer cells cultured on the scaffolds showed more aggressive behavior and the interplay with MG63 cells resulted in higher levels of alkaline phosphatase (ALP-bone mineralization marker) secretion similar to what is found in bone cancer patients. In another study, PLG (poly(lactide-co-glycolide)) scaffolds were produced by gas-foaming particulate leaching process and used to evaluate angiogenic factors secretion in three different cancer cell lines [98]. They compared their results to standard 3D Matrigel and found an increased secretion of angiogenic factors. Both studies show that seeding cells on top of 3D scaffolds could lead to the development of a relevant tumor microenvironment. Nevertheless, the direct mixing of cell population in a single compartment limits the dynamic and detailed observation of cell-cell and cell-matrix interaction to circumvent these limitation layered culture techniques have been proposed. For example Sittadjody *et al.,* developed double-layered alginate microcapsules to study the paracrine influence in pancreatic cancer [99]. In their model the two layers, one with epithelial prostate cancer cells (C4-2) and the other with prostate stromal myofibroblast cell line (WPMY-1) were separated by poly-L-ornithine (PLO) that served as a perm selective basement membrane which did not allowed direct cell-cell contact an important characteristic of the TME. Based also in layered approaches, Rijal *et al.* build a compartmentalized structure by seeding breast cancer (MDA-MB-231) cells on top of the scaffold and placing a hydrogel layer with

stromal cells (fibroblasts) around the structure [36]. A layer of blank hydrogel was used to separate the two compartments. They further analyzed cell outgrowth into that layer. This latter approach eventually will allow for cell-cell contact but still is limited in terms of architectural approach and ECM composition, as mentioned before they use decellularized mouse breast tissue.

Previous work in our group has combined two strategies to develop a vascular heterotypic 3D breast cancer model. The model consisted of a 3D tri-culture platform that combined an epithelial cell-laden hydrogel with pre-vascularized scaffold. Scaffold fabrication was optimized for pore size and distribution using freeze drying and particle leaching technique as described in 5.8. The co-culture conditions of hMF and OEC on scaffolds were optimized to obtain capillary-like structures. After establishing the vascularized scaffold, MDA-MB-231 were embedded in RGD-alginate at 1% w/v and seeded on top of the scaffold (Figure 22). Herein we propose the substitution of the RGD-alginate for our newly developed bioresponsive alginate hydrogel.

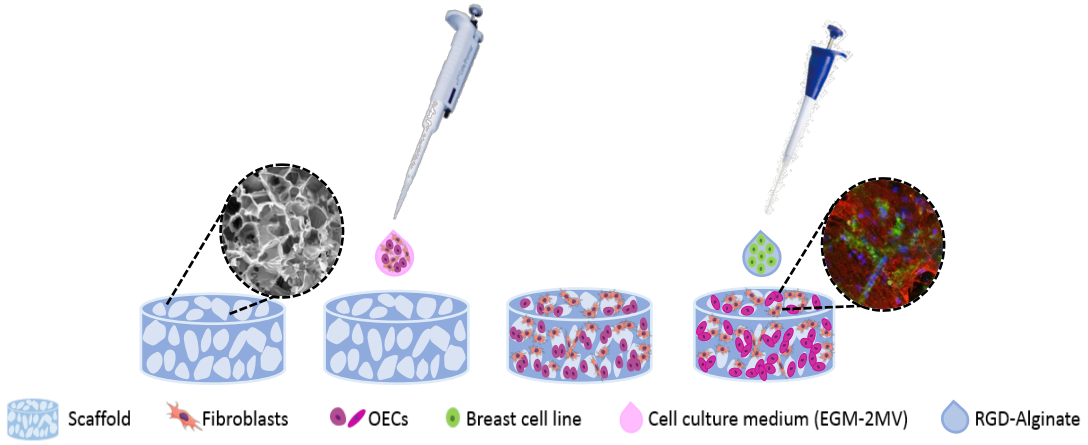


Figure 22 - Schematic representation of the 3D tri-culture platform that combined an epithelial cell-laden bioresponsive hydrogel with a pre-vascularized scaffold. Adapted from Filipa Teixeira MSc thesis

To evaluate the feasibility of using our hydrogel in this type of system we added the cell laden hydrogel, with the ratio R1, of MDA-MB-231 on top of RGD scaffold. To promote hydrogel infiltration into the scaffold the structures were centrifuged. In order to analyze the infiltration and organization of MDA-MB-231 within the scaffold, cells were pre-stained with Cell-Tracker™ Green and DAPI for nuclei staining (blue), and images were acquired at day 1 and day 7 of culture. In Figure 23 the porous structure of the scaffold is evident in gray scale and the cell distribution throughout the structure is evident by overlapping the image of the structure and the image of stained cells. As visualized in Figure 24 cell-laden hydrogel was able to penetrate in the porous scaffold from top to bottom and colonize it. At day 1, most of the cells were individually distributed cells, but at day 7 it was possible to identify some cell clusters (Figure 24). Nevertheless, some parameters of this experiment need to be optimized, such as the volume placed on top of the scaffold and the cell density used. For instance, based on this

preliminary study, it seems that 40 µL was excessive, some alginate slipped out of the scaffold. Overall, MDA-MB-231 seemed to adapt well to this environment and our hydrogel formulation shows promising results as a scaffold filler. Future work should focus on the pre-vascularization of the scaffold to validate the applicability of the bioresponsive alginate in this tri-culture platform.

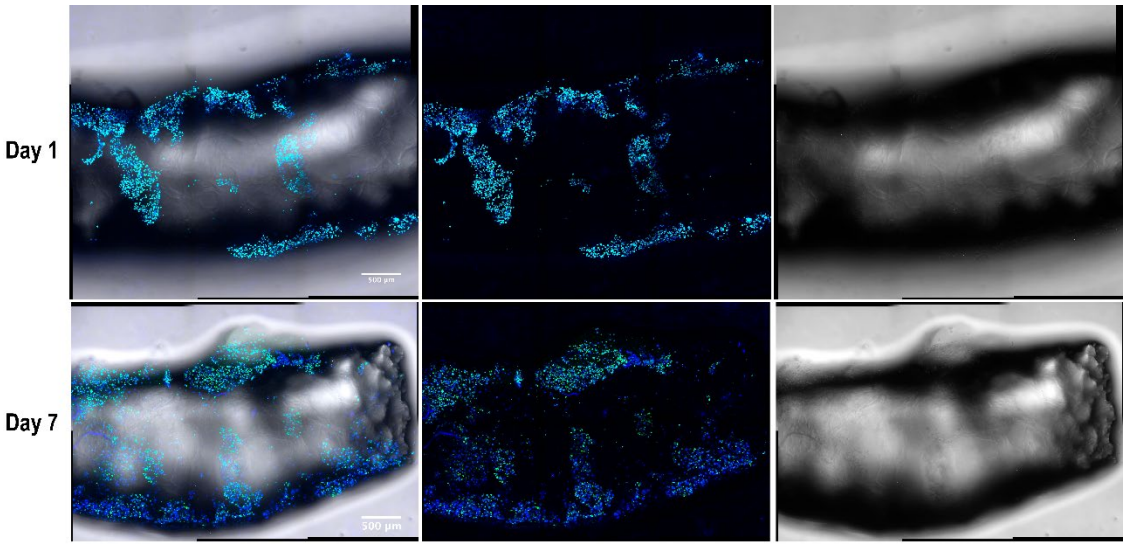


Figure 23 - Mosaic assembly of cross-sections of cell laden R1 hydrogel seeded on top of RGD alginate scaffolds after 1 and 7 days of culture, showing hydrogel penetration throughout the porous scaffold. From left to right we can see an overlapped image of the cell distribution and the scaffold structure at brightfield. Cells were labelled with CellTrackerGreen and DAPI (nuclei in blue) Scale bar = 500 µm.

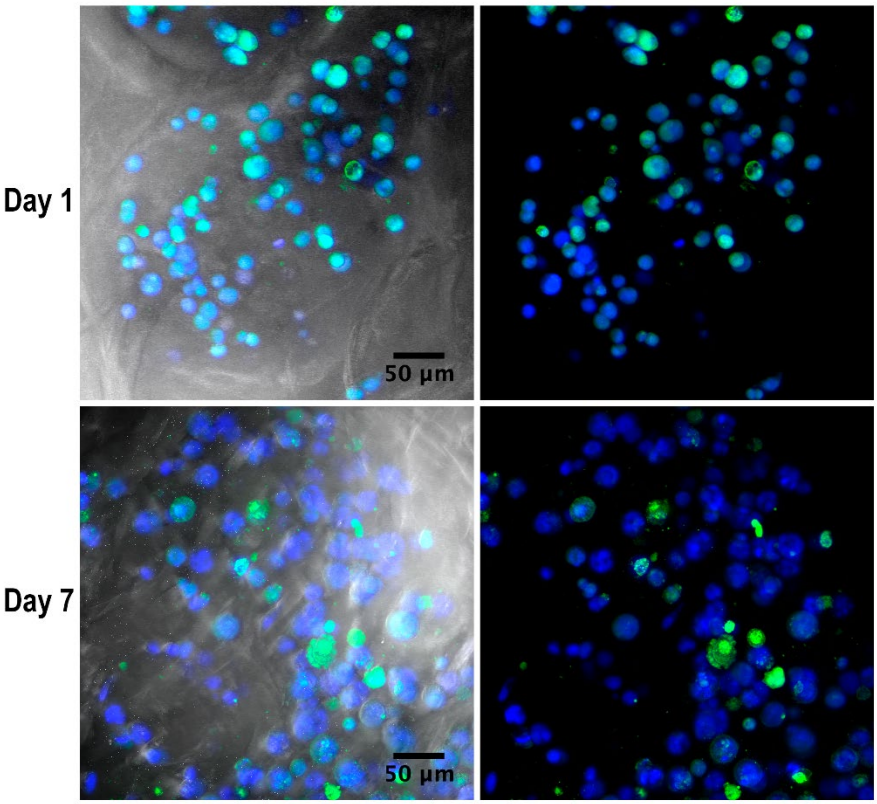


Figure 24 - Morphology of MDA-MB-231 embedded within R1 alginate and added to the porous scaffolds after 1 and 7 days of culture. Cells were able to proliferate within the scaffold and formed spheroids, which was monitored by taking brightfield images and by imaging labelled cells with CellTrackerGreen and DAPI (*nuclei in* blue). Scale bar = 50 µm.

The heterotypic model here proposed, besides combining the aforementioned advantages of alginate hydrogels will allow to recapitulate cell-cell and cell-matrix interactions of TME, alongside accumulation of ECM and secreted factors and mimic the close proximity between tumor and vascular cells found *in vivo*. In the future, this model can be further adapted to incorporate patient-derived cells for *in vitro* assessment of therapeutic efficacy using precision medicine approaches for translational research.

7. Concluding remarks and future perspectives

Breast Cancer (BC) is the second most frequently diagnosed cancer and one of the major causes of death in women. The most aggressive subtype of breast cancer is Triple Negative Breast Cancer (TNBC). This subtype represents a minority (10-20%) of all breast cancer cases, however, due to its poor prognostic, the need for cancer research directed to metastatic triple-negative disease is crucial to better identify effective treatment options and improve patients outcome. Despite an overwhelming amount of pre-clinical research on breast cancer models and chemotherapeutic strategies, the probability of approval of an oncology drug after completing Phase 1 trials is lower than 10%. This low efficiency is due in part to the inherent discrepancy between current preclinical cancer models and their ability to mimic the native breast cancer microenvironment in patients.

In breast cancer, as with any other cancer, the influence of the microenvironment, namely extracellular matrix (ECM) mechanical properties and composition, appear to have a key role in tumor progression and metastatic spread. The construction of a relevant 3D model to replicate the TME is a complex task and several approaches have been proposed to achieve this goal. From optimization of spheroid formation to the construction of more complex 3D models, the considerations to have in mind are the cellular composition of the tissue, vasculature formation, signaling molecules and of course the pillar to hold them all together, the ECM [3].

The growing number, of new approaches to study cancer biology with 3D systems using different materials is becoming the basis of the next generation of cancer research platforms. A 3D system makes it possible to study tumor cells behavior in a more biologically relevant setting and can be used for more specific drug screening to define treatments more accurately and personalized. In this context, the present work had the main objective of recreating an ECM equivalent based on a breast tumoroid of TNBC that recreates a tumor-like compartment. To achieve this goal we engineered bioresponsive ultra-pure alginate with tunable biochemical and biomechanical properties.

First, we demonstrated the possibility to tailor cell mediated degradation without compromising neither biochemical cues such as RGD presentation nor biomechanical properties such as hydrogel stiffness. Second, we evaluated the biological response of the MDA-MB-231 breast cancer cell line within our matrix regarding spheroid formation, outgrowth migration, MMP production and drug resistance. Third, the possibility to use our newly developed hydrogel to establish a relevant heterotypic breast cancer model was assessed in preliminary studies.

Regarding hydrogel optimization and characterization, we reported a successful functionalization of alginate with specific and highly reactive maleimide groups without compromising both viscoelastic properties and ionic crosslinking ability. Also, we have proved the ability of these groups to mediate thiol “click” crosslinking of alginate with a bifunctional

MMP sensitive peptide, (GI-linker), without precluding the addition of the cell suspension. Moreover, efficient incorporation of mono-cysteine adhesion ligand (RGD) via thiol "click" reaction was achieved without compromising the crosslinking mechanism. Rheological characterization revealed faster polymerization times with preservation of desired mechanical properties (G' values around 200 Pa, within the range of natural breast tissue).

The hMF cultured within the bioresponsive alginate were able to adhere and spread within the hydrogel. This behavior was dependent on the ratio thiol:maleimide (and consequently GI-linker concentration) that determines the number of cleavable sites and also the mechanical properties of the hydrogel. Cultures of MDA-MB-231 within this matrix confirmed this depended behavior and also showed that it was cell type related. The biochemical and biomechanical cues are tissue specific and are linked to their pathophysiological state. Thus, different cell types need distinct ECM properties, therefore we must adapt the composition accordingly. For instance, hMFs cultured in condition R2 were able to spread and withstand a longer period of culture within the matrix. On the other hand, MDA-MB-231 exhibited a higher ability to aggregate and form spheroids within R1 formulation. This demonstrates the versatility of our model since we were able to find optimal conditions for two different cell types by only adjusting the concentration of MMP sensitive peptide.

Besides spheroid formation, MDA-MB-231 exhibited enhanced capability to escape from the bioresponsive alginate R1 (120 µM of GI-linker and 156 µM RGD)) and maintained their characteristic levels of MMP production. Regarding co-cultures of MDA-MB-231 with hMF, we were able to observe phenotypic characteristics of both cell lines such as cell aggregates and elongated cells, along with enhanced collagen I deposition. However, further studies are still required to optimize co-culture parameters.

A drug screening test of Paclitaxel revealed an enhanced resistance to drug treatment of MDA-MB-231 cells cultured within bioresponsive alginate R1 for 7 days before drug treatment, which can be due to cell clustering and drug diffusion impairment. Co-cultures with hMF also exhibited higher values of drug resistance. However, to draw solid conclusions, further experiments are needed, such as, (1) the introduction of mono-cultures of hMFs as control and (2) a different method for cell viability evaluation. It is worth to mention that we aimed to compare our hydrogel culture with a 2D setting and scaffold-free spheroids, which are the golden standard so far for 3D culture. In our attempt to do so, we were able to successfully generate spheroids of MDA-MB-231 in mono- and co-culture using a MICROTISSUE© micro-mold system (82 wells) (Supplementary Figure 4). However, due to time constraints, we were not able to optimize the drug screening test of Paclitaxel in the scaffold-free spheroids.

Also, we successfully paved the way towards a relevant TME development with preliminary results on the use of bioresponsive alginate in a scaffold based heterotypic breast cancer model.

Furthermore, our hydrogel formulation enables independent control over chemical cues presented to the cells. This feature is achieved through highly specific orthogonal chemistries that can occur under mild and facile conditions, without affecting cell viability. Herein, we optimized the model for the RGD ligand and an MMP sensitive crosslinker. Nevertheless, the versatility of this model allows the tethering of the matrix with other relevant peptides, enhancing their potential for 3D cell culture and to further assess specific cell-matrix interactions. Moreover, the dual crosslinking mechanism allows for better mechanical control by simply changing the parameters of ionic crosslinking such as time of polymerization and ratio of divalent ion to carboxylic groups.

Importantly, our bioresponsive alginate could be adapted to culture patient-derived cells for *ex vivo* assessment of therapeutic efficacy using precision medicine approaches for translational research.

References

[1] C. F. O. R. All, “Who Report on Cancer,” 2020.

[2] H. Varmus, “The new era in cancer research,” *Science (80-.).*, vol. 312, no. 5777, pp. 1162–1165, 2006.

[3] G. Bahcecioglu, G. Basara, B. W. Ellis, X. Ren, and P. Zorlutuna, “Breast cancer models: Engineering the tumor microenvironment,” *Acta Biomater.*, vol. 106, pp. 1–21, 2020.

[4] M. Fedele, “The Epithelial-to-Mesenchymal Transition in Breast Cancer : Focus on Basal-Like Carcinomas,” pp. 1–19, 2017.

[5] C. Denkert, C. Liedtke, A. Tutt, and G. von Minckwitz, “Molecular alterations in triple-negative breast cancer—the road to new treatment strategies,” *Lancet*, vol. 389, no. 10087, pp. 2430–2442, 2017.

[6] C. Braicu *et al.*, “Novel insight into triple-negative breast cancers, the emerging role of angiogenesis, and antiangiogenic therapy,” *Expert Rev. Mol. Med.*, vol. 18, no. January 2019, 2016.

[7] G. Bianchini, J. M. Balko, I. A. Mayer, M. E. Sanders, and L. Gianni, “Triple-negative breast cancer: Challenges and opportunities of a heterogeneous disease,” *Nat. Rev. Clin. Oncol.*, vol. 13, no. 11, pp. 674–690, 2016.

[8] C. H. Wong, K. W. Siah, and A. W. Lo, “Estimation of clinical trial success rates and related parameters,” *Biostatistics*, vol. 20, no. 2, pp. 273–286, Apr. 2019.

[9] V. Papalazarou, M. Salmeron-Sanchez, and L. M. Machesky, “Tissue engineering the cancer microenvironment—challenges and opportunities,” *Biophys. Rev.*, vol. 10, no. 6, pp. 1695–1711, 2018.

[10] S. J. Bidarra, P. Oliveira, S. Rocha, D. P. Saraiva, C. Oliveira, and C. C. Barrias, “A 3D in vitro model to explore the inter-conversion between epithelial and mesenchymal states during EMT and its reversion,” *Sci. Rep.*, vol. 6, no. 1, pp. 1–14, Jun. 2016.

[11] D. Czaplinska, L. O. Elingaard-Larsen, M. G. Rolver, M. Severin, and S. F. Pedersen, “3D multicellular models to study the regulation and roles of acid–base transporters in breast cancer,” *Biochem. Soc. Trans.*, vol. 47, no. 6, pp. 1689–1700, 2019.

[12] E. M. Ahmed, “Hydrogel: Preparation, characterization, and applications: A review,” *J. Adv. Res.*, vol. 6, no. 2, pp. 105–121, Mar. 2015.

[13] I. W. Y. Mak, N. Evaniew, and M. Ghert, “Lost in translation: Animal models and clinical trials in cancer treatment,” *Am. J. Transl. Res.*, vol. 6, no. 2, pp. 114–118, 2014.

[14] J. Hoarau-Véchot, A. Rafii, C. Touboul, and J. Pasquier, “Halfway between 2D and animal models: Are 3D cultures the ideal tool to study cancer-microenvironment interactions?,” *Int. J. Mol. Sci.*, vol. 19, no. 1, 2018.

[15] L. P. Ferreira, V. M. Gaspar, and J. F. Mano, “Design of spherically structured 3D in vitro tumor models -Advances and prospects,” *Acta Biomater.*, vol. 75, pp. 11–34, 2018.

[16] S. Avnet, S. Lemma, M. Cortini, G. Di Pompo, F. Perut, and N. Baldini, “Pre-clinical Models for Studying the Interaction between Mesenchymal Stromal Cells and Cancer

Cells and the Induction of Stemness," *Front. Oncol.*, vol. 9, no. APR, pp. 1–8, 2019.

[17] M. Y. Choi *et al.*, "Engineered extracellular microenvironment with a tunable mechanical property for controlling cell behavior and cardiomyogenic fate of cardiac stem cells," *Acta Biomater.*, vol. 50, pp. 234–248, Mar. 2017.

[18] A. L. Torres *et al.*, "Microvascular engineering: Dynamic changes in microgel-entrapped vascular cells correlates with higher vasculogenic/angiogenic potential," *Biomaterials*, vol. 228, p. 119554, Jan. 2020.

[19] Caliari, "Review: Hydrogels," *Ecol. Austral*, vol. 26, no. 1, pp. 72–82, 2016.

[20] S. J. Bidarra, C. C. Barrias, and P. L. Granja, "Injectable alginate hydrogels for cell delivery in tissue engineering," *Acta Biomaterialia*, vol. 10, no. 4. Elsevier BV, pp. 1646–1662, 2014.

[21] S. J. Bidarra, A. L. Torres, and C. C. Barrias, "Injectable Cell Delivery Systems Based on Alginate Hydrogels for Regenerative Therapies," in *Reference Module in Materials Science and Materials Engineering*, Elsevier, 2016.

[22] E. L. S. Fong, D. A. Harrington, M. C. Farach-Carson, and H. Yu, "Heralding a new paradigm in 3D tumor modeling," 2016.

[23] S. V Sambasivarao, "A complex 3D human tissue culture system based on mammary stromal cells and silk scaffolds for modeling breast morphogenesis and function," vol. 18, no. 9, pp. 1199–1216, 2013.

[24] P. Friedl and S. Alexander, "Cancer invasion and the microenvironment: Plasticity and reciprocity," *Cell*, vol. 147, no. 5, pp. 992–1009, 2011.

[25] H. Jaganathan *et al.*, "Three-dimensional in vitro co-culture model of breast tumor using magnetic levitation," *Sci. Rep.*, vol. 4, pp. 1–9, 2014.

[26] P. Carranza-Rosales, N. E. Guzmán-Delgado, I. E. Carranza-Torres, E. Viveros-Valdez, and J. Morán-Martínez, "Breast Organotypic Cancer Models," Springer, Berlin, Heidelberg, 2018, pp. 1–25.

[27] K. K. Brodaczewska, C. Szczylik, M. Fiedorowicz, C. Porta, and A. M. Czarnecka, "Choosing the right cell line for renal cell cancer research," *Mol. Cancer*, vol. 15, no. 1, 2016.

[28] J. L. Inman, C. Robertson, J. D. Mott, and M. J. Bissell, "Mammary gland development: Cell fate specification, stem cells and the microenvironment," *Dev.*, vol. 142, no. 6, pp. 1028–1042, 2015.

[29] T. Alkasalias, L. Moyano-Galceran, M. Arsenian-Henriksson, and K. Lehti, "Fibroblasts in the tumor microenvironment: Shield or spear?," *International Journal of Molecular Sciences*, vol. 19, no. 5. MDPI AG, 21-May-2018.

[30] R. Baghban *et al.*, "Tumor microenvironment complexity and therapeutic implications at a glance," *Cell Communication and Signaling*, vol. 18, no. 1. BioMed Central Ltd., 07-Apr-2020.

[31] A. Bahrami *et al.*, *The Therapeutic Potential of Targeting Tumor Microenvironment in Breast Cancer: Rational Strategies and Recent Progress*, vol. 119, no. 1. 2018.

[32] Y. Mao, E. T. Keller, D. H. Garfield, K. Shen, and J. Wang, "Stromal cells in tumor microenvironment and breast cancer," *Cancer Metastasis Rev.*, vol. 32, no. 1–2, pp. 303–315, 2013.

[33] N. Anastasov *et al.*, "A 3D-microtissue-based phenotypic screening of radiation resistant tumor cells with synchronized chemotherapeutic treatment," *BMC Cancer*, vol. 15, no. 1, pp. 0–10, 2015.

[34] V. Brancato, F. Gioiella, G. Imparato, D. Guarnieri, F. Urciuolo, and P. A. Netti, "3D breast cancer microtissue reveals the role of tumor microenvironment on the transport and efficacy of free-doxorubicin in vitro," *Acta Biomater.*, vol. 75, pp. 200–212, Jul. 2018.

[35] T. Gudjonsson, L. Rønnov-Jessen, R. Villadsen, M. J. Bissell, and O. W. Petersen, "To create the correct microenvironment: Three-dimensional heterotypic collagen assays for human breast epithelial morphogenesis and neoplasia," *Methods*, vol. 30, no. 3, pp. 247–255, 2003.

[36] G. Rijal and W. Li, "A versatile 3D tissue matrix scaffold system for tumor modeling and drug screening," *Sci. Adv.*, vol. 3, no. 9, pp. 1–17, 2017.

[37] J. He *et al.*, "3D modeling of cancer stem cell niche," *Oncotarget*, vol. 9, no. 1, pp. 1326–1345, 2018.

[38] C. A. Whipple and M. Korc, "Angiogenesis signaling pathways as targets in cancer therapy," *Handb. Cell Signaling, 2/e*, vol. 3, pp. 2895–2905, 2010.

[39] L. Zhang, *Exosomes in tumor angiogenesis-multifunctional messengers with mixed intentions*. Elsevier Inc., 2018.

[40] G. G. Y. Chiew, N. Wei, S. Sultania, S. Lim, and K. Q. Luo, "Bioengineered three-dimensional co-culture of cancer cells and endothelial cells: A model system for dual analysis of tumor growth and angiogenesis," *Biotechnol. Bioeng.*, vol. 114, no. 8, pp. 1865–1877, 2017.

[41] S. Swaminathan, Q. Hamid, W. Sun, and A. M. Clyne, "Bioprinting of 3D breast epithelial spheroids for human cancer models," *Biofabrication*, vol. 11, no. 2, 2019.

[42] E. M. Langer *et al.*, "Modeling Tumor Phenotypes In Vitro with Three-Dimensional Bioprinting," *Cell Rep.*, vol. 26, no. 3, pp. 608-623.e6, 2019.

[43] A. V. Taubenberger *et al.*, "3D extracellular matrix interactions modulate tumour cell growth, invasion and angiogenesis in engineered tumour microenvironments," *Acta Biomater.*, vol. 36, pp. 73–85, 2016.

[44] D. T. Dao *et al.*, "Heparin impairs angiogenic signaling and compensatory lung growth after left pneumonectomy," *Angiogenesis*, vol. 21, no. 4, pp. 837–848, Nov. 2018.

[45] I. Rybinska, R. Agresti, A. Trapani, E. Tagliabue, and T. Triulzi, "Adipocytes in Breast Cancer, the Thick and the Thin," *Cells*, vol. 9, no. 3, p. 560, 2020.

[46] Q. Wu, B. Li, Z. Li, J. Li, S. Sun, and S. Sun, "Cancer-associated adipocytes: Key players in breast cancer progression," *J. Hematol. Oncol.*, vol. 12, no. 1, pp. 1–15, 2019.

[47] X. Y. Chen, J. Yeong, A. A. Thike, B. H. Bay, and P. H. Tan, "Prognostic role of immune infiltrates in breast ductal carcinoma in situ," *Breast Cancer Res. Treat.*, vol. 177, no. 1,

pp. 17–27, 2019.

[48] T. N. Augustine, T. Dix-Peek, R. Duarte, and G. P. Candy, “Establishment of a heterotypic 3D culture system to evaluate the interaction of TREG lymphocytes and NK cells with breast cancer,” *J. Immunol. Methods*, vol. 426, pp. 1–13, 2015.

[49] G. Benton, G. DeGray, H. K. Kleinman, J. George, and I. Arnaoutova, “In vitro microtumors provide a physiologically predictive tool for breast cancer therapeutic screening,” *PLoS One*, vol. 10, no. 4, pp. 1–18, 2015.

[50] S. Chaji, J. Al-Saleh, and C. T. Gomillion, “Bioprinted three-dimensional cell-laden hydrogels to evaluate adipocyte-breast cancer cell interactions,” *Gels*, vol. 6, no. 1, 2020.

[51] J. S. Jeon *et al.*, “Human 3D vascularized organotypic microfluidic assays to study breast cancer cell extravasation,” *Proc. Natl. Acad. Sci. U. S. A.*, vol. 112, no. 1, pp. 214–219, 2015.

[52] C. Chen, B. T. Mehl, A. S. Munshi, A. D. Townsend, D. M. Spence, and R. S. Martin, “3D-printed microfluidic devices: fabrication, advantages and limitations - a mini review,” *Anal. Methods*, vol. 8, no. 31, pp. 6005–6012, 2016.

[53] J. A. Burdick and M. M. Stevens, “Biomedical hydrogels,” *Biomater. Artif. Organs Tissue Eng.*, pp. 107–115, 2005.

[54] B. W. Kim, *Clinical regenerative medicine in urology*. 2017.

[55] H. Hecht and S. Srebnik, “Structural Characterization of Sodium Alginate and Calcium Alginate,” *Biomacromolecules*, vol. 17, no. 6, pp. 2160–2167, 2016.

[56] S. N. Pawar and K. J. Edgar, “Alginate derivatization: A review of chemistry, properties and applications,” *Biomaterials*, vol. 33, no. 11, pp. 3279–3305, 2012.

[57] M. Szekalska, A. Puciłowska, E. Szymańska, P. Ciosek, and K. Winnicka, “Alginate: Current Use and Future Perspectives in Pharmaceutical and Biomedical Applications,” *International Journal of Polymer Science*, vol. 2016. 2016.

[58] K. Y. Lee and D. J. Mooney, “Alginate: Properties and biomedical applications,” *Prog. Polym. Sci.*, vol. 37, no. 1, pp. 106–126, 2012.

[59] J. Sun and H. Tan, “Alginate-Based Biomaterials for Regenerative Medicine Applications,” *Materials (Basel).*, vol. 6, pp. 1285–1309, 2013.

[60] J. A. Rowley, G. Madlambayan, and D. J. Mooney, “Alginate hydrogels as synthetic extracellular matrix materials,” 1999.

[61] N. Huebsch *et al.*, “Harnessing traction-mediated manipulation of the cell/matrix interface to control stem-cell fate,” *Nat. Mater.*, vol. 9, no. 6, pp. 518–526, 2010.

[62] N. Huettner, T. R. Dargaville, and A. Forget, “Discovering Cell-Adhesion Peptides in Tissue Engineering: Beyond RGD,” *Trends Biotechnol.*, vol. 36, no. 4, pp. 372–383, 2018.

[63] N. C. Hunt *et al.*, “3D culture of human pluripotent stem cells in RGD-alginate hydrogel improves retinal tissue development,” *Acta Biomater.*, vol. 49, pp. 329–343, 2017.

[64] B. N. Lourenço, T. dos Santos, C. Oliveira, C. C. Barrias, and P. L. Granja, “Bioengineering

a novel 3D in vitro model of gastric mucosa for stomach permeability studies," *Acta Biomater.*, vol. 82, pp. 68–78, 2018.

[65] P. A. Williams, K. T. Campbell, and E. A. Silva, "Alginate hydrogels of varied molecular weight distribution enable sustained release of sphingosine-1-phosphate and promote angiogenesis," *J. Biomed. Mater. Res. - Part A*, vol. 106, no. 1, pp. 138–146, Jan. 2018.

[66] K. H. Bouhadir, K. Y. Lee, E. Alsberg, K. L. Damm, K. W. Anderson, and D. J. Mooney, "Degradation of partially oxidized alginate and its potential application for tissue engineering," *Biotechnol. Prog.*, vol. 17, no. 5, pp. 945–950, 2001.

[67] J. Jia *et al.*, "Engineering alginate as bioink for bioprinting," *Acta Biomater.*, vol. 10, no. 10, pp. 4323–4331, 2014.

[68] K. B. Fonseca *et al.*, "Injectable MMP-sensitive alginate hydrogels as hMSC delivery systems," *Biomacromolecules*, vol. 15, no. 1, pp. 380–390, Jan. 2014.

[69] K. B. Fonseca, S. J. Bidarra, M. J. Oliveira, P. L. Granja, and C. C. Barrias, "Molecularly designed alginate hydrogels susceptible to local proteolysis as three-dimensional cellular microenvironments," *Acta Biomater.*, vol. 7, no. 4, pp. 1674–1682, 2011.

[70] J. Sun *et al.*, "The development of cell-initiated degradable hydrogel based on methacrylated alginate applicable to multiple microfabrication technologies," *J. Mater. Chem. B*, vol. 5, no. 40, pp. 8060–8069, 2017.

[71] Y. Shtenberg, M. Goldfeder, A. Schroeder, and H. Bianco-Peled, "Alginate modified with maleimide-terminated PEG as drug carriers with enhanced mucoadhesion," *Carbohydr. Polym.*, vol. 175, pp. 337–346, 2017.

[72] D. Hanahan and R. A. Weinberg, "Hallmarks of cancer: The next generation," *Cell*, vol. 144, no. 5. Cell Press, pp. 646–674, 04-Mar-2011.

[73] I. WN, A. R. MSB, and D. AA, "Matrix Metalloproteinases In Cancer Biology: A Review," Aug. 2019.

[74] D. P. Nair *et al.*, "The Thiol-Michael addition click reaction: A powerful and widely used tool in materials chemistry," *Chem. Mater.*, vol. 26, no. 1, pp. 724–744, 2014.

[75] J. Patterson and J. A. Hubbell, "Enhanced proteolytic degradation of molecularly engineered PEG hydrogels in response to MMP-1 and MMP-2," *Biomaterials*, vol. 31, no. 30, pp. 7836–7845, Oct. 2010.

[76] A. Avagliano *et al.*, "Influence of fibroblasts on mammary gland development, breast cancer microenvironment remodeling, and cancer cell dissemination," *Cancers*, vol. 12, no. 6. MDPI AG, pp. 1–35, 01-Jun-2020.

[77] H. Li, Z. Qiu, F. Li, and C. Wang, "The relationship between MMP-2 and MMP-9 expression levels with breast cancer incidence and prognosis," *Oncol. Lett.*, vol. 14, no. 5, pp. 5865–5870, 2017.

[78] R. F. Pereira, C. C. Barrias, P. J. Bártolo, and P. L. Granja, "Cell-instructive pectin hydrogels crosslinked via thiol-norbornene photo-click chemistry for skin tissue engineering," *Acta Biomater.*, vol. 66, pp. 282–293, 2018.

[79] P. Farkaš and S. Bystrický, "Efficient activation of carboxyl polysaccharides for the preparation of conjugates," *Carbohydr. Polym.*, vol. 68, no. 1, pp. 187–190, 2007.

[80] M. D'Este, D. Eglin, and M. Alini, "A systematic analysis of DMTMM vs EDC/NHS for ligation of amines to Hyaluronan in water," *Carbohydr. Polym.*, vol. 108, no. 1, pp. 239–246, Aug. 2014.

[81] C. T. Moody, S. Palvai, and Y. Brudno, "Click cross-linking improves retention and targeting of refillable alginate depots," *Acta Biomater.*, vol. 112, pp. 112–121, 2020.

[82] H. W. Ooi, C. Mota, A. Tessa Ten Cate, A. Calore, L. Moroni, and M. B. Baker, "Thiol-Ene Alginate Hydrogels as Versatile Bioinks for Bioprinting," *Biomacromolecules*, vol. 19, no. 8, pp. 3390–3400, 2018.

[83] A. M. Kosinski, M. P. Sivasankar, and A. Panitch, "Varying RGD concentration and cell phenotype alters the expression of extracellular matrix genes in vocal fold fibroblasts," *J. Biomed. Mater. Res. - Part A*, vol. 103, no. 9, pp. 3094–3100, Sep. 2015.

[84] N. Huebsch *et al.*, "Harnessing traction-mediated manipulation of the cell/matrix interface to control stem-cell fate," *Nat. Mater.*, vol. 9, no. 6, pp. 518–526, 2010.

[85] J. M. Zuidema, C. J. Rivet, R. J. Gilbert, and F. A. Morrison, "A protocol for rheological characterization of hydrogels for tissue engineering strategies," *J. Biomed. Mater. Res. - Part B Appl. Biomater.*, vol. 102, no. 5, pp. 1063–1073, 2014.

[86] N. G. Ramião, P. S. Martins, R. Rynkevic, A. A. Fernandes, M. Barroso, and D. C. Santos, "Biomechanical properties of breast tissue, a state-of-the-art review," *Biomech. Model. Mechanobiol.*, vol. 15, no. 5, pp. 1307–1323, 2016.

[87] M. J. Paszek *et al.*, "Tensional homeostasis and the malignant phenotype," *Cancer Cell*, vol. 8, no. 3, pp. 241–254, Sep. 2005.

[88] K. R. Levental *et al.*, "Matrix Crosslinking Forces Tumor Progression by Enhancing Integrin Signaling," *Cell*, vol. 139, no. 5, pp. 891–906, Nov. 2009.

[89] B. L. Ekerdt, R. A. Segalman, and D. V. Schaffer, "Spatial organization of cell-adhesive ligands for advanced cell culture," *Biotechnology Journal*, vol. 8, no. 12. Wiley-VCH Verlag, pp. 1411–1423, 2013.

[90] K. M. Aw Yong *et al.*, "Heterogeneity at the invasion front of triple negative breast cancer cells," *Sci. Rep.*, vol. 10, no. 1, pp. 1–9, 2020.

[91] Z. Wei, Z. Shan, and Z. A. Shaikh, "Epithelial-mesenchymal transition in breast epithelial cells treated with cadmium and the role of Snail," *Toxicol. Appl. Pharmacol.*, vol. 344, pp. 46–55, Apr. 2018.

[92] A. C. Brown and T. H. Barker, "Fibrin-based biomaterials: Modulation of macroscopic properties through rational design at the molecular level," *Acta Biomater.*, vol. 10, no. 4, pp. 1502–1514, 2014.

[93] M. W. Roomi, J. C. Monterrey, T. Kalinovsky, M. Rath, and A. Niedzwiecki, "Patterns of MMP-2 and MMP-9 expression in human cancer cell lines," *Oncol. Rep.*, vol. 21, no. 5, pp. 1323–1333, May 2009.

[94] T. M. Abu Samaan, M. Samec, A. Liskova, P. Kubatka, and D. Büsselberg, "Paclitaxel's Mechanistic and Clinical Effects on Breast Cancer," *Biomolecules*, vol. 9, no. 12. NLM (Medline), 27-Nov-2019.

[95] P. Giannakakou, R. Robey, T. Fojo, and M. V Blagosklonny, "Low concentrations of

paclitaxel induce cell type-dependent p53, p21 and G1/G2 arrest instead of mitotic arrest: molecular determinants of paclitaxel-induced cytotoxicity."

[96] L. M. Zasadil *et al.*, "Cytotoxicity of paclitaxel in breast cancer is due to chromosome missegregation on multipolar spindles," *Sci. Transl. Med.*, vol. 6, no. 229, p. 229ra43, Mar. 2014.

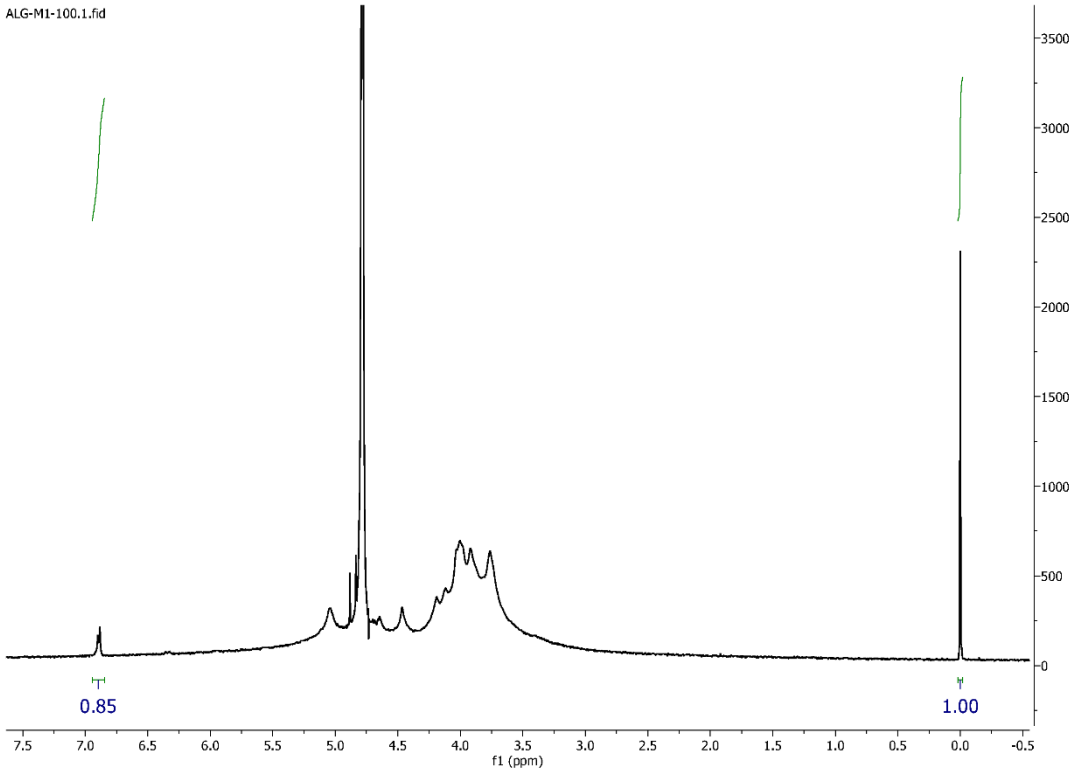
[97] B. Subia, T. Dey, S. Sharma, and S. C. Kundu, "Target specific delivery of anticancer drug in silk fibroin based 3D distribution model of bone-breast cancer cells," *ACS Appl. Mater. Interfaces*, vol. 7, no. 4, pp. 2269–2279, 2015.

[98] C. Fischbach *et al.*, "Engineering tumors with 3D scaffolds," *Nat. Methods*, vol. 4, no. 10, pp. 855–860, 2007.

[99] X. Sittadjody, S. Gyabaah, K. C. Opara, and E. C. Balaji, "Novel 3D Co-Culture Model for Epithelial-Stromal Cells Interaction in Prostate Cancer," *PLoS One*, vol. 8, no. 9, p. 75187, 2013.

Supplementary Information

Quantitative analysis of NMR spectra:



Supplementary Figure 1 - ^{1}H-NMR spectrum of AlgM1 and the integrals of the TSP (0.05M) standard (1.00) at 0.00 ppm and the maleimide signal (0.85) at 6.9 ppm.

Supplementary Table 1 - Calculus of the percentage of functionalization and the efficiency of the reaction based on quantitative NMR analysis.

% of activation	100%
Mass of NMR sample (mg)	9.56
NMR sample (µL)	717
[TSP] in sample (M)	4.17E-04
Integration of double bounds	0,85
Integration for 1H	0.425
[Maleimide] (M)	1.77E-04
No. Of mol of maleimide	1.27E-07
MW of maleimide	176.6
Mass of maleimide (mg)	0.0224
Mass of alginate (m.sample-m.mal)	9.54
MW of alginate	197.9
No. Of mol of alginate	4.82E-05
% of functionalization	0.26
% of theoretic functionalization	2.4
Efficiency	10,8%

Supplementary Table 2 - Table of ratios of peptide crosslinker to maleimide, final peptide concentration in 1% hydrogels composed of 100% of AlgM1 and the corresponding amount of thiol groups. This values are adjusted with the hydrogel polymer concentration and the amount of maleimide-alginate used, e.g ratio R5 in a hydrogel with 50% of AlgM1 is equivalent to a peptide concentration of 300µM.

Ratio P/MAL	GI-linker (µM)	Thiol Groups (mol)
R7	840	1.68×10^{-5}
R5	600	1.2×10^{-5}
R4	480	9.6×10^{-6}
R3	360	7.2×10^{-6}
R2	240	4.8×10^{-6}
R1	120	2.4×10^{-6}

Example of calculus for 1 g of alginate attending for 10% of efficiency in maleimide coupling reaction:

1 g of Alginate contains 1.2×10^{-5} mol of maleimide.

To occupy all the maleimides 1.2×10^{-5} mol of thiol is needed.

The cysteines flanking the peptide are responsible for the thiol groups present in the peptide:

$$\frac{2 \times Mw(Cysteine)}{Mw(Peptide)} = \frac{2 \times 103{,}14}{1048{,}2} = 0.2$$

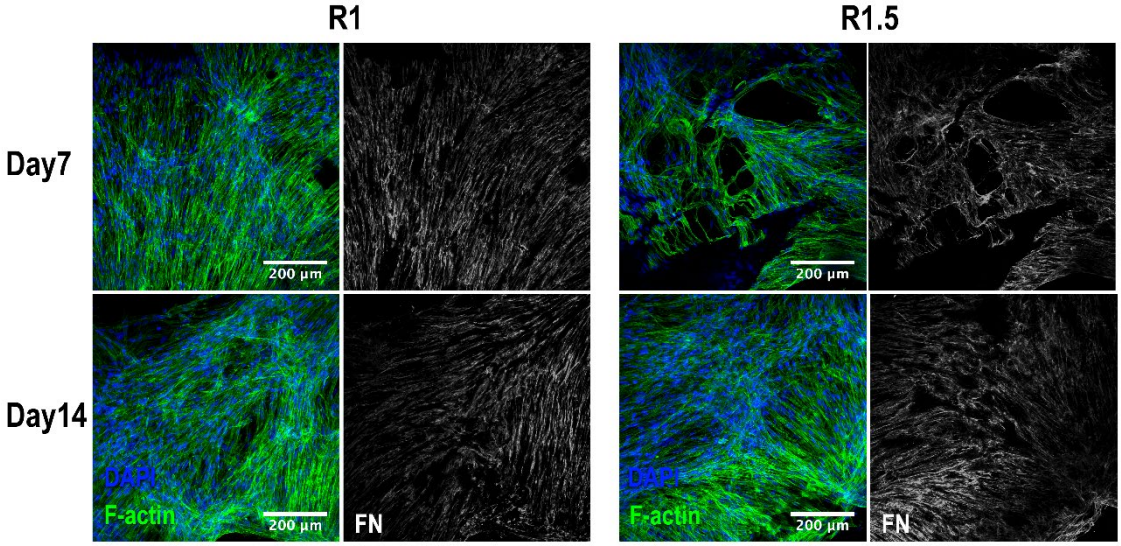
Amount of peptide needed:

$$\frac{1.2 \times 10^{-5}\ mol}{0.2} = 6 \times 10^{-5}\ mol$$

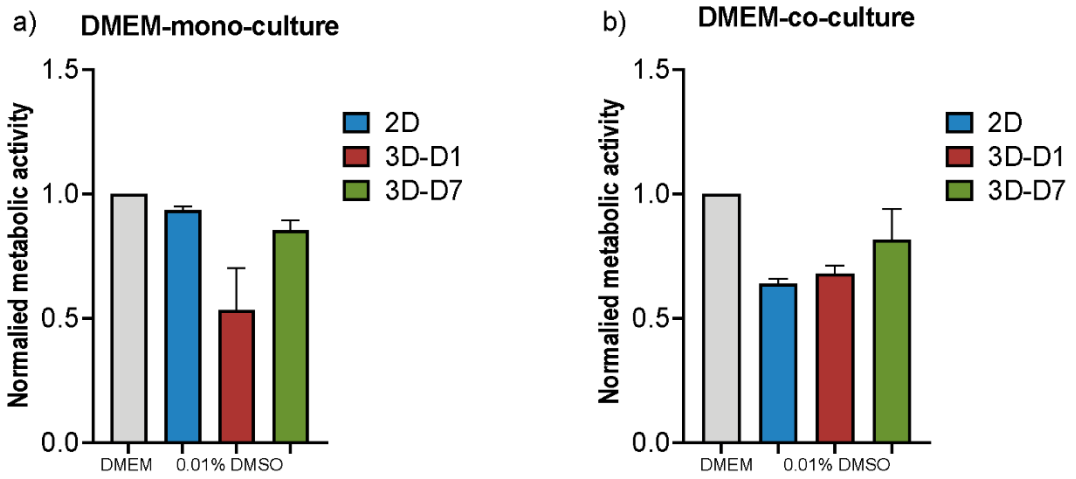
This means that it is needed 6×10^{-5} mol of peptide per 1 g of alginate to consume all the maleimides.

This corresponds to a molar concentration of peptide in 1% w/v hydrogels of:

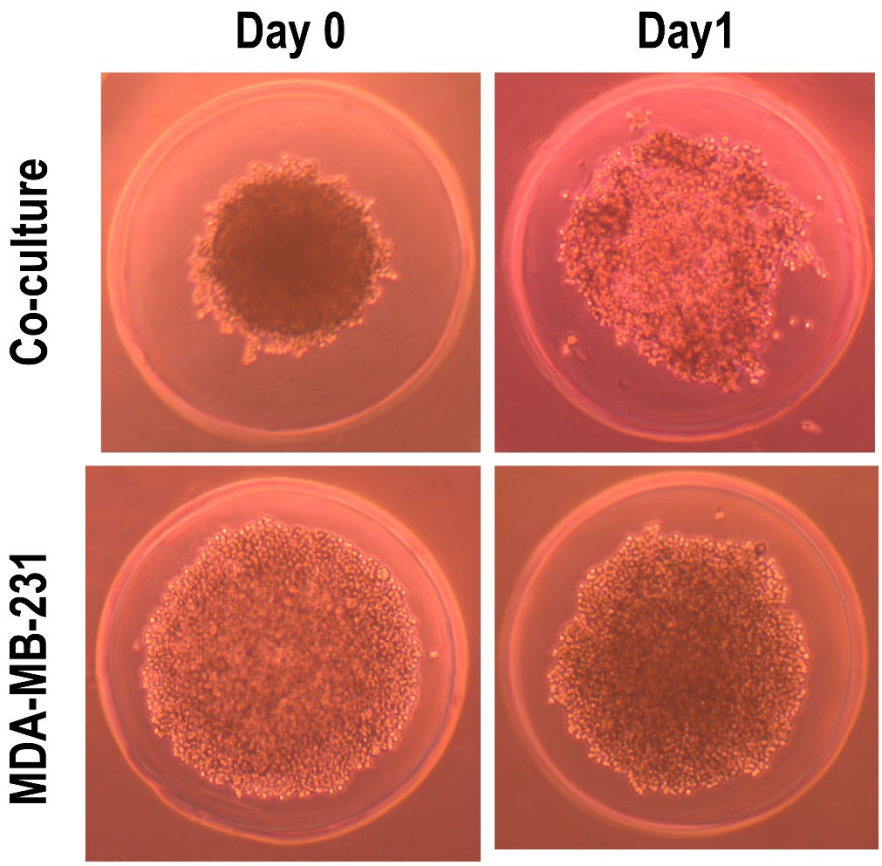
$$[Peptide] = \frac{6 \times 10^{-5}\ mol}{0.1\ L} = 6 \times 10^{-4}\ M$$



Supplementary Figure 2 –Top view of hMF cultured within bioresponsive alginate hydrogels after 7 and 14 days of culture within different alginate formulation: R1 and R1.5. Cells were stained for F-actin (green), fibronectin (grey) and DAPI (nucleu, blue). Images were taken by CLSM. Scale bars = 200 µm.



Supplementary Figure 3 - Effect of DMSO in metabolic activity of mono-cultures of MDA-MB-231 and co-culture of MDA-MB-231 with hMF after 72 hours. a) Response of mono-cultures and b) of co-cultures in 2D culture (blue bars) and 3D maintained for 1 day (3D-D1, red bars)) or 7 days (3D-D7, green bars)) in culture before adding DMSO. Values were normalized considering culture in DMEM as 100% of viability . Data is presented as means ± st*andard deviation* dev (n=3).



Supplementary Figure 4 – Brightfield images of MDA-MB-231/hMF spheroids (top row) and MDA-MB-231spheroids (bottom row). At day 0, cells aggregated, forming spherical structures. Co-cultures present higher cell cohesion, originating spheroids with smaller diameter. After 1 day, co-cultured spheroids seemed to lose their initial cohesion and circularity. On the other hand, mono-cultures spheroids seems to slightly decrease their diameter.